Dynamics and Synthesis of Kinematic Chains with Impact and Clearance

Except where reference is made to the work of others, the work described in this dissertation is my own or was done in collaboration with my advisory committee.

Eleonor D. Stoenescu

Certificate of Approval:

George T. Flowers
Professor
Department of Mechanical Engineering

Dan B. Marghitu, Chair
Professor
Department of Mechanical Engineering

David G. Beale
Professor
Department of Mechanical Engineering

Amnon J. Meir
Professor
Department of Mathematics

Stephen L. McFarland
Dean
Graduate School

Dynamics and Synthesis of Kinematic Chains with Impact and Clearance

Eleonor D. Stoenescu

A Dissertation

Submitted to

the Graduate Faculty of

Auburn University

in Partial Fulfillment of the

Requirements for the

Degree of

Doctor of Philosophy

Auburn, Alabama

May 13, 2005

Vita

Eleonor D. Stoenescu, son of Eleonor and Felicia Stoenescu, was born on January 15th, 1975, in Cisnadie, Romania. In 1993, he entered the University of Craiova, Department of Mechanical Engineering, where he received his B.S. Diploma in 1998. He received his M.S. Diploma from the same department in 1999. During 1999-2000 he worked as an instructor at the Department of Electrical Engineering of the University of Craiova. In August 2000 he joined the doctoral program of the Department of Mechanical Engineering at Auburn University, Alabama.

Dissertation Abstract

Dynamics and Synthesis of Kinematic Chains with Impact and Clearance

Eleonor D. Stoenescu

Doctor of Philosophy, May 13, 2005
(M.S., University of Craiova, Romania, 1999)
(B.S., University of Craiova, Romania, 1998)

162 Typed Pages

Directed by Dan B. Marghitu

In this dissertation, the dynamics and synthesis of open and closed kinematic chains with frictional impact and joint clearance is studied.

First, the impact between rigid bodies with friction is investigated. A new model of impact with friction is presented. The coefficient of rolling friction is defined and the moment of rolling friction is introduced to the impact equations. The influence of the moment of rolling friction and the geometrical characteristics of the links on the energy dissipated by friction during the impact is analyzed.

Next, the effect of prismatic joint inertia on the dynamics of kinematic chains is analyzed. The effect of the prismatic joint inertia on the position of the application point of the joint contact forces is investigated. The influence of the joint inertia on the dynamic response of a spatial robot arm with feedback control is analyzed. Also, the influence of the joint inertia on the dynamic parameters of a planar mechanism is exemplified using inverse dynamics.

Furthermore, a planar rigid-link mechanism with rotating prismatic joint and clearance is modeled. The influence of the clearance gap size, crank speed, friction, and

impact parameters on the dynamics of the system is analyzed. Nonlinear dynamics tools are applied to analyze the data captured from the connecting rod of the mechanism.

Finally, a new structural synthesis of spatial mechanisms is developed based on the system group classification. Spatial system groups of different families with one, two, and three independent contours are presented. The advantage of the analysis of spatial mechanisms based on the system group classification lies in its simplicity. The solution of mechanisms can be obtained by composing the partial solutions of system groups.

For the previous models of impact with friction, the effect of the rolling friction was neglected. In this dissertation, the moment of rolling friction is defined and introduced to the impact equations. Prismatic joint inertia must be included for modeling high-speed machine tools, manipulators, and robots. This problem is important, because in some cases the moment of inertia of the prismatic joints is comparable to the moment of inertia of the links and may significantly influence the dynamics of the system at high speeds. Periodic motion is observed for the mechanism with rotating prismatic joint and no clearance. The response of the mechanism with joint clearance is chaotic at relatively high crank speeds. Also, a general method is presented in order to determine all the configurations of complex spatial system groups and to automate the process.

Acknowledgments

The author would like to express his gratitude to his advisor Dr. Dan B. Marghitu, Associate Professor of Mechanical Engineering, for his valuable guidance, support, patience, and encouragement towards the completion of this dissertation. The author also wishes to acknowledge Dr. George T. Flowers, and Dr. David G. Beale, Professors of Mechanical Engineering, and Dr. Amnon J. Meir, Professor of Mathematics, for their helpful suggestions and serving as committee members.

The financial support provided by the Department of Mechanical Engineering, Auburn University, is gratefully appreciated.

The author would like to make a special acknowledgement to his parents, Eleonor and Felicia Stoenescu, for their education, love, and constant support during this years.

Style manual or journal used Journal of Sound and Vibration (together with the style known as "auphd"). Bibliography follows van Leunen's *A Handbook for Scholars.*

Computer software used The document preparation package TEX (specifically LATEX) together with the departmental style-file `auphd.sty`.

Table of Contents

List of Tables

List of Figures

Chapter 1

Introduction

Consideration of dynamic modeling is an important part in the analysis, design and control of mechanical systems such as mechanisms, manipulators, robots, etc. In general, mechanical systems have several desirable features relative to the coupling contact forces such as higher speed, improved mobility and stability, and reduced power consumption. The dynamics of mechanical systems with frictional contacts and impacts has been developed and applied to many industrial applications. One of the important factors that influence the dynamic stability and the performance of machines is joint clearance. In the last years, many researchers have been studied the effects of the clearance on the motion of mechanical systems.

In this dissertation the nonlinear dynamics of a mechanism with rotating prismatic joint and clearance is investigated. Nonlinear dynamics tools were applied in order to study the behavior of the mechanism. Frictional contacts and impacts and prismatic joint inertia have been considered to model the mechanism.

In Chapter 2 a new model of rigid body impact with friction is presented. The coefficient of rolling friction and the moment of rolling friction are introduced.

In Chapter 3 the influence of the prismatic joint inertia on the position of the application point of the joint reaction forces and the effect on the dynamics and control of open and closed kinematic chains is analyzed.

In Chapter 4 the nonlinear dynamics of a planar, rigid-link mechanism with prismatic joint clearance is investigated. The influence of the clearance gap size, crank speed, friction and impact parameters on the nonlinear behavior of the system are analyzed.

In Chapter 5 a new structural synthesis of spatial mechanisms is studied based on the system group classification. Structural synthesis of mechanisms with the specified number of contours and joint types is necessary in order to systematize the creative design process.

Finally, in Chapter 6, general conclusions are recorded. For mechanical systems with no clearance, the motion is periodic. Chaotic motion is observed for mechanical systems with joint clearance.

Chapter 2

Impact with moment of rolling friction

The impact between rigid bodies and rough surfaces is studied. The rolling friction moment and the coefficient of rolling friction are introduced, and an improved mathematical model of the planar impact with friction is presented. The influence of the moment of rolling friction on the energy dissipated by friction during the impact is analyzed. For a simple pendulum, using the energetic coefficient of restitution, more energy is dissipated for larger values of the coefficient of kinetic friction and contact radius, and for smaller values of the length of the beam. For a double pendulum, using the kinematic coefficient of restitution, in some cases one can obtain energetically inconsistent results. If the moment of rolling friction is introduced, this problem can be solved for some values of the coefficient of rolling friction.

2.1 Introduction

Newton [1] defines the coefficient of restitution e as a kinematic quantity that is used to derive a relation between the normal impact velocities of approach and separation at the contact point. Poisson [2] divides the collision period in two phases, compression and restitution. Poisson defines e as a kinetic quantity that relates the normal impulses at the contact point that occur during each phase. Routh [3] presented a graphical method based on Poisson's hypothesis [2] to treat collision problems. Later Whittaker [4] expanded Newton's method [1] considering the frictional impulse. Routh and Whittaker presented different approaches in the treatment of motion on the tangential direction at

the point of contact. Routh solves for the slipping velocity during collision and introduces the possibility of changes in slipping direction during contact. Considering Whittaker's method, slipping occurs when the ratio of the normal and tangential impulses are greater that the coefficient of friction μ.

Kane and Levinson [5] observed that the classical solution of rigid body impact problems using Newton's theory produces energetically inconsistent results. Keller [6] attributed this paradoxical behavior to slip reversals during collision subject to frictional effects. The Newtonian approach ignores the changes in the direction of slip, leading to the overestimation of the rebound velocity as a result of impact. Keller introduced a revised formulation of rigid body collision equations based on Poisson's hypothesis such that impact never increases energy. Stronge [7, 8] divided the energy that is dissipated during collision into two portions: dissipation due to frictional impulse and dissipation due to normal impulse. He solved the impact with friction problem using an energetic coefficient of restitution.

Brach [9, 10] has proposed a solution scheme based on revising Whittaker's method in order to avoid energy increases from resulting solutions. The approach treats the tangential impulse as a constant fraction μ of the normal impulse. Then energy loss is examined to determine the appropriate value of μ that can be used in the actual solution. He has expanded his approach, to treat contacts that take place over finite areas and introduced a moment coefficient e_m to solve the collision problem. The same author [11] has introduced a moment due to peeling at the trailing edge of the contact surface during rolling in the equations of a planar impact of a sphere in the presence of adhesion.

Marghitu [12] presented some impact friction versus impact angle plots for slender steel beams with semi-spherical ends impacting the hard surface of a massive concrete object. Similar impact friction plots were reported by Stoianovici and Hurmuzlu [13] for a slender beam impacting a half-space. The classical coefficient of restitution is found to depend strongly on the orientation of the bar, and the impacts are divided into a series of micro-impacts. Calsamiglia et al. [14] observed that the coefficient of friction for disks impacting a massive surface is found to depend on the inclination angle. Osakue and Rogers [15] presented an experimental study of friction during planar low-speed oblique impacts. Johansson and Kalbring [16] developed a numerical algorithm where the impenetrability condition and Coulomb's law of friction were formulated as equations in terms of velocities and impulses rather than displacements and forces.

Pfeiffer and Glocker [17] presented theoretical and applied aspects of the dynamics of multiple unilateral contacts in multibody mechanical systems. Kinetic restitution was considered for the normal direction as well as the tangential restitution effects. The problem of rigid body collision with multiple contact points was also studied by Marghitu and Hurmuzlu [18]. Hurmuzlu [19] introduced a new method to solve collision problems of slender bars with massive external surfaces on a revised energetic coefficient of restitution that resolves the effect of impact induced vibrations on the post-collision velocities of the impacting bars. The impulse-based rigid-body as well as the alternative compliance-based approaches have failed to produce valid solutions to the problem of predicting the post-impact velocities in multi-impact systems. Ceanga and Hurmuzlu [20] considered the impulse-momentum-based rigid-body approach and solved the non-uniqueness difficulty by introducing a new constant called the impulse transmission ratio.

In the new algebraic rigid-body collision model presented in Chatterjee and Ruina [21], it is possible to predict partially sliding disk collisions for suitable choices of the tangential coefficient of restitution. Lankarani [22] presented a general formulation for the analysis of impact problems with friction in both open- and closed-loop multibody mechanical systems. Newton's coefficient of friction and Poisson's coefficient of restitution were used as known quantities.

For the previous models of impact with friction, the effect of the rolling friction was neglected. In this paper, the moment of rolling friction is defined and introduced to the impact equations. For the simple pendulum, the energetic coefficient of restitution and the coefficient of rolling friction are used to model the impact. The influence of the coefficient of kinetic friction and the geometrical characteristics (the impact angle, the length and the contact radius of the beam) on the energy dissipated by friction during impact is analyzed. For the double pendulum, using the kinematic coefficient of restitution, in some cases one can obtain energetically inconsistent results. If the moment of rolling friction is introduced, this problem can be solved for some values of the coefficient of rolling friction.

2.2 Rolling friction

A homogeneous circular disk in motion on an inclined plane is shown in Fig. 2.1. The fixed cartesian reference frame $xOyz$ is chosen with the origin at O. The angle between the axis Ox and the horizontal is α. The contact point between the disk and the plane is B. The disk has the mass m, the radius r, and the center of mass at C. The gravitational acceleration is g.

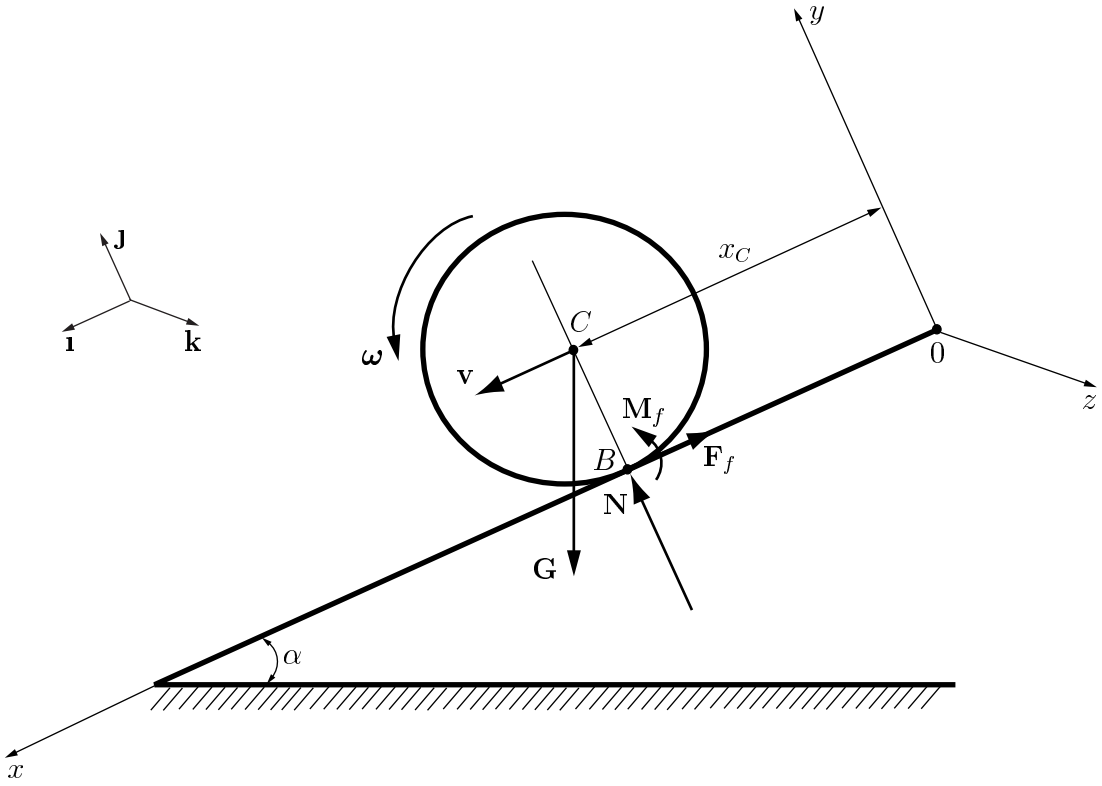

Figure 2.1: Homogeneous disk in motion on an inclined rough plane.

2.2.1 Pure rolling (no sliding)

The forces that act on the disk are the gravitational force $\mathbf{G} = -mg\mathbf{J}$ at the point C, the normal reaction force $\mathbf{N}$ of the plane and the friction force $\mathbf{F}_f$ at the contact point B. The rolling friction is considered negligible. The position vector $\mathbf{r}_C$ of the center of mass C of the disk is

$$\mathbf{r}_C = x_C\mathbf{I} + r\mathbf{J}. \tag{2.1}$$

The velocity vector $\mathbf{v}_C$ of the center of mass C of the disk is

$$\mathbf{v}_C = \dot{\mathbf{r}}_C = \dot{x}_C\mathbf{I} + \dot{r}\mathbf{J} = \dot{x}_C\mathbf{I}. \tag{2.2}$$

Denoting $\dot{x}_C = v$, the velocity of the center of mass C becomes

$$\mathbf{v}_C = v\mathbf{I}. \tag{2.3}$$

Thus, the acceleration vector of $\mathbf{a}_C$ of the center of mass C of the disk is

$$\mathbf{a}_C = \dot{\mathbf{v}}_C = \dot{v}\mathbf{I}. \tag{2.4}$$

One can express the velocity $\mathbf{v}_B$ of the contact point B as

$$\mathbf{v}_B = \mathbf{v}_C + \boldsymbol{\omega} \times \mathbf{CB} = v\mathbf{I} + (-\omega\mathbf{k}) \times (-r\mathbf{J}) = (v - r\omega)\mathbf{I}. \tag{2.5}$$

In order to find the equation of motion for the disk, one can write the Newton's equation

$$m\mathbf{a}_C = \sum \mathbf{F}. \tag{2.6}$$

The sum of the external forces can be written as

$$\sum \mathbf{F} = m\mathbf{g} + \mathbf{F}_f + \mathbf{N} = (mg\sin\alpha - F_f)\mathbf{\imath} + (N - mg\cos\alpha)\mathbf{\jmath}, \tag{2.7}$$

where $\mathbf{F}_f = -F_f\mathbf{\imath}$ is the friction force, and $\mathbf{N} = N\mathbf{\jmath}$ is the reaction force of the plane on the disk. From Eqs. (2.4), (2.6), and (2.7) one can write the following equations

$$m\dot{v} = mg\sin\alpha - F_f, \tag{2.8}$$

$$N = mg\cos\alpha. \tag{2.9}$$

The following moment equation can be written for the disk with respect to its center of mass C

$$I_C\boldsymbol{\alpha} = \sum \mathbf{M}_C, \tag{2.10}$$

where I_C is the mass moment of inertia with respect to the point C, $\boldsymbol{\alpha} = \dot{\boldsymbol{\omega}} = -\dot{\omega}\mathbf{k}$ is the angular acceleration, and $\boldsymbol{\omega} = -\omega\mathbf{k}$ is the angular velocity of the disk. The sum of the external moments can be written as

$$\sum \mathbf{M}_C = \mathbf{CB} \times \mathbf{F} = (-r\mathbf{\jmath}) \times (-F\mathbf{\imath}) = -rF_f\mathbf{k}. \tag{2.11}$$

From Eqs. (2.10) and (2.11) one can write the following equation

$$I_C\dot{\omega} = rF_f. \tag{2.12}$$

For no sliding, the velocity $\mathbf{v}_B$ is zero ($\mathbf{v}_B = \mathbf{0}$). Thus, from Eq. (2.5) one can write $\omega = v/r$ and Eq. (2.12) becomes

$$I_C\frac{\dot{v}}{r^2} = F_f. \tag{2.13}$$

From Eqs. (2.8) and (2.13) the following equation of motion can be derived

$$\left(m + \frac{I_C}{r^2}\right)\dot{v} = mg\sin\alpha. \tag{2.14}$$

A homogeneous disk is considered in our case and the mass moment of inertia with respect to its center of mass is $I_C = m\frac{r^2}{2}$. Thus, Eq. (2.14) can be written as

$$\dot{v} = \frac{2}{3}g\sin\alpha. \tag{2.15}$$

Condition for pure rolling

From Eq. (2.8) and Eq. (2.15) one can compute the friction force F_f as

$$F_f = \frac{m}{3}g\sin\alpha. \tag{2.16}$$

The condition for the disk of rolling without sliding on the plane is

$$F_f \leq \mu_k N, \tag{2.17}$$

where μ_k is the coefficient of kinetic friction. From Eq. (2.9), Eq. (2.16), and Eq. (2.17) one can obtain

$$\tan\alpha \leq 3\mu_k, \tag{2.18}$$

or

$$\alpha \leq \Phi, \tag{2.19}$$

where the sliding friction angle Φ can be determined from the equation

$$\tan\Phi = 3\mu_k, \text{ where } \mu_k = \tan\phi. \tag{2.20}$$

Eq. (2.19) represents the condition for rolling without sliding of the disk on the plane. If the angle α of the plane is smaller than the sliding friction angle Φ, the disk rolls on the plane without sliding. If the angle α of the plane is greater than the sliding friction angle Φ, the disk rolls and slides on the plane simultaneously.

Moment of rolling friction

Experimentally one can observe that if the angle α of the plane is small enough, the disk does not move. The equilibrium conditions for the disk are $v = 0$, and $\omega = 0$. The rolling is stopped by a rolling resistant moment M_f that balances the active moment rF_f

$$M_f = rF_f. \tag{2.21}$$

The acceleration $\dot{v}$ is zero and from Eq. (2.8) one can express the friction force as $F_f = G\sin\alpha$. Thus, one can write

$$M_f = rmg\sin\alpha = rN\tan\alpha. \tag{2.22}$$

If α_0 is the value of the angle α when the rolling starts, the moment M_f is called the *rolling friction moment* and has the value

$$M_f = rN \tan \alpha_0. \tag{2.23}$$

The constant $r \tan \alpha_0$ is denoted by s and represents the coefficient of rolling friction

$$s = r \tan \alpha_0. \tag{2.24}$$

The rolling friction moment M_f become

$$M_f = sN. \tag{2.25}$$

The rolling friction moment M_f is proportional to the normal reaction N and has the expression

$$\mathbf{M}_f = -sN \frac{\boldsymbol{\omega}}{|\boldsymbol{\omega}|}. \tag{2.26}$$

2.2.2 Rolling with moment of friction

In this case, Eq. (2.10) becomes

$$I\dot{\omega} = rF_f - sN. \tag{2.27}$$

From Eq. (2.8) and Eq. (2.27) one can write

$$\dot{v} = \frac{2}{3}(\sin \alpha - \cos \alpha \tan \alpha_0)g = \frac{2 \sin(\alpha - \alpha_0)}{3 \cos \alpha_0} g. \tag{2.28}$$

In this case, the rolling condition is

$$\frac{sin(\alpha - \alpha_0)}{\cos \alpha_0} \leq 3\frac{sin(\phi - \alpha_0)}{\cos \phi}, \tag{2.29}$$

or

$$\tan \alpha \leq \tan \phi + 2(\tan \phi - \tan \alpha_0). \tag{2.30}$$

Eq. (2.30) can also be written as

$$\alpha \leq \Phi, \tag{2.31}$$

where the angle Φ can be obtained from

$$\tan \Phi = \tan \phi + 2(\tan \phi - \tan \alpha_0). \tag{2.32}$$

For the motion of the homogeneous disk on the plane of slope α, the following three cases are possible:

Case 1. $\alpha < \alpha_0$ (Eq. (2.28)). The disk has no motion.

Case 2. $\alpha_0 \leq \alpha < \Phi$ (Eq. (2.32)). The disk has pure rolling (no sliding) motion.

Case 3. $\alpha \geq \Phi$. The disk has rolling and sliding motion simultaneously .

2.3 Impact with moment of rolling friction

2.3.1 Simple pendulum and energetic coefficient of restitution

The planar rigid pendulum with mass M and length L pivots around the frictionless pin joint O, and the tip impacts an inelastic horizontal surface S at point C (Fig. 2.2). The fixed cartesian reference frame $xOyz$ is chosen. The inclination of the pendulum

with respect to the vertical axis Oy is the angle θ. At the impact point C, the coefficients of kinetic and static friction are μ_k and μ_s, the coefficient of rolling friction is s, and the energetic coefficient of restitution is e_*. The ratio ω_s/ω_a of the separation angular speed $\omega_s = \omega(t_s)$ and the approach angular speed $\omega_s = \omega(t_a)$ at impact is calculated. The kinetic energy of the pendulum is

$$T = \frac{1}{2} I \boldsymbol{\omega} \cdot \boldsymbol{\omega}, \tag{2.33}$$

where I is the mass moment of inertia with respect to the joint O and $\boldsymbol{\omega} = \omega \mathbf{k}$ is the angular velocity of the pendulum.

The position of the contact point C relative to the center of axis O can be expressed as

$$\mathbf{r}_C = -x\mathbf{\imath} - y\mathbf{\jmath}, \tag{2.34}$$

where $x = L\sin\theta$ and $y = L\sin\theta$. Thus, the velocity of the point C is

$$\mathbf{v}_C = \boldsymbol{\omega} \times \mathbf{r}_C. \tag{2.35}$$

The differential of the impulse $d\mathbf{p} = dp_t\mathbf{\imath} + dp_n\mathbf{\jmath}$ at the contact point C satisfies the Amontons-Coulomb law

$$\begin{aligned} dp_t = \mu_k dp_n,\ \mathbf{v}_C \cdot \mathbf{\imath} < 0, \\ -\mu_k dp_n < dp_t < \mu_k dp_n,\ \mathbf{v}_C \cdot \mathbf{\imath} = 0, \\ dp_t = -\mu_k dp_n,\ \mathbf{v}_C \cdot \mathbf{\imath} > 0, \end{aligned} \tag{2.36}$$

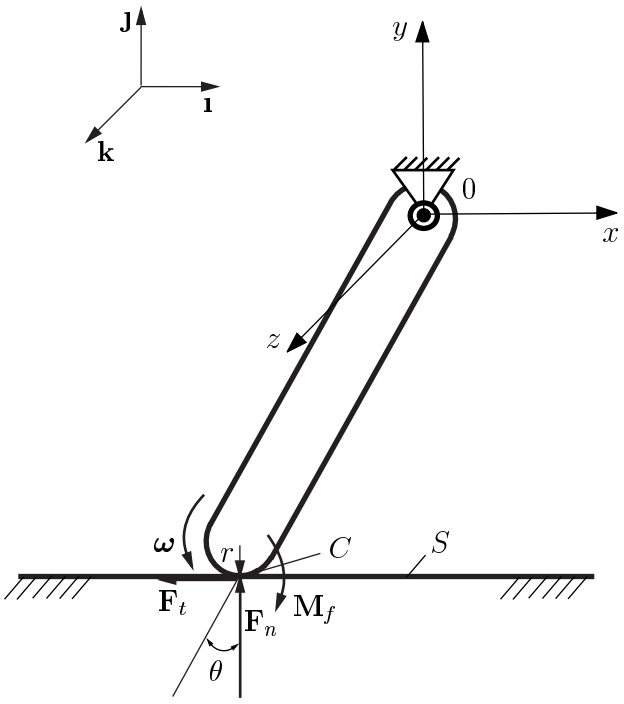

Figure 2.2: Impact of a rigid simple pendulum with a rough horizontal surface.

where p_t is the tangential impulse and p_n is the normal impulse to the surface S at the point C.

The impact equation for the pendulum can be written as

$$\left(\frac{\partial T}{\partial \omega}\right)_{t_s} - \left(\frac{\partial T}{\partial \omega}\right)_{t_a} = \frac{\partial \mathbf{v}_C}{\partial \omega} \cdot (p_t \mathbf{1} + p_n \mathbf{J}) + \frac{\partial \boldsymbol{\omega}}{\partial \omega} \cdot \mathbf{M}_f, \tag{2.37}$$

where t_a and t_s are the approach and separation moments at the impact and $\mathbf{M}_f = -sp_n \dfrac{\boldsymbol{\omega}}{|\boldsymbol{\omega}|}$ is the rolling friction moment at the point C.

The slip reverses in the direction of the compression impulse p_c simultaneously with the transition from compression to restitution. From Eq. (2.53) one can obtain the angular velocity ω as a function of the normal impulse $p_n = p$

$$\omega(p) = \begin{cases} \omega_a - \dfrac{x + \mu_k y + s}{I} p, \ 0 < p \le p_c, \\ -\dfrac{x - \mu_k y - s}{I}(p - p_c), \ p_c < p < p_s, \end{cases} \tag{2.38}$$

where p_s is the separation impulse.

In order to have slip reversal, the following condition must be satisfied $\mu_s < \tan\theta$. Otherwise the pendulum sticks after compression ($\omega_s = 0$).

The compression impulse p_c can be calculated from $\mathbf{J} \cdot \mathbf{v}_C(p_c) = 0$ as

$$p_c = \frac{I\omega_a}{x + \mu_k y + s}. \tag{2.39}$$

The work of the normal impulse during compression $W_n(p_c)$ is

$$W_n(p_c) = \int_0^{p_c} \mathbf{J} \cdot \mathbf{v}_C(p) dp = -\frac{x(x + \mu_k y + s)}{2I} p_c^2. \tag{2.40}$$

The work of the normal impulse during restitution $W_n(p_s) - W_n(p_c)$ is

$$W_n(p_s) - W_n(p_c) = \int_{p_c}^{p_f} \mathbf{J} \cdot \mathbf{v}_C(p) dp = \frac{x(x - \mu_k y - s)}{2I} (p_s - p_c)^2 . \tag{2.41}$$

The energetic coefficient of restitution e_* (Stronge [7]) can be written as

$$e_*^2 = -\frac{W_n(p_s) - W_n(p_c)}{W_n(p_c)} = \frac{x - \mu_k y - s}{x + \mu_k y + s} \left(\frac{p_s}{p_c} - 1 \right)^2 . \tag{2.42}$$

From Eq. (2.42) one can compute the separation impulse p_s as

$$p_s = p_c \left(1 + e_* \sqrt{\frac{x + \mu_k y + s}{x - \mu_k y - s}} \right) . \tag{2.43}$$

The ratio of the angular velocities of separation $\omega(p_s)$ and approach $\omega(0)$ becomes

$$\frac{\omega_s}{\omega_a} = \frac{\omega(p_s)}{\omega(0)} = e_* \sqrt{\frac{x - \mu_k y - s}{x + \mu_k y + s}} . \tag{2.44}$$

For no rolling friction moment ($s = 0$) the ratio $\dfrac{\omega_s}{\omega_a}$ becomes

$$\frac{\omega_s}{\omega_a} = e_* \sqrt{\frac{1 - \mu_k \cot\theta}{1 + \mu_k \cot\theta}} . \tag{2.45}$$

2.3.2 Double pendulum and kinematic coefficient of restitution

In Fig. 2.3, two uniform rigid rods 1 and 2 with lengths L_1 and L_2 and masses m_1 and m_2 are joined at point B by a frictionless pin joint in order to form a planar double pendulum. The end of the rod 1 pivots around a frictionless pin joint at O. The free end of the rod 2 strikes a rough horizontal surface S at the point C. The rods

have the angles of inclination from axis Oy denoted by θ_1 and θ_2 and angular speeds of magnitudes $\omega_1 = \dot{\theta}_1$ and $\omega_2 = \dot{\theta}_2$, respectively. The fixed cartesian reference frame $xOyz$ is chosen. At the impact point C, the coefficients of kinetic and static friction are μ_k and μ_s, the coefficient of rolling friction is s, and the kinematic coefficient of restitution is e. The separation angular speeds ω_{s1} and ω_{s2} are calculated with respect to the approach angular speeds ω_{a1} and ω_{a2} and the initial angles θ_{10} and θ_{20}. Also, the difference $\Delta T = T_s - T_a$ of the kinetic energies of separation and approach T_s and T_a at the impact is computed. The positions of the center of masses C_1 and C_2 of the rods 1 and 2 are

$$\mathbf{r}_{C1} = -\frac{L_1}{2}\sin\theta_1 \mathbf{\imath} - \frac{L_1}{2}\cos\theta_1 \mathbf{J}, \tag{2.46}$$

$$\mathbf{r}_{C2} = -(L_1\sin\theta_1 + \frac{L_2}{2}\sin\theta_2)\mathbf{\imath} - (L_1\cos\theta_1 + \frac{L_2}{2}\cos\theta_2)\mathbf{J}. \tag{2.47}$$

The velocities of the center of masses C_1 and C_2 are

$$\mathbf{v}_{C1} = \dot{\mathbf{r}}_{C1}, \text{ and } \mathbf{v}_{C2} = \dot{\mathbf{r}}_{C2}. \tag{2.48}$$

The position of the contact point C is

$$\mathbf{r}_{C2} = -(L_1\sin\theta_1 + \frac{L_2}{2}\sin\theta_2)\mathbf{\imath} - (L_1\cos\theta_1 + \frac{L_2}{2}\cos\theta_2)\mathbf{J}. \tag{2.49}$$

The velocity of the contact point C is $\mathbf{v}_C = \dot{\mathbf{r}}_C$.

The kinetic energies T_1 and T_2 of the rods 1 and 2 are

$$T_i = \frac{1}{2}(m_i\mathbf{v}_{Ci}\cdot\mathbf{v}_{Ci} + I_{Ci}\boldsymbol{\omega}_i\cdot\boldsymbol{\omega}_i),\ i = 1, 2, \tag{2.50}$$

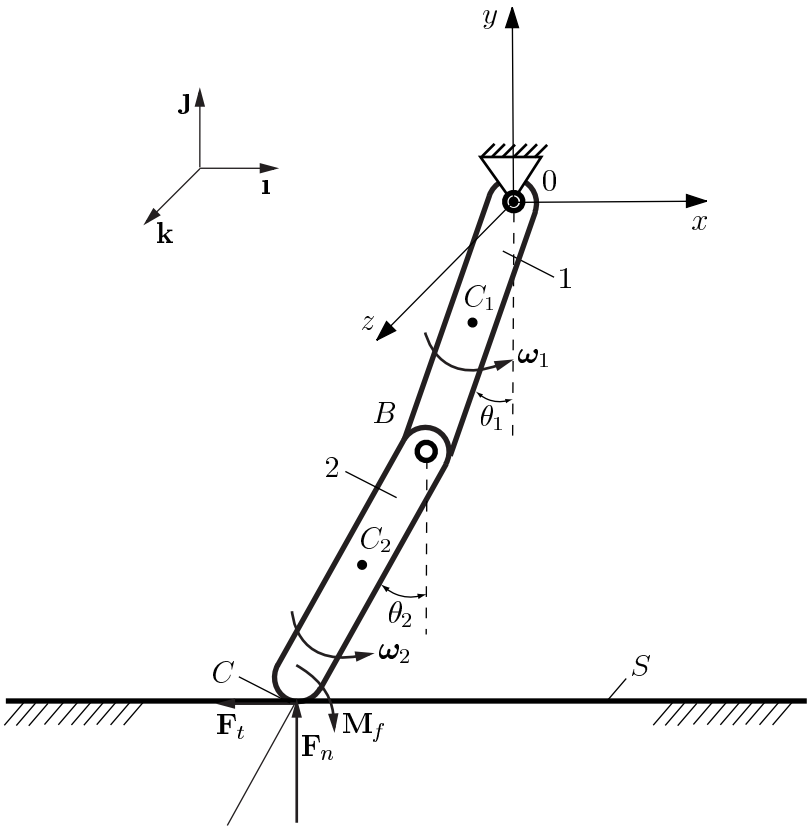

Figure 2.3: Impact of a rigid double pendulum with a rough horizontal surface.

where I_{Ci} is the mass moment of inertia with respect to the point C_i and $\boldsymbol{\omega}_i = \omega_i \mathbf{k}$ is the angular velocity of the rod i, for $i = 1, 2$.

The kinetic energy T of the double pendulum is

$$T = T_1 + T_2. \tag{2.51}$$

The differential of the impulse $d\mathbf{p} = dp_t \boldsymbol{\imath} + dp_n \mathbf{J}$ at the contact point C satisfies the Amontons-Coulomb law

$$\begin{aligned} dp_t = \mu_k dp_n,\ \mathbf{v}_C \cdot \boldsymbol{\imath} < 0, \\ -\mu_k dp_n < dp_t < \mu_k dp_n,\ \mathbf{v}_C \cdot \boldsymbol{\imath} = 0, \\ dp_t = -\mu_k dp_n,\ \mathbf{v}_C \cdot \boldsymbol{\imath} > 0, \end{aligned} \tag{2.52}$$

where p_t is the tangential impulse and p_n is the normal impulse to the surface S at the point C.

The impact equation for the rod i can be written as

$$\left(\frac{\partial T}{\partial \omega_i}\right)_{t_s} - \left(\frac{\partial T}{\partial \omega_i}\right)_{t_a} = \frac{\partial \mathbf{v}_C}{\partial \omega_i} \cdot (p_t \boldsymbol{\imath} + p_n \mathbf{J}) + \frac{\partial \boldsymbol{\omega}_i}{\partial \omega_i} \cdot \mathbf{M}_f,\ i = 1, 2, \tag{2.53}$$

where t_a and t_s are the approach and separation moments at the impact and $\mathbf{M}_f = -sp_n \dfrac{\boldsymbol{\omega}_2}{|\boldsymbol{\omega}_2|}$ is the rolling friction moment at the point C.

The velocities of approach and separation $\mathbf{v}_{Ca}$ and $\mathbf{v}_{Cs}$ of the point C can be expressed as

$$\mathbf{v}_{Ca} = \mathbf{v}_C(t_a),\ \text{and}\ \mathbf{v}_{Cs} = \mathbf{v}_C(t_s). \tag{2.54}$$

In order to have slip reversal, the following condition must be satisfied $\mu_s < \left|\frac{p_t}{p_n}\right|$, otherwise the rod 2 sticks after compression ($\mathbf{v}_{Cs} \cdot \mathbf{\imath} = 0$).

Using the kinematic coefficient of restitution e (Newton [1]) the following equation can be written

$$e = -\frac{\mathbf{v}_{Cs} \cdot \mathbf{J}}{\mathbf{v}_{Ca} \cdot \mathbf{J}}. \tag{2.55}$$

From Eqs. (2.53) and (4.107) one can compute the angular velocities of separation ω_{1s} and ω_{2s} for the rods 1 and 2.

The kinetic energy dissipated by friction ΔT is

$$\Delta T = T(t_s) - T(t_a), \tag{2.56}$$

where $T(t_a)$ and $T(t_s)$ are the kinetic energies before and after the impact for the double pendulum.

2.4 Results

2.4.1 Simple pendulum

In this section, results from computer simulations are presented. The rigid pendulum impacting a rough horizontal surface is shown in Fig. 2.2. The energetic coefficient of restitution is $e_* = 0.3$. Figures 2.4, 2.5, and 2.6 illustrate the ratio of the separation angular speed ω_s, the approach angular speed ω_a, and the coefficient e_* as a function of the angle θ at the impact. The effect of the energy dissipated by friction at the impact between the pendulum and the horizontal surface S is shown. At small values of the angle θ the contact sticks ($\omega_s = 0$), if the coefficient of static friction is sufficiently large

($\mu_s \geq \tan\theta$). Also, for small angles θ the work done by the friction force F_t is large in comparison with the work done by the normal contact force F_n.

In Fig. 2.4 the pendulum with the length $L = 0.2$ m and the contact radius $r = 0.002$ m is considered. The ratio $(\omega_s/\omega_a)/e_*$, that characterizes the energy dissipated by friction at the impact, is plotted as function of the angle θ using different values of the coefficient of kinetic friction μ_k. The results for no friction moment ($M_f = 0$) are represented with continuous line and the results for nonzero friction moment ($M_f \neq 0$) are represented with dotted line. For larger values of μ_k, larger differences between the ratios considering zero and nonzero friction moment M_f are observed. For example, for $\theta = 1.044$ rad and $\mu_k = 0.3$ the difference of ratios is $d_I = 0.010$, and for $\theta = 1.044$ rad and $\mu_k = 0.9$ the difference of ratios is $d_{IV} = 0.025$.

In Fig. 2.5 the length L of the pendulum is modified while all the other parameters are kept constant. Less energy is dissipated by friction for larger values of L. For example, for $r = 0.002$ m, $\mu_k = 0.3 =$ constant, and $\theta = 1.044$ rad, the ratio $(\omega_s/\omega_a)/e_* = 0.784$ corresponds to $L = 0.040$ m and the ratio $(\omega_s/\omega_a)/e_* = 0.801$ corresponds to $L = 0.060$ m.

A relation can also be established between the contact radius r of the pendulum and the energy dissipated at impact (Fig. 2.6). Less energy is dissipated by friction for smaller values of r. For example, for $L = 0.200$ m, $\mu_k = 0.5 =$ constant, and $\theta = 1.044$ rad, the ratio $(\omega_s/\omega_a)/e_* = 0.729$ corresponds to $r = 0.001$ m and the ratio $(\omega_s/\omega_a)/e_* = 0.706$ corresponds to $r = 0.004$ m.

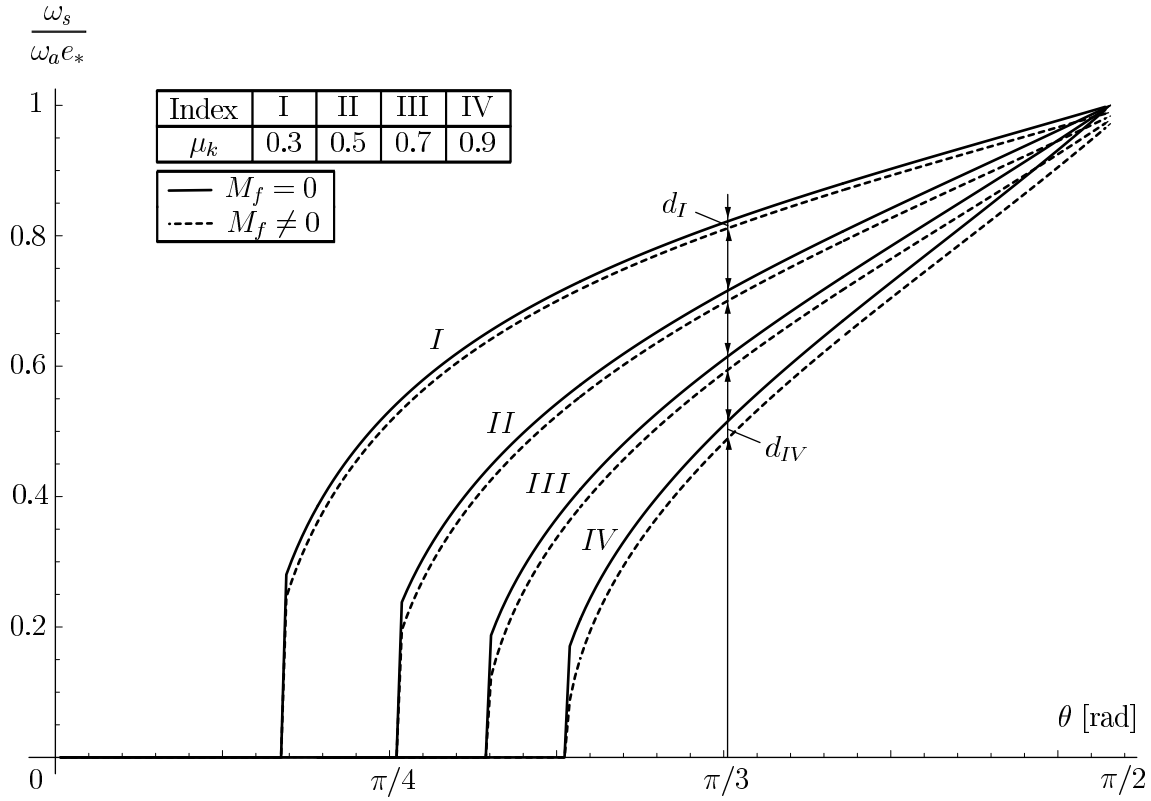

Figure 2.4: The influence of the coefficient μ_k and the angle θ on the ratio $(\omega_s/\omega_a)/e_*$ for $M_f = 0$ and $M_f \neq 0$.

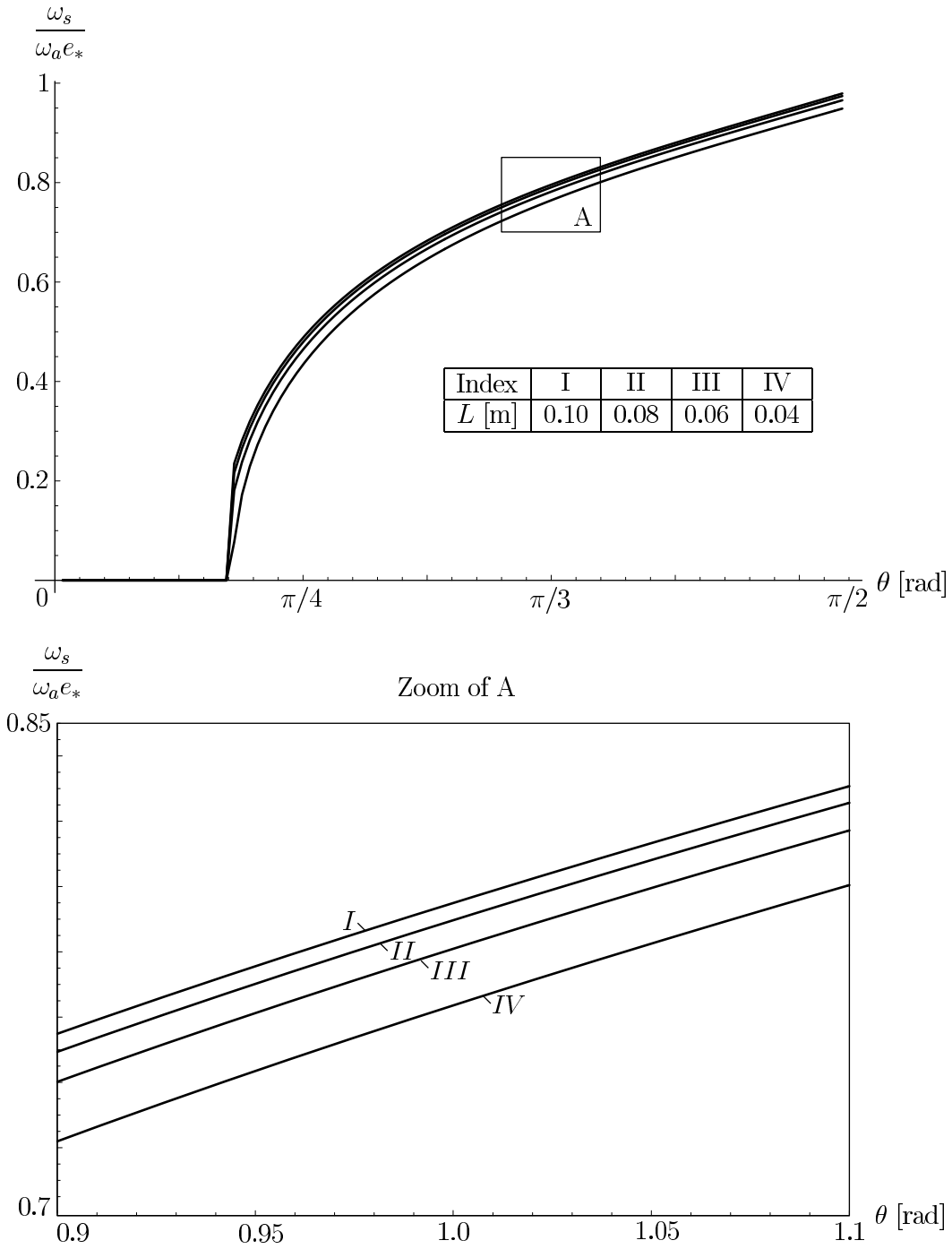

Figure 2.5: The influence of the length L and the angle θ on the ratio $(\omega_s/\omega_a)/e_*$ for $M_f \neq 0$.

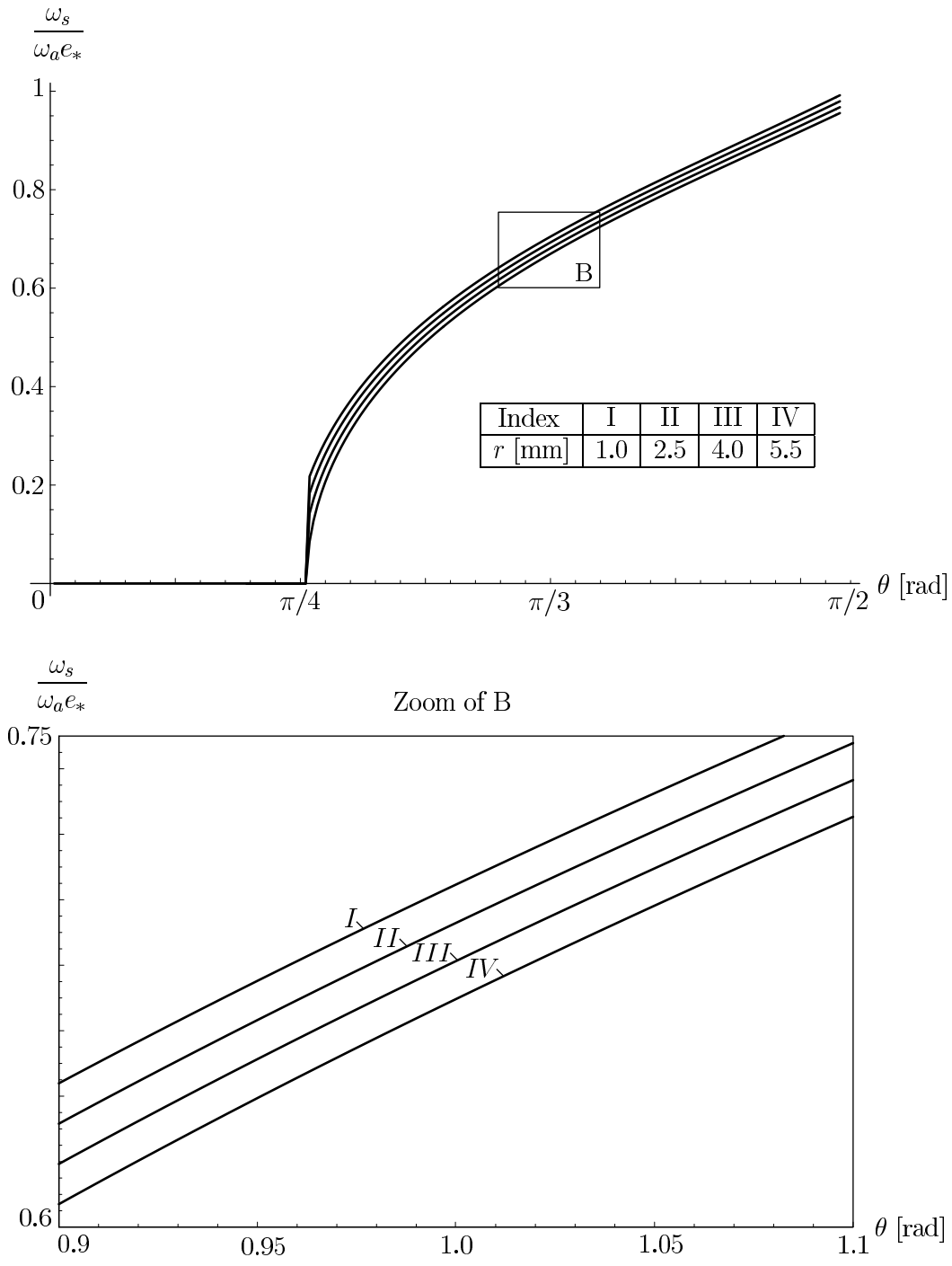

Figure 2.6: The influence of the radius r and the angle θ on the ratio $(\omega_s/\omega_a)/e_*$ for $M_f \neq 0$.

2.4.2 Double pendulum

The rigid double pendulum impacting a rough horizontal surface is shown in Fig. 2.3. For the rods 1 and 2, the following data are given: the masses $m_1 = m_2 = 3$ kg, the lengths $L_1 = L_2 = 2$ m, the mass moments of inertia with respect to the axis Oz are $I_{C1} = I_{C2} = 1$ kg m^2, the inclination angles with respect to the axis Oy are $\theta_1 = 20^\circ$ and $\theta_1 = 30^\circ$, and the magnitudes of the angular speeds are $\omega_1 = 1$ rad/s and $\omega_2 = 2$ rad/s.

Figure 2.7 illustrates the energy variation ΔT as function of the coefficient e, for different values of the coefficient s and constant coefficient of kinetic friction $\mu_k = 0.3 =$ constant. For $s = 0$ (no moment of rolling friction) and $0.45 < e < 0.65$, the energy variation ΔT is positive and a paradoxical increase of energy is observed. Using a moment of rolling friction, negative energy variation ΔT is obtained and energetically consistent results for $s > 0.16$ and $0.45 < e < 0.65$. For example, for $e = 0.55$ and $s = 0$, it results $\Delta T = 2.455$ J, and for $e = 0.55$ and $s = 0.16$, it results $\Delta T = -1.783$ J. For $s = 0.08$, the energy variation ΔT is negative for $0.45 < e < 0.55$ and positive for $0.55 < e < 0.65$. For example, for $s = 0.08$ and $e = 0.5$, it results $\Delta T = -0.779$ J, and for $s = 0.08$ and $e = 0.6$, it results $\Delta T = 0.926$ J.

Figure 2.8 illustrates the energy variation ΔT as function of the coefficient μ_k, for different values of the coefficient s and constant kinematic coefficient of restitution $e = 0.5 =$ constant. For $s = 0$ (no moment of rolling friction) and $0.3 < \mu_k < 0.4$, the energy variation ΔT is positive and a paradoxical increase of energy is observed. Using a moment of rolling friction, negative energy variation ΔT is obtained and energetically consistent results for $s > 0.25$ and $0.3 < \mu_k < 0.4$. For example, for $\mu_k = 0.35$ and $s = 0$,

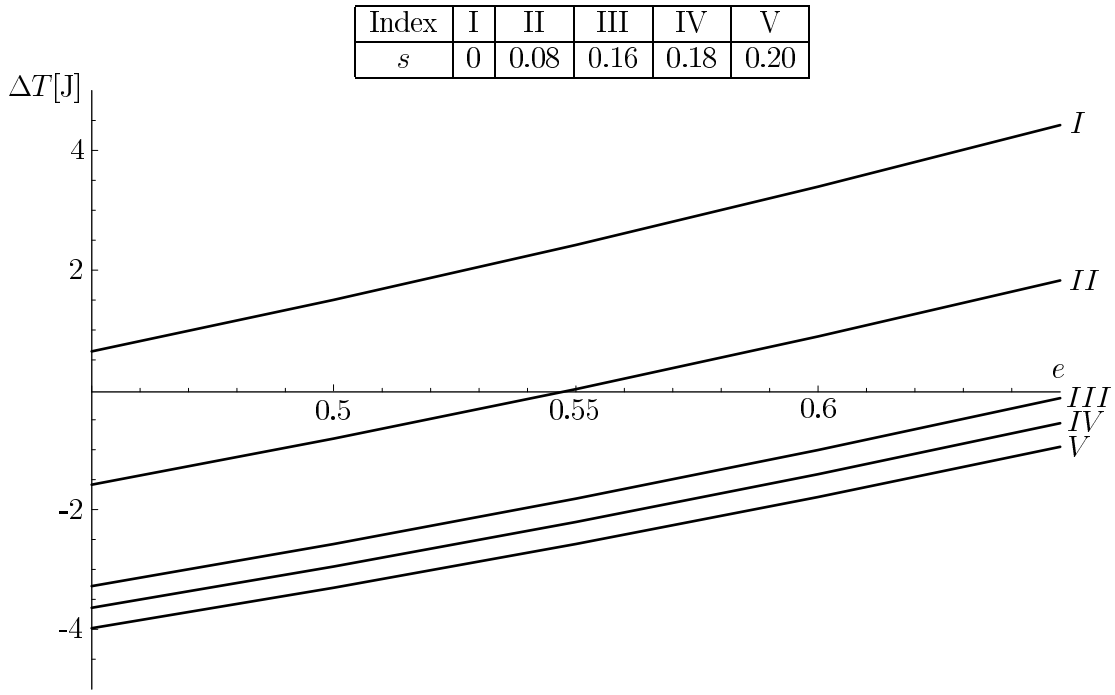

Figure 2.7: The influence of the coefficients s and e on the energy variation ΔT.

it results $\Delta T = 1.538$ J, and for $\mu_k = 0.35$ and $s = 0.25$, it results $\Delta T = -2.354$ J. For $s = 0.15$, the energy variation ΔT is negative for $0.3 < \mu_k < 0.35$ and positive for $0.35 < \mu_k < 0.4$. For example, for $s = 0.15$ and $\mu_k = 0.3$, it results $\Delta T = -2.344$ J, and for $s = 0.15$ and $\mu_k = 0.4$, it results $\Delta T = 3.037$ J.

Using the kinematic coefficient of restitution e to model the impact, for no rolling friction moment ($M_f = 0$), the energy variation ΔT is positive in the cases considered above and paradoxical results are observed (Kane and Levinson [5]). Using a rolling friction moment ($M_f \neq 0$), the energy variation ΔT becomes negative for sufficiently large values of s and energetically consistent results are obtained.

2.5 Conclusions

The results show the influence of the moment M_f on the energy dissipated by friction during the impact for different values of the parameters θ, s, μ_k, e, L, and r. More energy is dissipated during impact for larger values of s. For the simple pendulum, using the rolling friction moment, the ratios of the separation angular speed, approach angular speed, and the energetic coefficient of restitution are compared for a constant value of μ_k and different values of the length L and the radius r of the beam. For the double pendulum, when the kinematic coefficient of restitution e is used to model the impact, an energy increase is observed in some cases. One can partially solve this problem and obtain energetically consistent results introducing the moment of rolling friction M_f to the impact equations. In order to validate the analytical results, experimental data are needed.

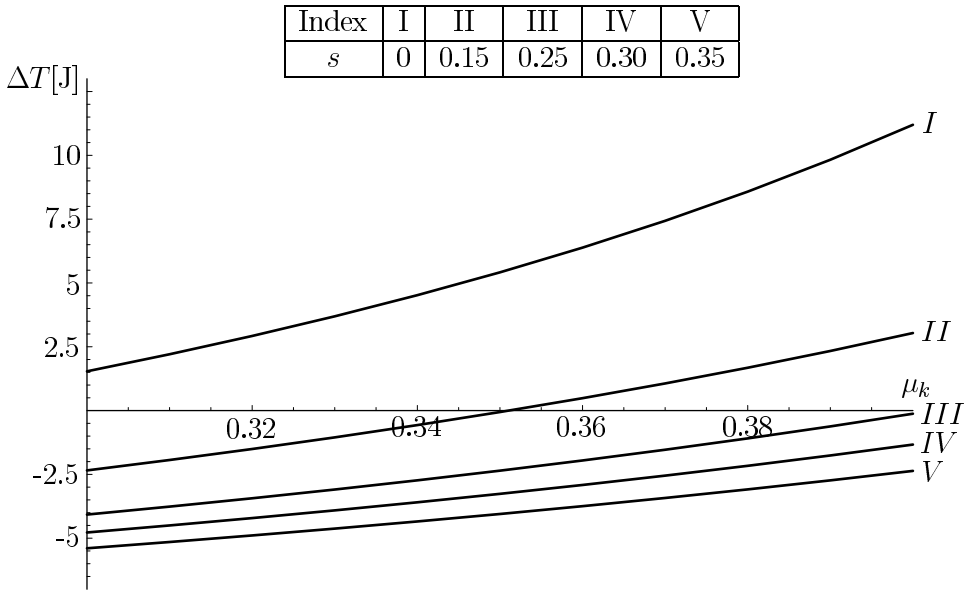

Figure 2.8: The influence of the coefficients s and μ_k on the energy variation ΔT.

Chapter 3

Effect of prismatic joint inertia

The effect of prismatic joint inertia on dynamics of kinematic chains with friction is investigated. The mathematical model of a planar kinematic chain consisting of a prismatic joint sliding along a link that is connected to a revolute joint is developed. The influence of the slider inertia on the position of the application point of the joint forces is analyzed. The effect of the slider link inertia on the dynamic response of a spatial robot arm with feedback control is analyzed using Kane's formulation. Larger values of the initial condition response characteristics are observed for larger values of the slider link inertia. Also, the effect of the prismatic joint inertia on the dynamic parameters of a planar mechanism is exemplified using inverse dynamics based on the Newton-Euler's method. Numerical results are obtained and compared for zero and larger values of the prismatic joint inertia at different speeds. The numerical simulations reveal that the effect of slider inertia may be negligible at low speeds, but becomes significant at high speeds.

3.1 Introduction

The center of mass simplifies the translational motion of the body, but it gives no information about the distribution of the mass on the body. The mass of the body represents the amount of matter contained in the body and the resistance of the body to translational motion. The quantity that is dependent on how the mass is distributed and

describes the resistance of the body to rotation is the mass moment of inertia. Consideration of dynamic modeling is an important part in the analysis, design and control of mechanical systems such as mechanisms, robots, manipulators, etc. In general, mechanical systems have several desirable features relative to the coupling contact forces such as higher speed, improved mobility and control, and reduced power consumption. The dynamics of mechanical systems with frictional contacts has been developed and applied to many industrial applications. Examples in this area include fingered grippers [23] and manipulation systems [24]. The contact normal and tangential forces can be determined if the contacts are known for systems with independent constraints [25]. The contact forces cannot be uniquely determined when the constraints are not all independent. It has been shown that the initial value problem has no solution or multiple solutions for some initial conditions [26].

The dynamics of elastic manipulators with prismatic joints has been investigated by Kim [27] and Buffinton [28]. They examine the motion of a single beam moving longitudinally over two distinct points. The equations of motion are formulated by treating the beam's supports as kinematical constraints imposed on an unrestrained beam. Gordaninejad, Azhdari, and Chalhoub [29] examined the motion of a planar robot arm consisting of one revolute and one prismatic joint. Benson and Talke [30] investigated the dynamics of a magnetic recording slider of a rigid disk during its transition between sliding and flying. The slider is modeled as a three degree-of-freedom system, capable of lift, pitch, and roll. In addition to the load from the suspension arm and the impulsive load arising from slider/disk collisions, they also considered the load due to inertia.

Do and Yang [31] solved the inverse dynamics of the Stewart platform manipulator [32] assuming the joints are frictionless and the moment of inertia of the legs has not been updated as a function of configuration in the simulation algorithm for path tracking. Ji [33] considered the question of leg inertia and studied its effect on the dynamics of the Stuart platform. The dynamic and gravity effects as well as the viscous friction at the joints were considered for the inverse dynamic formulation of the general Stuart platform presented by Dasgupta and Mruthyunjaya [34]. Important research related to the subject of the present paper has been done by Xi, Sinatra, and Han [35]. The authors investigated the effect of leg inertia on dynamic parameters of sliding-leg hexapods. The theory presented in this study can be applied to the dynamic modeling of parallel manipulators with prismatic joints [36].

In the present paper, the effect of slider link mass moment of inertia on the dynamics of mechanical systems with friction is investigated. The mathematical model of an open kinematic chain is developed using Lagrange's method for unconstrained and constrained systems. Also, a controlled three-link planar robot arm is modeled by using Kane's method. A conventional feedback control [37] is used for the robot. The three-link planar mechanism and the controlled three-link planar robot arm with prismatic joint are presented as applications. The influence of the prismatic joint mass moment of inertia on dynamic parameters as the application point of the joint contact forces, angular speed of the links, actuator torques and forces is analyzed.

In general, the effect of prismatic joint inertia may be negligible at low speeds, but becomes significant at high speeds. Hence, prismatic joint inertia must be included for

modeling high-speed machine tools, manipulators, and robots. This problem is important, because in some cases the moment of inertia of the prismatic joints is comparable to the moment of inertia of the links and may significantly influence the dynamics of the system at high speeds.

3.2 Mathematical background

The planar two-link mechanical system shown in Fig. 3.1 is considered. The cartesian reference frame $x_O O y_O$ is chosen. The mobile reference frame xOy attached to the link 1 is considered. The angle between the axis Ox and Ox_O is θ. For the links 1 and 2 the masses are m_1 and m_2, and the center of mass locations are designated by C_1 and C_2. The length of the link 1 is L. The distance OC_2 is denoted by r. The coefficient of friction between the links 1 and 2 is μ. The gravitational acceleration g is considered. The gravitational forces $\mathbf{G}_1$ and $\mathbf{G}_2$ that act on the links 1 and 2 are

$$\mathbf{G}_1 = -m_1 g \left(\sin\theta \mathbf{1} + \cos\theta \mathbf{J}\right), \ \mathbf{G}_2 = -m_2 g \left(\sin\theta \mathbf{1} + \cos\theta \mathbf{J}\right). \tag{3.1}$$

The reaction force $\mathbf{F}_{12}$ and the friction force $\mathbf{F}_{f12}$ exerted by the link 1 to the link 2 can be written as

$$\mathbf{F}_{12} = N\mathbf{J}, \ \mathbf{F}_{f12} = -\mu N \text{sign}(\dot{r})\mathbf{1}. \tag{3.2}$$

The reaction force $\mathbf{F}_{21}$ and the friction force $\mathbf{F}_{f21}$ exerted by the link 1 to the link 2 are

$$\mathbf{F}_{21} = -\mathbf{F}_{12}, \ \mathbf{F}_{f12} = -\mathbf{F}_{f12}. \tag{3.3}$$

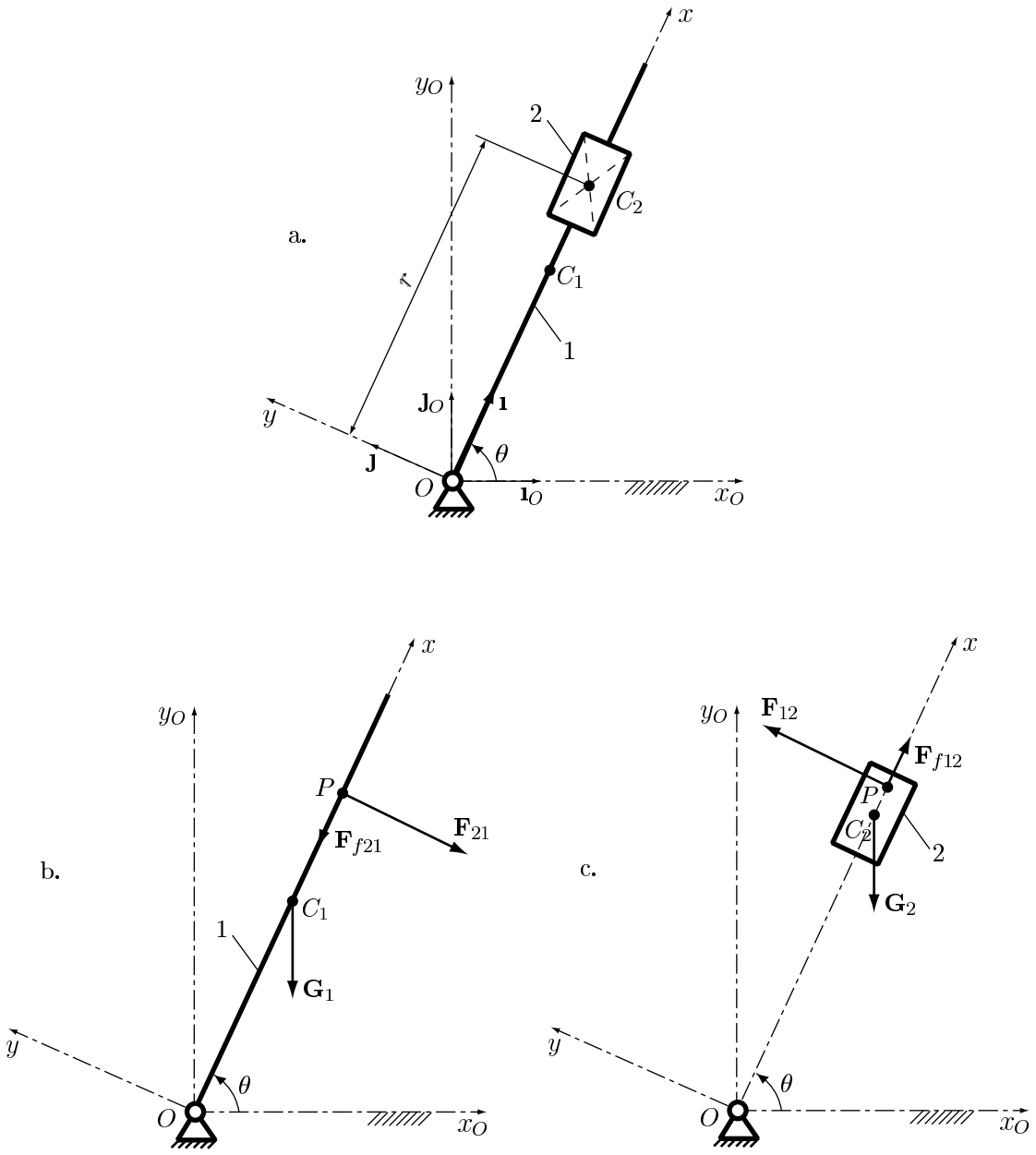

Figure 3.1: a. Open kinematic chain with slider and friction; b. Force diagram for the link 1; c. Force diagram for the link 2.

3.2.1 Newton-Euler equations

The dynamic system presented above is considered (Fig. 3.1) and the equations of motion are derived by using the Newton-Euler's method.

The position $\mathbf{r}_P$ of the point P is

$$\mathbf{r}_P = p\mathbf{\imath}, \tag{3.4}$$

where P is the application point of the reaction force N between the links 1 and 2.

The sum of the moments for the link 2 with respect to the center of mass C_2 is zero (Fig. 3.1.c)

$$(\mathbf{r}_P - \mathbf{r}_{C_2}) \times \mathbf{F}_{12} - I_{C_2}\boldsymbol{\alpha} = \mathbf{0}. \tag{3.5}$$

One can solve the linear equation Eq. (3.5) with respect to p

$$p = r + \frac{I_{C_2}}{N}\ddot{\theta}. \tag{3.6}$$

The sum of the forces that act on the link 2 is zero (Fig. 3.1.c)

$$\mathbf{G}_2 + \mathbf{F}_{12} + \mathbf{F}_{f12} - m_2\mathbf{a}_{C_2} = \mathbf{0}. \tag{3.7}$$

One can project Eq. (3.7) on $\mathbf{\jmath}$ direction and find the reaction force N

$$N = m_2(g\cos\theta + 2\dot{r}\dot{\theta} + r\ddot{\theta}). \tag{3.8}$$

One can project Eq. (3.7) on $\mathbf{\imath}$ direction

$$m_2(g\sin\theta - r\dot{\theta}^2 + \ddot{r}) + \mu N \text{sign}(\dot{r}) = 0. \tag{3.9}$$

The sum of the moments for the link 1 with respect to the point O is zero (Fig. 3.1.b)

$$\mathbf{r}_{C_1} \times \mathbf{G}_1 + \mathbf{r}_P \times \mathbf{F}_{21} - I_{C_1 O}\boldsymbol{\alpha} = \mathbf{0}. \tag{3.10}$$

One can project Eq. (3.10) on $\mathbf{k}$ direction

$$\frac{1}{6}m_1 L_1(3g\cos\theta + 2L\ddot{\theta}) + Np = 0. \tag{3.11}$$

From Eqs. (3.9) and (3.11) one can derive and solve the equations of motion with respect to r and θ.

3.2.2 Lagrange equations (unconstrained system)

For the mechanical system shown in Fig. 3.1 the equations of motion for the unconstrained system are derived using Lagrange's method. The polar coordinates $q_1 = r$ and $q_2 = \theta$ are chosen as generalized coordinates.

The positions $\mathbf{r}_{C_1}$ and $\mathbf{r}_{C_2}$ of the centers of mass C_1 and C_2 are

$$\mathbf{r}_{C_1} = \frac{L}{2}\mathbf{\imath},\ \mathbf{r}_{C_2} = r\mathbf{\imath}. \tag{3.12}$$

The angular velocity $\boldsymbol{\omega}$ and angular acceleration $\boldsymbol{\alpha}$ of the links 1 and 2 are

$$\boldsymbol{\omega} = \dot{\theta}\mathbf{k},\ \boldsymbol{\alpha} = \ddot{\theta}\mathbf{k}. \tag{3.13}$$

The velocities $\mathbf{v}_{C_1}$ and $\mathbf{v}_{C_2}$ of the points C_1 and C_2 can be expressed as

$$\mathbf{v}_{C_1} = \dot{\mathbf{r}}_{C_1} + \boldsymbol{\omega} \times \mathbf{r}_{C_1},\ \mathbf{v}_{C_2} = \dot{\mathbf{r}}_{C_2} + \boldsymbol{\omega} \times \mathbf{r}_{C_2}. \tag{3.14}$$

The position $\mathbf{r}_P$ of the point P is

$$\mathbf{r}_P = p\boldsymbol{\imath}, \tag{3.15}$$

where P is the application point of the reaction force F_{12}.

The sum of the moments for the link 2 with respect to C_2 is zero (Fig. 3.1.c)

$$(\mathbf{r}_P - \mathbf{r}_{C_2}) \times \mathbf{F}_{12} - I_{C_2}\boldsymbol{\alpha} = \mathbf{0}. \tag{3.16}$$

One can solve the linear equation Eq. (3.16) with respect to p

$$p = r + \frac{I_{C_2}}{N}\ddot{\theta}. \tag{3.17}$$

The sum of the forces that act on the link 2 is zero

$$\mathbf{G}_2 + \mathbf{F}_{12} + \mathbf{F}_{f12} - m_2\mathbf{a}_{C_2} = \mathbf{0}. \tag{3.18}$$

One can project the constraint Eq. (3.18) on $\mathbf{j}$ direction and find the reaction force N

$$N = m_2(g\cos\theta + 2\dot{r}\dot{\theta} + r\ddot{\theta}). \tag{3.19}$$

The Lagrange differential equations are

$$\frac{d}{dt}\left(\frac{\partial T}{\partial \dot{q}_i}\right) - \frac{\partial T}{\partial q_i} = Q_i,\ i = 1, 2, \tag{3.20}$$

where T is the total kinetic energy and Q_i is the generalized force corresponding to q_i.

The kinetic energy T_1 for the link 1 is

$$T_1 = \frac{1}{2} I_O \boldsymbol{\omega} \cdot \boldsymbol{\omega}, \tag{3.21}$$

where I_O is the mass moment of inertia of the link 1 with respect to the point O.

The kinetic energy T_2 for the link 2 is

$$T_2 = \frac{1}{2} m_2 \mathbf{v}_{C_2} \cdot \mathbf{v}_{C_2} + \frac{1}{2} I_{C_2} \boldsymbol{\omega} \cdot \boldsymbol{\omega}, \tag{3.22}$$

where I_{C_2} is the mass moment of inertia of the link 2 with respect to the center of mass C_2.

The total kinetic energy is

$$T = T_1 + T_2. \tag{3.23}$$

The velocity $\mathbf{v}_{P_1}$ and $\mathbf{v}_{P_2}$ of the point P attached to the links 1 and 2 can be written as

$$\mathbf{v}_{P_1} = \boldsymbol{\omega} \times \mathbf{r}_P,\ \mathbf{v}_{P_2} = \boldsymbol{\omega} \times \mathbf{r}_P + \dot{\mathbf{r}}_P. \tag{3.24}$$

The relative velocity $\mathbf{v}_{P_{21}}$ of the link 2 with respect to the link 1 is

$$\mathbf{v}_{P_{21}} = \mathbf{v}_{P_2} - \mathbf{v}_{P_1} = \dot{\mathbf{r}}_P. \tag{3.25}$$

The generalized force Q_i for the link i is

$$Q_i = \frac{\partial \mathbf{v}_{C_1}}{\partial \dot{q}_i} \cdot \mathbf{G}_1 + \frac{\partial \mathbf{v}_{C_2}}{\partial q_i} \cdot \mathbf{G}_2 + \frac{\partial \mathbf{v}_{P_1}}{\partial \dot{q}_i} \cdot (\mathbf{F}_{21} + \mathbf{F}_{f21}) + \frac{\partial \mathbf{v}_{P_2}}{\partial \dot{q}_i} \cdot (\mathbf{F}_{12} + \mathbf{F}_{f12}),\ i = 1, 2. \tag{3.26}$$

From Eqs. (3.26), (3.25), and (3.3) one can write the generalized force Q_i as

$$Q_i = \frac{\partial \mathbf{v}_{C_1}}{\partial \dot{q}_i} \cdot \mathbf{G}_1 + \frac{\partial \mathbf{v}_{C_2}}{\partial q_i} \cdot \mathbf{G}_2 + \frac{\partial \mathbf{v}_{P_{21}}}{\partial \dot{q}_i} \cdot (\mathbf{F}_{12} + \mathbf{F}_{f12}),\ i = 1, 2. \tag{3.27}$$

From Eq. (3.20) one can derive and solve the equations of motion with respect to q_1 and q_2.

3.2.3 Lagrange equations (constrained system)

For the mechanical system shown in Fig. 3.1 the equations of motion for the constrained system are derived using Lagrange's method. The rod (link 1) and the slider (link 2) are considered separately. The motion of the slider is expressed using the polar coordinates r and θ. To express the motion of the rod the angle ϕ is introduced. One can chose the generalized coordinates $q_1 = r$, $q_2 = \theta$, and $q_3 = \phi$.

The constraint equation is

$$\theta - \phi = 0. \tag{3.28}$$

The Lagrange differential equations are

$$\frac{d}{dt}\left(\frac{\partial T}{\partial \dot{q}_i}\right) - \frac{\partial T}{\partial q_i} = Q_i,\ i = 1, 2, 3, \tag{3.29}$$

where T is the total kinetic energy and Q_i is the generalized force corresponding to q_i.

The kinetic energy T_1 for the link 1 is

$$T_1 = \frac{1}{2} I_O \boldsymbol{\omega}_1 \cdot \boldsymbol{\omega}_1, \tag{3.30}$$

where $\boldsymbol{\omega}_1 = \dot{\phi}\mathbf{k}$.

The kinetic energy T_2 for the link 2 is

$$T_2 = \frac{1}{2} m_2 \mathbf{v}_{C_2} \cdot \mathbf{v}_{C_2} + \frac{1}{2} I_{C_2} \boldsymbol{\omega}_2 \cdot \boldsymbol{\omega}_2, \tag{3.31}$$

where $\boldsymbol{\omega}_2 = \dot{\theta}\mathbf{k}$ and $\mathbf{v}_{C_2} = \dot{\mathbf{r}}_{C_2} + \boldsymbol{\omega}_2 \times \mathbf{r}_{C_2}$.

The total kinetic energy is

$$T = T_1 + T_2. \tag{3.32}$$

The velocity $\mathbf{v}_{P_1}$ of the point P attached to the link 1 can be written as

$$\mathbf{v}_{P_1} = \boldsymbol{\omega}_1 \times \mathbf{r}_{P_1}, \tag{3.33}$$

where $\mathbf{r}_{P_1} = p\,(\cos\phi\mathbf{\imath} + \sin\phi\mathbf{\jmath})$.

The velocity $\mathbf{v}_{P_2}$ of the point P attached to the link 2 can be written as

$$\mathbf{v}_{P_2} = \boldsymbol{\omega}_2 \times \mathbf{r}_{P_2} + \dot{p}\mathbf{\imath}, \tag{3.34}$$

where $\mathbf{r}_{P_2} = p\,(\cos\theta\mathbf{\imath} + \sin\theta\mathbf{\jmath})$.

The generalized force Q_i for the link i is

$$Q_i = \frac{\partial \mathbf{v}_{C_1}}{\partial \dot{q}_i} \cdot \mathbf{G}_1 + \frac{\partial \mathbf{v}_{C_2}}{\partial q_i} \cdot \mathbf{G}_2 + \frac{\partial \mathbf{v}_{P_1}}{\partial \dot{q}_i} \cdot (\mathbf{F}_{21} + \mathbf{F}_{f21}) + \frac{\partial \mathbf{v}_{P_2}}{\partial \dot{q}_i} \cdot (\mathbf{F}_{12} + \mathbf{F}_{f12}),\ i = 1, 2, 3. \tag{3.35}$$

The sum of the moments for the link 2 with respect to C_2 is zero

$$(\mathbf{r}_{P_2} - \mathbf{r}_{C_2}) \times \mathbf{F}_{12} - I_{C_2}\boldsymbol{\alpha}_2 = \mathbf{0}, \tag{3.36}$$

where $\boldsymbol{\alpha}_2 = \ddot{\theta}\mathbf{k}$.

One can solve Eq. (3.36) and find p.

$$p = r + \frac{I_{C_2}}{N}\ddot{\theta}. \tag{3.37}$$

From Eq. (3.29), for $i = 3$, one can find the reaction force N.

From Eq. (3.29), for $i = 1, 2$, and by using the constraint Eq. (3.28), one can derive and solve the equations of motion.

3.2.4 Kane equations

For the system shown in Fig. 3.1, equations of motion are derived by using Kane's method. There are two generalized speeds $u_1 = \dot{r}$ and $u_2 = \dot{\theta}$ corresponding to the generalized coordinates r and θ. To find the value of the reaction force N one can introduce the third generalized speed u_3 on Ox-axis. Thus, from Eq. (3.25) one can

write the relative velocity $\mathbf{v}_{P_{21}}$ as

$$\mathbf{v}_{P_{21}} = \dot{\mathbf{r}}_P + u_{3\mathbf{J}}. \tag{3.38}$$

From Eqs. (3.24) and (3.38) the velocity $\mathbf{v}_{P_2}$ becomes

$$\mathbf{v}_{P_2} = \mathbf{v}_{P_1} + \mathbf{v}_{P_{21}} = \boldsymbol{\omega} \times \mathbf{r}_P + \dot{\mathbf{r}}_P + u_{3\mathbf{J}}. \tag{3.39}$$

Furthermore, the velocity $\mathbf{v}_{C_2}$ becomes

$$\mathbf{v}_{C_2} = \boldsymbol{\omega} \times \mathbf{r}_{C_2} + \dot{\mathbf{r}}_{C_2} + u_{3\mathbf{J}}. \tag{3.40}$$

The generalized forces Q_j associated to the generalized speeds u_j can be computed as

$$\begin{aligned} Q_j = \frac{\partial \mathbf{v}_{C_1}}{\partial u_j} \cdot \mathbf{G}_1 + \frac{\partial \mathbf{v}_{C_2}}{\partial u_j} \cdot \mathbf{G}_2 + \frac{\partial \mathbf{v}_{P_1}}{\partial u_j} \cdot (\mathbf{F}_{21} + \mathbf{F}_{f21}) + \\ \frac{\partial \mathbf{v}_{P_2}}{\partial u_j} \cdot (\mathbf{F}_{12} + \mathbf{F}_{f12}),\ j = 1, 2, 3. \end{aligned} \tag{3.41}$$

One can use Eq. (3.3) and rewrite Eq. (3.41) as

$$Q_j = \frac{\partial \mathbf{v}_{C_1}}{\partial u_j} \cdot \mathbf{G}_1 + \frac{\partial \mathbf{v}_{C_2}}{\partial u_j} \cdot \mathbf{G}_2 + \frac{\partial \mathbf{v}_{P_{21}}}{\partial u_j} \cdot (\mathbf{F}_{12} + \mathbf{F}_{f12}),\ j = 1, 2, 3. \tag{3.42}$$

The generalized inertia forces F_j^* can be written as

$$F_j^* = \sum_{i=1}^{2} \frac{\partial \mathbf{v}_{C_i}}{\partial u_j} \cdot (-m_i \mathbf{a}_{C_i}) + \sum_{i=1}^{2} \frac{\partial \boldsymbol{\omega}_i}{\partial u_j} \cdot (-I_{C_i} \boldsymbol{\alpha}_i),\ j = 1, 2, 3. \tag{3.43}$$

One can write Kane's equations associated to the generalized speeds u_j as

$$F_j^* + Q_j = 0,\ j = 1, 2, 3. \tag{3.44}$$

From Eq.(3.44), for $j = 3$, one can find the reaction force N.

From Eq.(3.44), for $j = 1, 2$, one can derive and solve the equations of motion with respect to r and θ.

3.3 Kinematic chains

The basic theory presented in the previous section can be applied for the study of open and closed kinematic chains with prismatic joints.

3.3.1 Open kinematic chains

The equations of motion for the three-link spatial robot arm with prismatic joint (Fig. 3.2) are derived by using Kane's method. The cartesian reference frame $x_O O y_O z_O$ is chosen. The mobile reference frame $x_i O y_i z_i$ is attached to the link i, $i = 1, 2$. The robot arm has three degrees of freedom, those are the angles q_1, q_2, and the distance q_3. The link i has length L_i, mass m_i, center of mass C_i, and central inertia dyadic $\bar{I}_{C_i}$, $i = 1, 2, 3$. The coefficient of friction between the links 2 and 3 is μ. Friction is negligible for the rotational joints. The gravitational acceleration g is considered. The initial conditions at $t = 0$ are $q_1(0) = q_{1_0}$, $q_2(0) = q_{2_0}$, $q_3(0) = q_{3_0}$ m, and $\dot{q}_1(0) = \dot{q}_2(0) = \dot{q}_3(0) = 0$. The feedback control is implemented using the actuator torques $\mathbf{M}_{c01}$ and $\mathbf{M}_{c12}$ applied to the rotational joints O and A and the actuator force $\mathbf{F}_{c23}$ acting to the translational joint at A. The desired final state of the system is $q_1 = q_{1f}$, $q_2 = q_{2f}$, and $q_3 = q_{3f}$. The

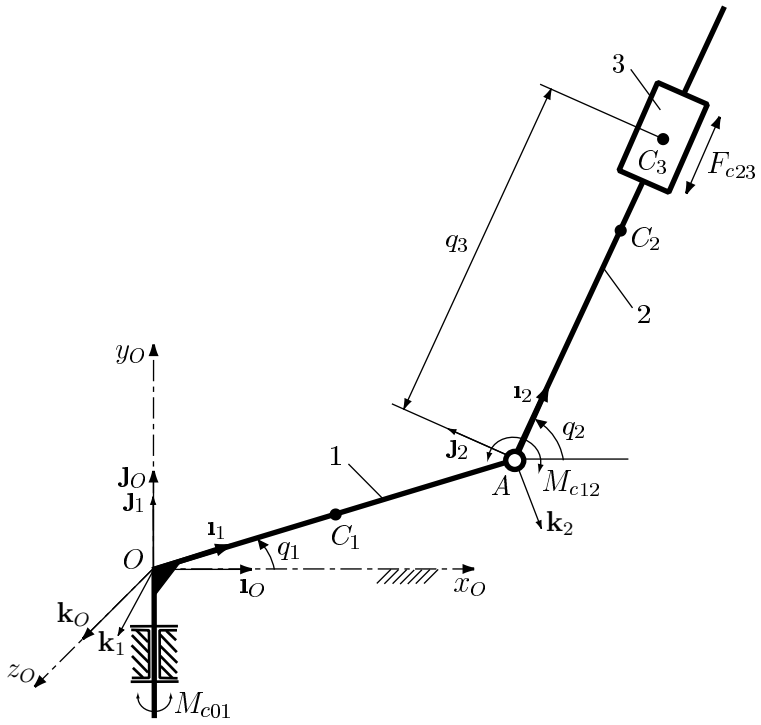

Figure 3.2: Three-link robot arm with prismatic joint.

position $\mathbf{r}_{C_i}$ of the center of mass C_i, $i = 1, 2, 3$, is

$$\begin{aligned} \mathbf{r}_{C_1} &= \frac{L_1}{2}\mathbf{i}_1, \\ \mathbf{r}_{C_2} &= L_1\mathbf{i}_1 + \frac{L_2}{2}\mathbf{i}_2, \\ \mathbf{r}_{C_3} &= L_1\mathbf{i}_1 + q_3\mathbf{i}_2. \end{aligned} \tag{3.45}$$

The angular velocities and angular accelerations of the links 1 and 2 are

$$\boldsymbol{\omega}_1 = \dot{q}_1\mathbf{J}_1, \ \boldsymbol{\alpha}_1 = \ddot{q}_1\mathbf{J}_1, \tag{3.46}$$

$$\boldsymbol{\omega}_2 = \dot{q}_1\mathbf{J}_1 + \dot{q}_2\mathbf{k}_2, \ \boldsymbol{\alpha}_2 = \ddot{q}_1\mathbf{J}_1 + \ddot{q}_2\mathbf{k}_2. \tag{3.47}$$

The velocities $\mathbf{v}_{C_i}$ and accelerations $\mathbf{a}_{C_i}$ of the points C_i, $i = 1, 2, 3$, can be expressed as

$$\mathbf{v}_{C_i} = \dot{\mathbf{r}}_{C_i} + \boldsymbol{\omega}_i \times \mathbf{r}_{C_i}, \ \mathbf{a}_{C_i} = \dot{\mathbf{v}}_{C_i} + \boldsymbol{\omega}_i \times \mathbf{v}_{C_i}. \tag{3.48}$$

The gravitational forces $\mathbf{G}_1$, $\mathbf{G}_2$, and $\mathbf{G}_3$ that act on the links 1, 2 and 3 are

$$\begin{aligned} \mathbf{G}_1 &= -m_1 g\mathbf{J}_1, \\ \mathbf{G}_2 &= -m_2 g\left(\sin q_2\mathbf{i}_2 + \cos q_2\mathbf{J}_2\right), \\ \mathbf{G}_3 &= -m_3 g\left(\sin q_2\mathbf{i}_2 + \cos q_2\mathbf{J}_2\right). \end{aligned} \tag{3.49}$$

The reaction force $\mathbf{F}_{23}$ and the friction force $\mathbf{F}_{f23}$ exerted by the link 2 to the link 3 can be written as

$$\mathbf{F}_{23} = N\mathbf{J}_2, \ \mathbf{F}_{f23} = -\mu N \text{sign}(\dot{q}_3)\mathbf{i}_2. \tag{3.50}$$

The reaction force $\mathbf{F}_{32}$ and the friction force $\mathbf{F}_{f32}$ exerted by the link 1 to the link 2 are

$$\mathbf{F}_{32} = -\mathbf{F}_{23},\ \mathbf{F}_{f32} = -\mathbf{F}_{f23}. \tag{3.51}$$

The feedback control of the arm is realized using the actuator torques and forces

$$\begin{aligned}
M_{c01} &= -[c_{11}\dot{q}_1 + c_{12}(q_1 - q_{10})],\\
M_{c12} &= -[c_{21}\dot{q}_2 + c_{22}(q_2 - q_{20})] + \left(\frac{m_2}{2}L_2 + m_3 q_3\right) g\cos q_2 + NL_1\cos q_2 +\\
&\quad + [F_{c23} - \mu N \mathrm{sign}(\dot{q}_3)]L_1 \sin q_2,\\
F_{c23} &= -[c_{31}\dot{q}_3 + c_{32}(q_3 - q_{30})] + m_3 g\sin q_2 + \mu N \mathrm{sign}(\dot{q}_3),
\end{aligned} \tag{3.52}$$

where $c_{11},\ c_{12},\ c_{21},\ c_{22},\ c_{31},\ c_{32}$ are constants.

The position of the application point P of the reaction force $\mathbf{F}_{23}$ is

$$\mathbf{r}_P = L_1\mathbf{1}_1 + p\mathbf{1}_2, \tag{3.53}$$

where $p = q_3 + \dfrac{I_{C_3}}{N}\ddot{q}_2$.

The velocities $\mathbf{v}_{P_2}$ and $\mathbf{v}_{P_3}$ of the point P attached to the links 2 and 3 can be written as

$$\mathbf{v}_{P_2} = \boldsymbol{\omega}_2 \times \mathbf{r}_P,\ \mathbf{v}_{P_3} = \boldsymbol{\omega}_2 \times \mathbf{r}_P + \dot{\mathbf{r}}_P. \tag{3.54}$$

The relative velocity $\mathbf{v}_{P_{32}}$ between the links 3 and 2 is

$$\mathbf{v}_{P_{23}} = \mathbf{v}_{P_3} - \mathbf{v}_{P_2} = \dot{\mathbf{r}}_P. \tag{3.55}$$

One can define the generalized speeds $u_i = \dot{q}_i$ corresponding to the generalized coordinates q_i, $i = 1, 2, 3$. To find the reaction force N one can introduce the generalized speed u_4 on the direction Ox_2 in the expression of the relative velocity $\mathbf{v}_{P_{23}}$

$$\mathbf{v}_{P_{23}} = \dot{\mathbf{r}}_P + u_4 \mathbf{J}_2. \tag{3.56}$$

Thus, the velocities $\mathbf{v}_{P_3}$ and $\mathbf{v}_{C_3}$ become

$$\begin{aligned} \mathbf{v}_{P_3} &= \boldsymbol{\omega}_2 \times \mathbf{r}_P + \dot{\mathbf{r}}_P + u_4 \mathbf{J}_2, \\ \mathbf{v}_{C_3} &= \boldsymbol{\omega}_2 \times \mathbf{r}_{C_3} + \dot{\mathbf{r}}_{C_3} + u_4 \mathbf{J}_2. \end{aligned} \tag{3.57}$$

The generalized forces Q_j associated to the generalized speeds u_j can be written as

$$\begin{aligned} Q_j = \frac{\partial \mathbf{v}_{C_1}}{\partial u_j} \cdot \mathbf{G}_1 + \frac{\partial \mathbf{v}_{C_2}}{\partial u_j} \cdot \mathbf{G}_2 + \frac{\partial \mathbf{v}_{C_3}}{\partial u_j} \cdot \mathbf{G}_3 + \frac{\partial \boldsymbol{\omega}_1}{\partial u_j} \cdot \mathbf{M}_{c01} + \\ \frac{\partial (\boldsymbol{\omega}_2 - \boldsymbol{\omega}_1)}{\partial u_j} \cdot \mathbf{M}_{c12} + \frac{\partial \mathbf{v}_{P_{23}}}{\partial u_j} \cdot (\mathbf{F}_{23} + \mathbf{F}_{f23} + \mathbf{F}_{c23}),\ j = 1, 2, 3. \end{aligned} \tag{3.58}$$

The generalized inertia forces F_j can be written as

$$F_j = \sum_{i=1}^{3} \frac{\partial \mathbf{v}_{C_i}}{\partial u_j} \cdot (-m_i \mathbf{a}_{C_i}) + \sum_{i=1}^{3} \frac{\partial \boldsymbol{\omega}_i}{\partial u_j} \cdot (-\bar{I}_{C_i} \cdot \boldsymbol{\alpha}_i),\ j = 1, 2, 3. \tag{3.59}$$

One can write Kane's equations associated to the generalized speeds u_j as

$$F_j + Q_j = 0,\ j = 1, 2, 3. \tag{3.60}$$

From Eq. (4.120), for $j = 4$, one can find the reaction force N.

From Eq. (4.120), for $j = 1, 2, 3$, one can derive and solve the equations of motion with respect to the generalized co-ordinates q_1, q_2, and q_3.

3.3.2 Closed kinematic chains

The three moving link planar mechanism shown in Fig. 3.3 is considered. The angle between the link 1 and Ox-axis is the driver angle θ_1. A motor torque M_m is acting on the link 1 while an external torque M_e is applied on the link 3. The distance from the center of mass C_2 of the link 2 to the application point P of the reaction force F_{23} between links 2 and 3 is d. The coefficient of friction between the links 2 and 3 is μ. The link i has the length L_i, the mass m_i, the center of mass C_i, the mass moments of inertia I_{C_i}, the linear acceleration $\mathbf{a}_{C_i}$, and the angular acceleration $\boldsymbol{\alpha}_i$, for $i = 1, 2, 3$. The gravitational force that acts on the link i is $\mathbf{G}_i = -m_i g \mathbf{J}$, where g is the gravitational acceleration. The distance d and the motor torque M_m can be computed using the Newton-Euler's equations. The Newton-Euler's equations for the link 3 are

$$m_3 \mathbf{a}_{C_3} = \mathbf{F}_{03} + \mathbf{F}_{23} + \mathbf{F}_{f23} + \mathbf{G}_3, \tag{3.61}$$

$$I_{C_3} \boldsymbol{\alpha}_3 = \mathbf{C}_3\mathbf{C} \times \mathbf{F}_{03} + \mathbf{C}_3\mathbf{P} \times \mathbf{F}_{23} + \mathbf{M}_e, \tag{3.62}$$

where $\mathbf{F}_{03}$ is the reaction force from the link 0 (the ground) on the link 3, and $\mathbf{F}_{23} = F_{23}(-\sin\theta_3 \mathbf{I} + \cos\theta_3 \mathbf{J})$ is the reaction force from the link 2 on the link 3.

The friction force $\mathbf{F}_{f23}$ has opposite direction to the relative translational velocity $\mathbf{v}_{23}$

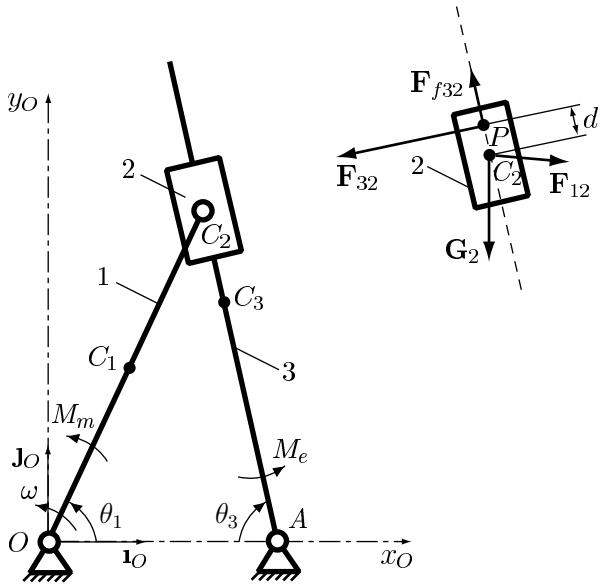

Figure 3.3: Three-link mechanism with prismatic joint.

between the links 2 and 3

$$\mathbf{F}_{f23} = -\frac{\mathbf{v}_{23}}{|\mathbf{v}_{23}|}\mu F_{23}. \tag{3.63}$$

The application point $P(x_P, y_P)$ of the reaction force $\mathbf{F}_{23}$ is not known but it is located on the sliding direction

$$\tan\theta_3 = \frac{y_P}{x_P - OA}, \tag{3.64}$$

where θ_3 is the angle between the link 3 and the Ox-axis.

The Newton-Euler's equations for the link 2 are

$$m_2\mathbf{a}_{C_2} = \mathbf{F}_{12} + \mathbf{F}_{32} + \mathbf{F}_{f32} + \mathbf{G}_2, \tag{3.65}$$

$$I_{C_2}\boldsymbol{\alpha}_2 = \mathbf{C}_2\mathbf{P} \times \mathbf{F}_{32}, \tag{3.66}$$

where $\mathbf{F}_{12}$ is the reaction force from the link 1 on the link 2, $\mathbf{F}_{32} = -\mathbf{F}_{23}$, and $\mathbf{F}_{f32} = -\mathbf{F}_{f23}$.

From Eqs. (4.70), (4.71), (4.64), (3.64), (4.68), and (4.69) one can compute the reaction forces $\mathbf{F}_{03}$, $\mathbf{F}_{23}$, $\mathbf{F}_{12}$, the friction force $\mathbf{F}_{f23}$, and the position of the point $P(x_P, y_P)$.

The Newton-Euler's equations for the link 1 are

$$m_1\mathbf{a}_{C_1} = \mathbf{F}_{01} + \mathbf{F}_{21}, \tag{3.67}$$

$$I_{C_1}\boldsymbol{\alpha}_1 = \mathbf{C}_1\mathbf{C}_2 \times \mathbf{F}_{21} + \mathbf{C}_1\mathbf{O} \times \mathbf{F}_{01} + \mathbf{M}_m, \tag{3.68}$$

where $\mathbf{F}_{01}$ is the reaction force from the link 0 (the ground) on the link 1, and $\mathbf{F}_{21} = -\mathbf{F}_{12}$.

From Eqs. (4.66) and (4.67) one can compute the reaction force $\mathbf{F}_{01}$ and the motor torque $\mathbf{M}_m$.

3.4 Results

3.4.1 Open kinematic chain

In this section, results from computer simulations are presented. Numerical data captured from the three-link spatial robot arm shown in Fig. 3.2 is analyzed. The lengths of the links 1 and 2 are $L_1 = L_2 = 0.1$ m. The masses of the links 1, 2, and 3 are $m_1 = m_2 = 1$ kg, and $m_3 = 0.2$ kg. The mass moments of inertia of the links 1, 2, and 3 are $I_{C_1x} = 0$, $I_{C_1y} = I_{C_1z} = 0.01$ kg m^2, $I_{C_2x} = 0$, $I_{C_2y} = I_{C_2z} = 0.01$ kg m^2, $I_{C_3x} = I_{C_3y} = 0$, and $I_{C_3z} = I_{C_3}$. The coefficient of friction between the links 2 and 3 is $\mu = 0.5$. The gravitational acceleration is $g = 9.807$ m/s^2. The initial conditions at $t = 0$ are $q_1(0) = \pi/6$ rad, $q_2(0) = \pi/4$ rad, $q_3(0) = 0.01$ m, and $\dot{q}_1(0) = \dot{q}_2(0) = \dot{q}_3(0) = 0$. The feedback control is implemented using the constants $c_{11} = c_{12} = 10$, $c_{21} = c_{22} = 0.1$, and $c_{31} = c_{32} = 1$. The desired final state of the system is $q_{1f} = q_{2f} = \pi/3$ rad, and $q_{3f} = 0.1$ m. The initial conditions response of the co-ordinate $q_2(t)$ for $I_{C_3} = 0$, $I_{C_3} = 0.05$ kg m^2, $I_{C_3} = 0.1$ kg m^2, and $I_{C_3} = 0.15$ kg m^2 is illustrated in Fig. 3.4.a-d.

One can define the error $e_i(t) = q_i(t) - q_{if}$ for the co-ordinate q_i, $i = 1, 2, 3$. The maximum overshoot $e_{imax} = \max |e_i(t)|$ and the settling time t_{si} ($e_i(t) < e_{i_0}$ for $t > t_{s_i}$), can be computed for $i = 1, 2, 3$, where e_{i_0} is a constant. The maximum overshoot e_{2max} and the settling time t_{s_2} are computed for different values of I_{C_3}, where $e_{2_0} = 10^{-3}$ (Table 1). For $I_{C_3} = 0$, the maximum overshoot is approximately zero ($e_{2max} \approx 0$) and the settling time is $t_{s_2} = 4.83$ s. Larger values of e_{2max} and t_{s_2} are observed for larger

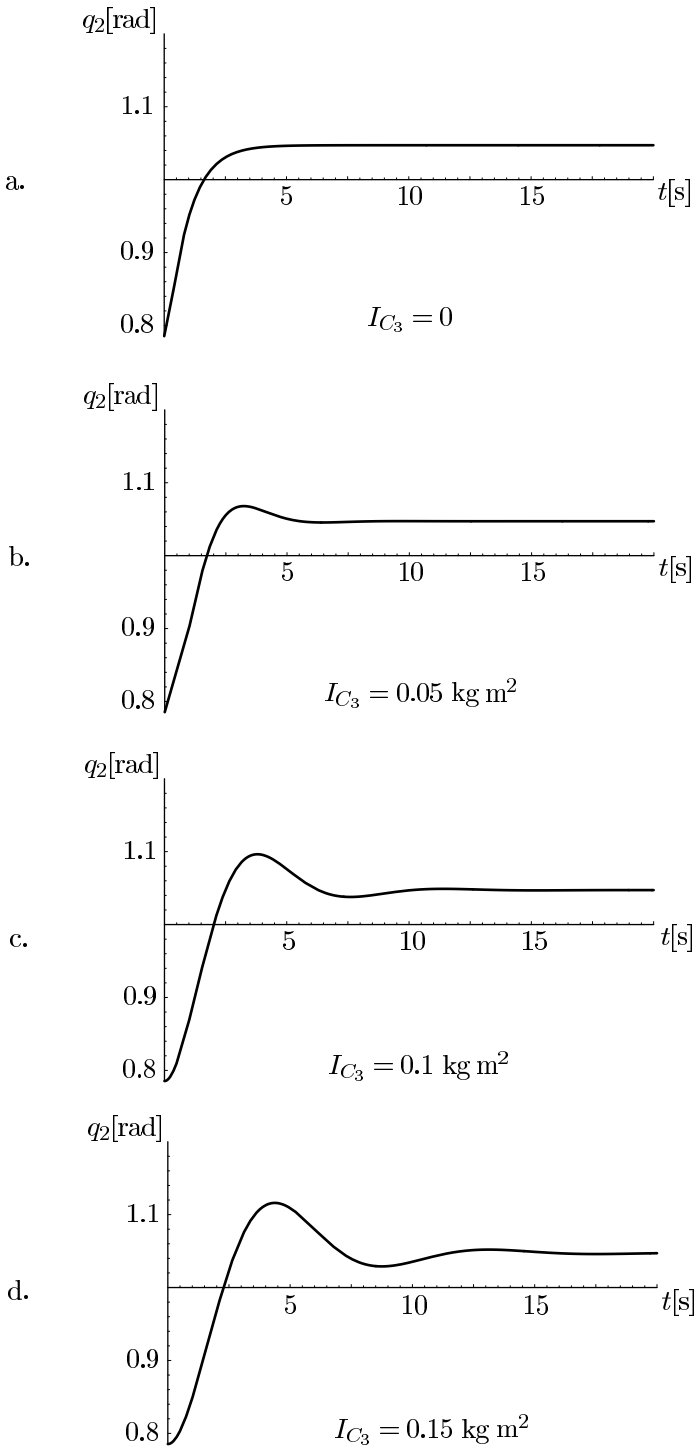

Figure 3.4: The dynamic response of the co-ordinate q_2 for the robot arm in the cases: a. $I_{C_3} = 0$, b. $I_{C_3} = 0.05$ kg m^2, c. $I_{C_3} = 0.1$ kg m^2, and d. $I_{C_3} = 0.15$ kg m^2.

values of I_{C_3} for the same control parameters values. For example, for $I_{C_3} = 1$ kg m^2, the maximum overshoot is $e_{2max} = 0.049$ and the settling time is $t_{s_2} = 12.66$ s.

Similar results can be obtained for the generalized co-ordinates q_1 and q_3.

I_{C_3}[kg m^2]	0	0.05	0.1	0.15
e_{2max}	≈0	0.02	0.049	0.068
t_{s_2}[s]	4.83	7.42	12.66	18.45

Table 3.1: The maximum overshoot e_{2max} and the settling time t_{s_2} computed for different values of I_{C_3}.

3.4.2 Closed kinematic chain

Simulation results captured from the planar three-link mechanism shown in Fig. 3.3 are presented. The cartesian reference frame $x_O O y_O$ is considered. The masses of the links 1, 2, and 3 are $m_1 = 0.5$ kg, $m_2 = 0.2$ kg, and $m_3 = 0.8$ kg, respectively. The lengths of the links 1 and 3 are $L_1 = 0.5$ m and $L_3 = 0.8$ m. The distance between the points O and A is $OA = 0.2$ m. The mass moments of inertia for the links 1 and 3 are $I_{C_1} = 0.01$ kg m^2 and $I_{C_3} = 0.042$ kg m^2. An external torque $M_e = 500$ Nm is applied on the link 3. The angle $\theta_1 = \pi/3$ is chosen for the simulations. The gravitational acceleration is $g = 9.807$ m/s^2.

Figures 3.5 and 3.6 illustrate the distance d and the torque M_m plotted for different values of the mass moment of inertia I_{C_2} and angular speeds $\omega_1 = \dot{\theta}_1$, while the coefficient of friction is $\mu = 0.5$=constant. The distance d is zero ($d = 0$) for $I_{C_2} = 0$. In Fig. 3.5 larger values of d are observed for larger values of I_{C_2} and ω_1. For example, for $\omega_1 = 20$ rad/s and $I_{C_2} = 0.004$ kg m^2 it results $d = 0.0009$ m, and for $\omega_1 = 20$ rad/s and $I_{C_2} = 0.008$ kg m^2 it results $d = 0.0019$ m. Also, for $I_{C_2} = 0.006$ kg m^2 and $\omega_1 = 10$

rad/s it results $d = 0.0003$ m, and for $I_{C_2} = 0.006$ kg m^2 and $\omega_1 = 30$ rad/s it results $d = 0.0037$ m. Simultaneously, smaller values of M_m are observed for larger values of I_{C_2} and ω_1 (Fig. 3.6). For example, for $\omega_1 = 20$ rad/s and $I_{C_2} = 0.004$ kg m^2 it results $M_m = 725.145$ Nm, and for $\omega_1 = 20$ rad/s and $I_{C_2} = 0.008$ kg m^2 it results $M_m = 723.158$ Nm. Also, for $I_{C_2} = 0.006$ kg m^2 and $\omega_1 = 10$ rad/s it results $M_m = 789.958$ Nm, and for $I_{C_2} = 0.006$ kg m^2 and $\omega_1 = 30$ rad/s it results $M_m = 614.474$ Nm. The distance d increases and significantly modifies the value of the torque M_m for relatively high values of the angular velocity ω_1.

3.5 Conclusions

The effect of prismatic joint inertia on the dynamic parameters of planar kinematic chains is presented. The application point of the slider contact forces changes its position for different values of the slider inertia. The effect of the slider inertia may be negligible at low speeds but becomes significant at relatively high speeds. Dynamic response characteristics of a planar robot arm are compared for different values of the slider inertia. The maximum overshoot may be negligible for small values of the mass moment of inertia and for some control parameters. Larger values of the maximum overshoot and the settling time are observed for larger values of the mass moment of inertia for the same control parameters. Experimental data are needed in order to validate the analytical results.

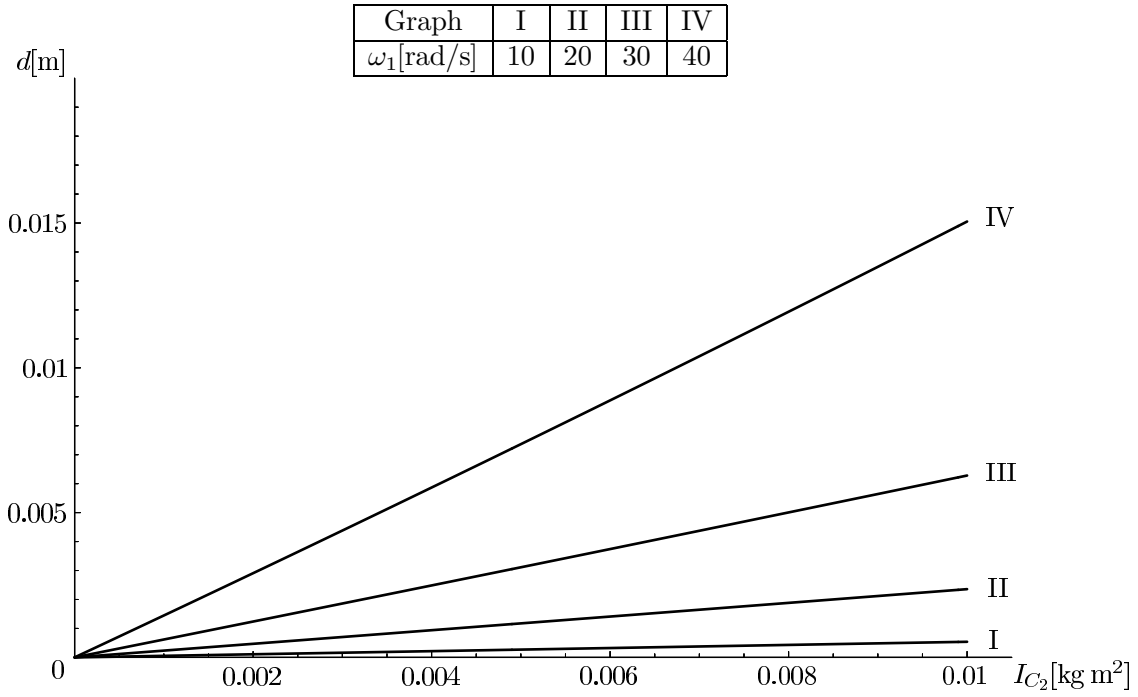

Figure 3.5: The influence of the mass moment of inertia I_{C_2} and angular speed ω_1 on the distance d.

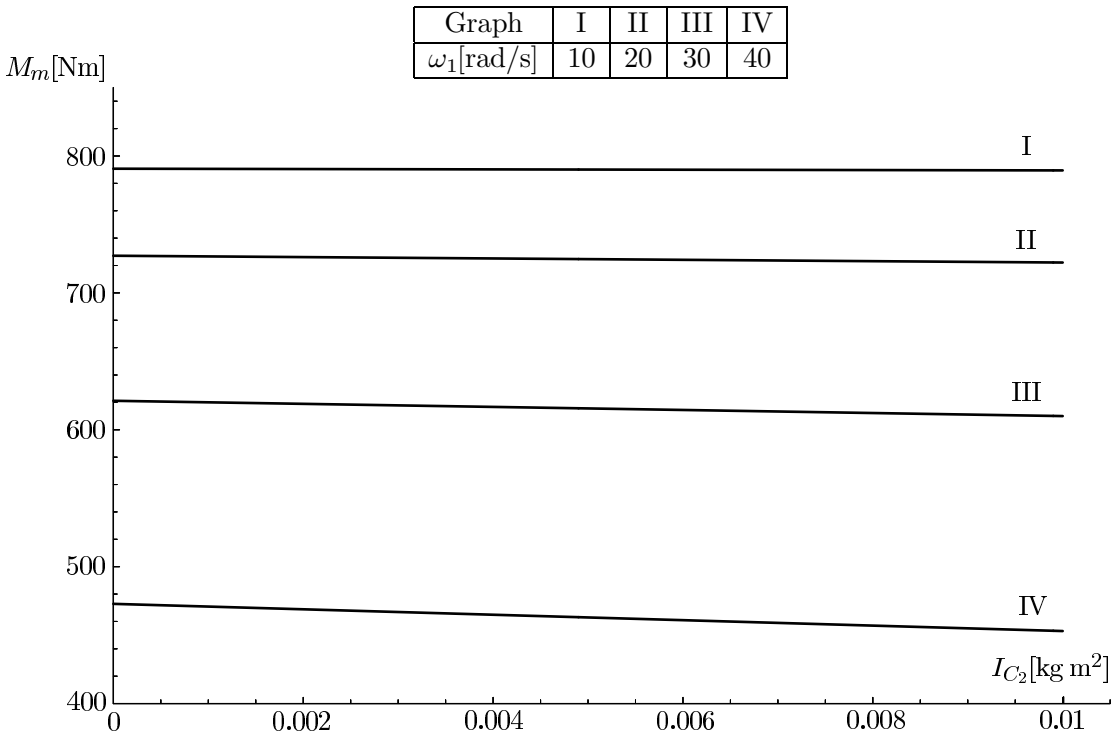

Figure 3.6: The influence of the mass moment of inertia I_{C_2} and angular speed ω_1 on the motor torque M_m.

Chapter 4

Rigid body contact and impact

In this study a planar rigid-link mechanism with a rotating slider joint and clearance is investigated. The influence of the clearance gap size, crank speed, friction and impact parameters on the nonlinear behavior of the system are analyzed. Periodic response is observed for zero clearance and also at low crank speeds and low values of the coefficient of restitution for the mechanism with clearance. Chaotic motion is observed for relatively high crank speeds. The sliding joint with clearance is modelled using a kinematic coefficient of friction and a coefficient of restitution. Nonlinear dynamics tools are applied to analyze the simulation data captured from the connecting rod of the mechanism. The largest Lyapunov exponent is used as an index for studying the stability of the system and a diagnostic tool.

4.1 Introduction

One of the important factors that influence the dynamic stability and the performance of mechanisms is the joint clearance. In the last years, many researchers have been studied the effects of the clearance on the motion of mechanical systems. Farahanchi and Shaw [38] considered the model of a planar, rigid-link mechanism with clearance at the slider joint. They observed that the response of the system appears to be chaotic, although periodic motion become more common as dissipation effects are increased. Abarbanel et al. [39, 40, 41] developed dynamic tools for analyzing observed chaotic

data. Nonlinear dynamic tools were presented by Nayfeh and Balachadran [42]. Related papers in the field of chaotic motion in mechanical systems are those of Kapitaniak [43], and Ott et al. [44]. Deck and Dubowski [45] studied the problems encountered in predicting the dynamic response of machines with clearance connections. Recent research has contributed to the development of simulation methods for specific multibody systems. Gilmore and Cipra [46] discussed a simulation method for planar dynamical mechanical systems with changing topologies. The information provided by the rigid bodies' boundary descriptions was used to automatically predict and detect impacts. Conti et al. [47] described a unified method to predict the contact changes due to kinematics. Contact and friction constraints were used by Pfeiffer [48] to study the stick-slip phenomena. The first trials to model impacts with friction can be found in Brach [49], and Wang and Mason [50]. Brach [49] considered only single collisions and formulates the impact equations using Newton's law. Wang and Mason [50] applied a time-scaling method and solve the impact equations by using Poisson's Law and Coulomb's law for a single contact. Jean and Moreau [51] reformulated Newton's law in an unilateral manner for multiple impacts with friction. In this work, the models of rigid and flexible body impacts described by Marghitu et al. [52, 53, 54] were used. In a closely related paper, Marghitu and Stoenescu [55] developed a dynamic analysis of children gait.

In this section, the dynamic analysis of a planar rigid-link mechanism with prismatic joint and clearance is investigated [56, 57]. Periodic motion is observed for the system with no clearance. The response of the system with clearance is chaotic at relatively high crank speeds and low values of the coefficient of restitution.

4.2 R-RTR mechanism

In this section, the planar R-RTR mechanism shown in Fig. 4.1 is considered. A fixed reference frame $xAyz$ is chosen. The lengths of the links are $L_1 = 0.001$ m, $L_2 = 0.470$ m, and $L3 = 0.047$ m. The links 1 and 2 are rectangular prisms with the depth $d = 0.001$ m and height $h = 0.01$ m. The link 3 has the height $h_3 = 0.02$ m, and the depth $d_3 = 0.05$ m. The mass density of the links is $\rho = 7850$ Kg/m^3. The center of mass locations of the links $i = 1,\ 2,\ 3$ are designated by $G_i(x_{G_i}, y_{G_i}, 0)$. The initial conditions $\theta_1(0) = \pi/6$ rad and $\omega_1(0) = \dot{\theta}_1(0) = 0$ rad/s are given.

Generalized coordinates

The number of degrees of freedom for the mechanism can be computed using the relation

$$M = 3n - 2c_5 - c_4,$$

where n is the number of moving links, c_5 is the number of pin joints or slider joints with one degree of freedom, and c_4 is the number of pin joints or slider joints with two degrees of freedom.

In our case, $n = 3,\ c_5 = 4\ (A(R),\ B(R),\ C(T),\ C(R)),\ c_4 = 0$, and the mechanism has one degree of freedom ($M = 1$). One can choose the angle $q_1(t) = \theta_1(t)$ as the generalized coordinate.

Kinematics

a. Position vectors

The position vector r_{G_1} of the center of the mass G_1 is

$$\mathbf{r}_{G_1} = x_{G_1}\mathbf{I} + y_{G_1}\mathbf{J}, \tag{4.1}$$

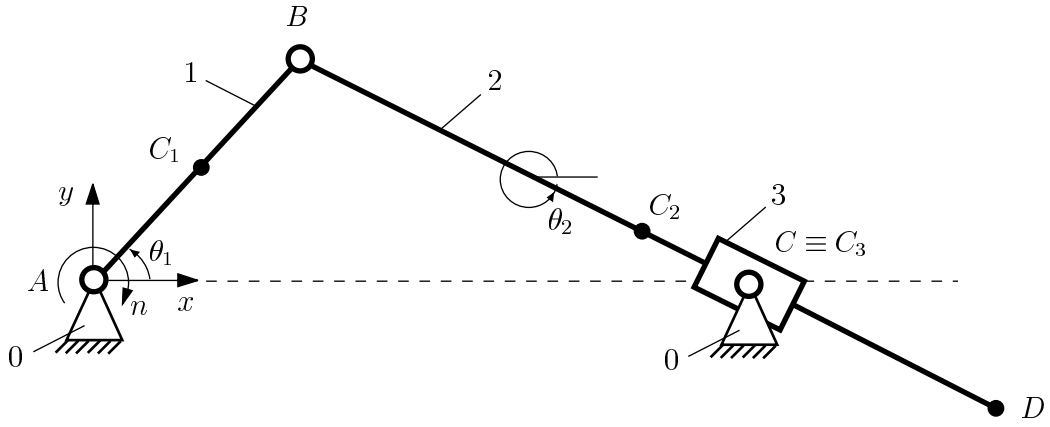

Figure 4.1: Rigid body diagram for the R-RTR mechanism with rotating prismatic joint.

where x_{G_1} and y_{G_1} are the coordinates of G_1

$$x_{G_1} = \frac{L_1}{2}\cos q_1,\ y_{G_1} = \frac{L_1}{2}\sin q_1. \tag{4.2}$$

The position vector r_{G_2} of the center of the mass G_2 is

$$\mathbf{r}_{G_2} = x_{G_2}\mathbf{1} + y_{G_2}\mathbf{J}, \tag{4.3}$$

where x_{G_2} and y_{G_2} are the coordinates of G_2

$$x_{G_2} = L_1\cos q_1 + \frac{L_2}{2}\cos\theta_2,\ y_{G_2} = L_1\sin q_1 + \frac{L_2}{2}\sin\theta_2, \tag{4.4}$$

where $\theta_2 = \arctan\dfrac{L_1\sin q_1}{L_1\cos q_1 - AC}$.
The position vector r_{G_3} of the center of the mass G_3 is

$$\mathbf{r}_{G_3} = AC\mathbf{1}. \tag{4.5}$$

b. Velocity vectors

The velocity vector $\mathbf{v}_{G_1}$ is the derivative with respect to time of the position vector $\mathbf{r}_{G_1}$

$$\mathbf{v}_{G_1} = \dot{\mathbf{r}}_{G_1} = \dot{x}_{G_1}\mathbf{1} + \dot{y}_{G_1}\mathbf{J}, \tag{4.6}$$

where

$$\dot{x}_{G_1} = -\frac{L_1}{2}\dot{q}_1\sin q_1,\ \dot{y}_{G_1} = \frac{L_1}{2}\dot{q}_1\cos q_1. \tag{4.7}$$

The velocity vector $\mathbf{v}_{G_2}$ is the derivative with respect to time of the position vector $\mathbf{r}_{G_2}$

$$\mathbf{v}_{G_2} = \dot{\mathbf{r}}_{G_2} = \dot{x}_{G_2}\mathbf{\imath} + \dot{y}_{G_2}\mathbf{J}, \tag{4.8}$$

where

$$\begin{aligned} \dot{x}_{G_2} &= -L_1\dot{q}_1 \sin q_1 - \frac{L_2}{2}\dot{\theta}_2 \sin\theta_2, \\ \dot{y}_{G_2} &= L_1\dot{q}_1 \cos q_1 + \frac{L_2}{2}\dot{\theta}_2 \cos\theta_2. \end{aligned} \tag{4.9}$$

The velocity vector $\mathbf{v}_{G_3}$ is zero

$$\mathbf{v}_{G_3} = \mathbf{0}. \tag{4.10}$$

c. Acceleration vectors

The acceleration vector $\mathbf{a}_{G_1}$ is the double derivative with respect to time of the position vector $\mathbf{r}_{G_1}$

$$\mathbf{a}_{G_1} = \ddot{\mathbf{r}}_{G_1} = \ddot{x}_{G_1}\mathbf{\imath} + \ddot{y}_{G_1}\mathbf{J}, \tag{4.11}$$

where

$$\begin{aligned} \ddot{x}_{G_1} &= -\frac{L_1}{2}\ddot{q}_1 \sin q_1 - \frac{L_1}{2}\dot{q}_1^2 \cos q_1, \\ \ddot{y}_{G_1} &= \frac{L_1}{2}\ddot{q}_1 \cos q_1 - \frac{L_1}{2}\dot{q}_1^2 \sin q_1. \end{aligned} \tag{4.12}$$

The acceleration vector $\mathbf{a}_{G_2}$ is the double derivative with respect to time of the position vector $\mathbf{r}_{G_2}$

$$\mathbf{a}_{G_2} = \ddot{\mathbf{r}}_{G_2} = \ddot{x}_{G_2}\mathbf{\imath} + \ddot{y}_{G_2}\mathbf{J}, \tag{4.13}$$

where

$$\begin{aligned} \ddot{x}_{G_2} &= -L_1\ddot{q}_1 \sin q_1 - L_1\dot{q}_1^2 \cos q_1 - \frac{L_2}{2}\ddot{\theta}_2 \sin\theta_2 - \frac{L_2}{2}\dot{\theta}_2^2 \cos\theta_2, \\ \ddot{y}_{G_2} &= L_1\ddot{q}_1 \cos q_1 - L_1\dot{q}_1^2 \sin q_1 + \frac{L_2}{2}\ddot{\theta}_2 \cos\theta_2 - \frac{L_2}{2}\dot{\theta}_2^2 \sin\theta_2. \end{aligned} \tag{4.14}$$

The acceleration vector of $\mathbf{a}_{G_3}$ is zero

$$\mathbf{a}_{G_3} = \mathbf{0}. \tag{4.15}$$

d. Angular velocity vectors

The angular velocity vectors of the links 1, 2, and 3 are

$$\begin{aligned} \boldsymbol{\omega} &= \dot{q}_1 \mathbf{k}, \\ \boldsymbol{\omega}_2 &= \boldsymbol{\omega}_3 = \dot{\theta}_2 \mathbf{k}. \end{aligned} \tag{4.16}$$

e. Angular acceleration vectors

The angular acceleration vectors of the links 1, 2, and 3 are

$$\begin{aligned} \boldsymbol{\alpha} &= \ddot{q}_1 \mathbf{k}, \\ \boldsymbol{\alpha}_2 &= \boldsymbol{\alpha}_3 = \ddot{\theta}_2 \mathbf{k}. \end{aligned} \tag{4.17}$$

Force analysis

a. Masses

The masses of the links 1, 2 and 3 are

$$\begin{aligned} m_1 &= \rho L_1 h d, \\ m_2 &= \rho L_2 h d, \\ m_3 &= m_{3a} - m_{3b}, \end{aligned}$$

where $m_{3a} = \rho L_3 h_3 d_3,\ m_{3b} = \rho L_3 h d.$

b. Gravitational forces

The gravitational forces of the link 1, 2, and 3 are

$$\begin{aligned} \mathbf{G}_1 &= -m_1 g_{\mathbf{J}}, \\ \mathbf{G}_2 &= -m_2 g_{\mathbf{J}}, \\ \mathbf{G}_3 &= -m_3 g_{\mathbf{J}}. \end{aligned} \tag{4.18}$$

c. Mass moments of inertia

The mass moment of inertia of the link 1 with respect to the center of mass G_1 is

$$I_{G_1} = \frac{m_1}{12}\left(L_1^2 + h^2\right).$$

The mass moment of inertia of the link 2 with respect to the center of mass G_2 is

$$I_{G_2} = \frac{m_2}{12}\left(L_2^2 + h^2\right).$$

The mass moment of inertia of the link 3 with respect to the center of mass G_3 is

$$I_{G_3} = \frac{m_{3a}}{12}\left(L_3^2 + h_3^2\right) - \frac{m_{3b}}{12}\left(L_3^2 + h^2\right).$$

d. Motor torque

The motor torque acts on the link 1

$$\mathbf{M}_m = M\mathbf{k}. \tag{4.19}$$

For a D.C. electric motor, $M = M_0 \left(1 - \frac{\omega_1}{\omega_0}\right)$, where M_0 and ω_0 are given in catalogues. In our case, $M_0 = 1$ Nm, and $\omega_0 = 4$ rad/s (Fig. 4.2).

4.2.1 Newton-Euler's method

In this section the equation of motion for the mechanism is solved by using Newton-Euler's formulation. There are three rigid bodies in the system and one can write the Newton-Euler equations for each link.

a. Link 1

The Newton-Euler equations for the link 1 are (see Fig. 4.3.a)

$$m_1 \mathbf{a}_{G_1} = \mathbf{F}_{01} + \mathbf{F}_{21} + \mathbf{G}_1, \tag{4.20}$$

$$I_{G_1} \boldsymbol{\alpha}_1 = \mathbf{G}_1\mathbf{A} \times \mathbf{F}_{01} + \mathbf{G}_1\mathbf{B} \times \mathbf{F}_{21} + \mathbf{M}_m, \tag{4.21}$$

where $\mathbf{F}_{01}$ is the joint reaction of the ground 0 on the link 1 at the point A, and $\mathbf{F}_{21}$ is the joint reaction of the link 2 on the link 1 at the point B

$$\begin{aligned} \mathbf{F}_{01} &= F_{01x}\mathbf{I} + F_{01y}\mathbf{J}, \\ \mathbf{F}_{21} &= F_{21x}\mathbf{I} + F_{21y}\mathbf{J}. \end{aligned} \tag{4.22}$$

b. Link 2

The Newton-Euler equations for the link 2 are (see Fig. 4.3.b)

$$m_2 \mathbf{a}_{G_2} = \mathbf{F}_{12} + \mathbf{F}_{32} + \mathbf{G}_2, \tag{4.23}$$

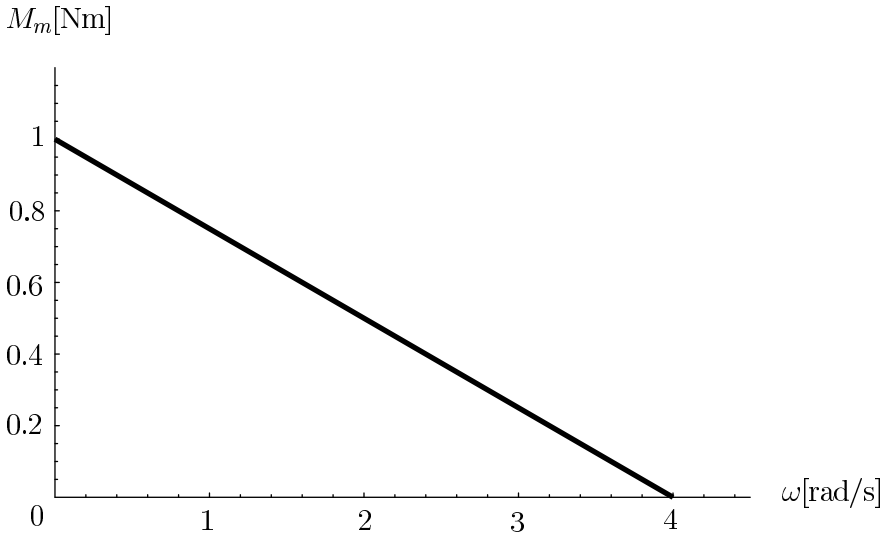

Figure 4.2: The variation of the driver motor torque with respect to the angular speed for the R-RTR mechanism.

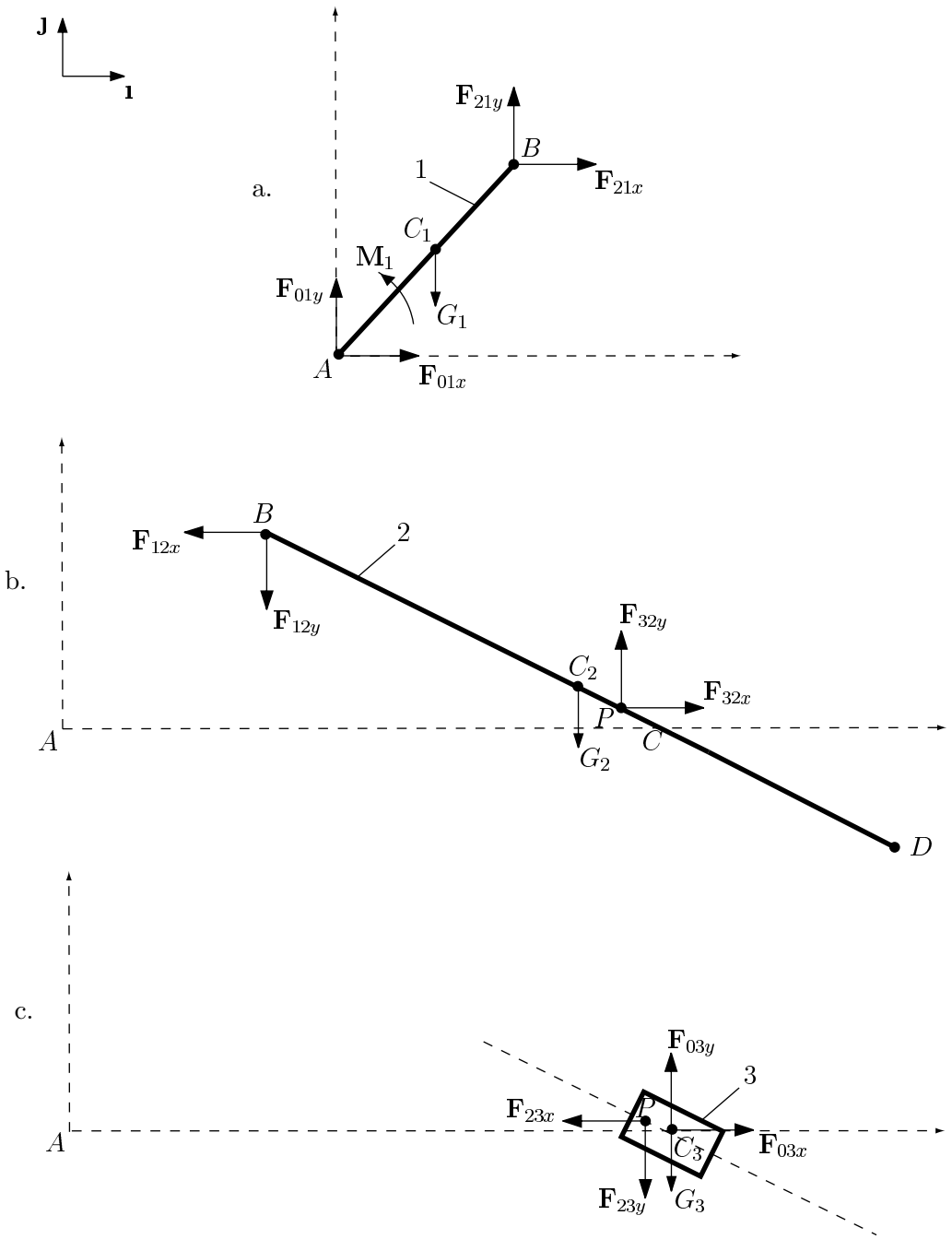

Figure 4.3: Rigid body diagram for the R-RTR mechanism.

$$I_{G_2}\boldsymbol{\alpha}_2 = \mathbf{G_2B} \times \mathbf{F}_{12} + \mathbf{G_2P} \times \mathbf{F}_{32}, \tag{4.24}$$

where $\mathbf{F}_{12}$ is the joint reaction of the link 1 on the link 2 at the point B and $\mathbf{F}_{32}$ is the joint reaction of the link 3 on the link 2 at the point P

$$\begin{aligned} \mathbf{F}_{12} &= -\mathbf{F}_{21}, \\ \mathbf{F}_{32} &= F_{32x}\mathbf{1} + F_{32y}\mathbf{J}. \end{aligned} \tag{4.25}$$

The application point $P(x_P, y_P)$ of the reaction force $\mathbf{F}_{32}$ is not known but it is located on the sliding direction

$$\tan\theta_2 = \frac{y_P}{x_P - AC}, \tag{4.26}$$

where $x_P,\ y_P$ are the coordinates of the point P.

The reaction force $\mathbf{F}_{32}$ is perpendicular to the sliding direction BD

$$\mathbf{F}_{32} \cdot \mathbf{BD} = 0. \tag{4.27}$$

c. Link 3

The Newton-Euler equations for the link 3 are (see Fig. 4.3.c)

$$m_3\mathbf{a}_{G_3} = \mathbf{F}_{23} + \mathbf{F}_{03} + \mathbf{G}_3 = 0, \tag{4.28}$$

$$I_{G_3}\boldsymbol{\alpha}_3 = \mathbf{CP} \times \mathbf{F}_{23}, \tag{4.29}$$

where

$$\begin{aligned} \mathbf{F}_{23} &= -\mathbf{F}_{32}, \\ \mathbf{F}_{03} &= F_{03x}\mathbf{1} + F_{03y}\mathbf{J}. \end{aligned} \tag{4.30}$$

There are ten scalar equations with ten unknowns. From the Eqs. (4.39), (4.40), (4.44), (4.45), (4.26), (4.42), and (4.47) one can find the unknown joint reaction forces F_{01x}, F_{01y}, F_{21x}, F_{21y}, F_{32x}, F_{32y}, F_{03x}, F_{03y}, and the coordinates x_P and y_P of the point P. Knowing the reaction forces and the position vector $\mathbf{r}_P$ as functions of $q_1(t)$, $\dot{q}_1(t)$, and $\ddot{q}_1(t)$, one can derive the equation of motion for the mechanism from Eq. (4.48).

4.2.2 Lagrange's method

In this section the equation of motion for the mechanism is solved using Lagrange's formulation. The Lagrange differential equation for the mechanism with one degree of freedom is

$$\frac{d}{dt}\left(\frac{\partial T}{\partial \dot{q}_1}\right) - \frac{\partial T}{\partial q_1} = Q, \tag{4.31}$$

where T is the total kinetic energy of the system, and Q is the generalized force.
The kinetic energy T_1 for the link 1 is

$$T_1 = \frac{1}{2} m_1 \mathbf{v}_{G_1} \cdot \mathbf{v}_{G_1} + \frac{1}{2} I_{G_1} \boldsymbol{\omega}_1 \cdot \boldsymbol{\omega}_1. \tag{4.32}$$

The kinetic energy T_2 for the link 2 is

$$T_2 = \frac{1}{2} m_2 \mathbf{v}_{G_2} \cdot \mathbf{v}_{G_2} + \frac{1}{2} I_{G_2} \boldsymbol{\omega}_2 \cdot \boldsymbol{\omega}_2. \tag{4.33}$$

The kinetic energy T_3 for the link 3 is

$$T_3 = \frac{1}{2} I_{G_3} \boldsymbol{\omega}_3 \cdot \boldsymbol{\omega}_3. \tag{4.34}$$

The total kinetic energy is

$$T = \sum_{i=1}^{3} T_i. \tag{4.35}$$

The generalized force Q_i for the link i is

$$Q_i = \frac{\partial \mathbf{r}_{G_i}}{\partial q_1} \cdot \mathbf{G}_i. \tag{4.36}$$

The generalized force Q_m for the motor is

$$Q_m = \frac{\partial \boldsymbol{\omega}_1}{\partial \dot{q}_1} \cdot \mathbf{M}_m = M_0 \left(1 - \frac{\dot{q}_1}{\omega_0}\right). \tag{4.37}$$

The total generalized force Q for the mechanism is

$$Q = \sum_{i=1}^{3} Q_i + Q_m = \sum_{i=1}^{3} \frac{\partial \mathbf{r}_{G_i}}{\partial q_1} \cdot \mathbf{G}_i + \frac{\partial \boldsymbol{\omega}_1}{\partial \dot{q}_1} \cdot \mathbf{M}_m. \tag{4.38}$$

For the link 1 some calculations are given

$$T_1 = \frac{1}{2}(I_{G_1} + \frac{1}{4}L_1^2 m_1)\dot{q}_1^2.$$

$$\frac{\partial T_1}{\partial \dot{q}_1} = (I_{G_1} + \frac{1}{4}L_1^2 m_1)\dot{q}_1.$$

$$\frac{\partial \mathbf{r}_{G_1}}{\partial \dot{q}_1} = -\frac{1}{2}L_1(\sin q_1 \mathbf{i} + \cos q_1 \mathbf{J}).$$

$$Q_1 = \frac{\partial \mathbf{r}_{G_1}}{\partial \dot{q}_1} \cdot (-m_1 g \mathbf{J}) = -\frac{1}{2}m_1 g L_1 \cos q_1.$$

From Eqs. (4.31), (4.35), and (4.38) one can derive and solve the equation of motion for the mechanism.

Remark: Lagrange's method does not require the calculation of the joint forces.

4.3 R-RTR mechanism with friction

The mechanism described in Section 4.2 is considered. The coefficient of kinetic friction is $\mu_k = 0.4$. The mechanism has one degree of freedom. One can chose the angle $q_1(t) = \theta(t)$ as the generalized coordinate for the system.

4.3.1 Newton-Euler's method

The equation of motion for the mechanism is solved using Newton-Euler's formulation. There are three rigid bodies in the system and one can write the Newton-Euler equations for each link.

a. Link 1

The Newton-Euler equations for the link 1 are (see Fig. 4.3.a)

$$m_1 \mathbf{a}_{G_1} = \mathbf{F}_{01} + \mathbf{F}_{21} + \mathbf{G}_1, \tag{4.39}$$

$$I_{G_1} \boldsymbol{\alpha}_1 = \mathbf{G}_1\mathbf{A} \times \mathbf{F}_{01} + \mathbf{G}_1\mathbf{B} \times \mathbf{F}_{21} + \mathbf{M}_m, \tag{4.40}$$

where $\mathbf{F}_{01}$ is the joint reaction of the ground 0 on the link 1 at the point A, and $\mathbf{F}_{21}$ is the joint reaction of the link 2 on the link 1 at the point B

$$\begin{aligned} \mathbf{F}_{01} &= F_{01x}\mathbf{1} + F_{01y}\mathbf{J}, \\ \mathbf{F}_{21} &= F_{21x}\mathbf{1} + F_{21y}\mathbf{J}. \end{aligned} \tag{4.41}$$

b. Link 2

The reaction force $\mathbf{F}_{32}$ is perpendicular to the sliding direction BD

$$\mathbf{F}_{32} \cdot \mathbf{BD} = 0. \tag{4.42}$$

The friction force $\mathbf{F}_{f_{32}}$ that acts on the link 2 is

$$\mathbf{F}_{f_{32}} = \mathbf{F}_f = -\frac{\mathbf{v}_{C_2}}{|\mathbf{v}_{C_2}|}\mu_k F_{32}. \tag{4.43}$$

The Newton-Euler equations for the link 2 are (see Fig. 4.3.b)

$$m_2\mathbf{a}_{G_2} = \mathbf{F}_{12} + \mathbf{F}_{32} + \mathbf{G}_2 + \mathbf{F}_{f_{32}}, \tag{4.44}$$

$$I_{G_2}\boldsymbol{\alpha}_2 = \mathbf{G}_2\mathbf{B} \times \mathbf{F}_{12} + \mathbf{G}_2\mathbf{P} \times \mathbf{F}_{32}, \tag{4.45}$$

where $\mathbf{F}_{12}$ is the joint reaction of the link 1 on the link 2 at the point B and $\mathbf{F}_{32}$ is the joint reaction of the link 3 on the link 2 at the point P

$$\begin{aligned} \mathbf{F}_{12} &= -\mathbf{F}_{21}, \\ \mathbf{F}_{32} &= F_{32x}\mathbf{1} + F_{32y}\mathbf{J}. \end{aligned} \tag{4.46}$$

c. Link 3

The Newton-Euler equations for the link 3 are (see Fig. 4.3.c)

$$m_3\mathbf{a}_{G_3} = \mathbf{F}_{23} + \mathbf{F}_{03} + \mathbf{G}_3 - \mathbf{F}_{f_{32}}, \tag{4.47}$$

$$I_{G_3}\boldsymbol{\alpha}_3 = \mathbf{CP} \times \mathbf{F}_{23}, \tag{4.48}$$

where

$$\begin{aligned} \mathbf{F}_{23} &= -\mathbf{F}_{32}, \\ \mathbf{F}_{03} &= F_{03x}\mathbf{I} + F_{03y}\mathbf{J}. \end{aligned} \tag{4.49}$$

There are eight scalar equations with eight unknowns. From the Eqs. (4.39), (4.40), (4.44), (4.42), and (4.47) one can find the unknown joint reaction forces F_{01x}, F_{01y}, F_{21x}, F_{21y}, F_{32x}, F_{32y}, F_{03x}, F_{03y}.

Knowing the reaction forces as functions of $q_1(t)$, $\dot{q}_1(t)$, and $\ddot{q}_1(t)$, one can derive the equation of motion for the mechanism from Eq. (4.45).

4.3.2 Kane's method

The equation of motion for the mechanism is solved using Kane's formulation.

The total kinetic energy is

$$T = \sum_{i=1}^{3} T_i, \tag{4.50}$$

where T_i is the kinetic energy of the link i.

Generalized speeds

One can chose the generalized speed

$$u_1 = \dot{q}_1. \tag{4.51}$$

The velocity vector of the point C_2 located on the link 2 can be written as

$$\mathbf{v}_{C_2} = \mathbf{v}_{G_2} + \boldsymbol{\omega}_2 \times \mathbf{G_2C}, \tag{4.52}$$

where $\mathbf{G_2C} = \mathbf{r}_C - \mathbf{r}_{G_2}$.

In order to take in consideration the reaction force N between the links 2 and 3 one can introduce a new generalized speed u_2 in the expression of the relative velocity vector $\mathbf{v}_{C_{32}}$

$$\mathbf{v}_{C_{23}} = \mathbf{v}_{C_2} - \mathbf{v}_{C_3} + u_2\mathbf{e}_{2n}, \tag{4.53}$$

where $\mathbf{e}_{2n} = -\sin\theta_2\mathbf{\imath} + \cos\theta_2\mathbf{J}$ and $\theta_2 = \arctan\dfrac{L_1\sin q_1}{L_1\cos q_1 - AC}$. Thus, one can write $\mathbf{v}_{G_3} = \mathbf{v}_{C_3} = -u_2\mathbf{e}_{2n}$.

Generalized forces

The reaction force $\mathbf{F}_{32}$ of the link 3 on the link 2 is

$$\mathbf{F}_{32} = \mathbf{N} = N\mathbf{e}_{2n}. \tag{4.54}$$

The reaction force $\mathbf{F}_{23}$ of the link 3 on the link 2 is

$$\mathbf{F}_{23} = -\mathbf{F}_{32} = -\mathbf{N}. \tag{4.55}$$

The friction force $\mathbf{F}_{f_{32}}$ that acts on the link 2 is

$$\mathbf{F}_{f_{32}} = \mathbf{F}_f = -\frac{\mathbf{v}_{C_2}}{|\mathbf{v}_{C_2}|}\mu_k N. \tag{4.56}$$

The friction force $\mathbf{F}_{f_{23}}$ that acts on the link 3 is

$$\mathbf{F}_{f_{23}} = -\mathbf{F}_{f_{32}} = -\mathbf{F}_f. \tag{4.57}$$

The generalized forces Q_j associated to the generalized speeds u_j, for j=1,2, can be computed as

$$Q_j = \sum_{i=1}^{3} \frac{\partial \mathbf{v}_{G_i}}{\partial u_j} \cdot \mathbf{G}_i + \frac{\partial \mathbf{v}_{C_2}}{\partial u_j} \cdot (\mathbf{N} + \mathbf{F}_f) + \frac{\partial \mathbf{v}_{C_3}}{\partial u_j} \cdot (-\mathbf{N} - \mathbf{F}_f) + \frac{\partial \boldsymbol{\omega}_1}{\partial u_j} \cdot \mathbf{M}_m. \tag{4.58}$$

Generalized inertia forces

The forces F_j^* can be written as

$$F_j^* = \sum_{i=1}^{3} \frac{\partial \mathbf{v}_{G_i}}{\partial u_j} \cdot (-m_i \mathbf{a}_{G_i}) + \sum_{i=1}^{3} \frac{\partial \boldsymbol{\omega}_i}{\partial u_j} \cdot (-I_{G_i} \boldsymbol{\alpha}_i). \tag{4.59}$$

Kane's equations

One can write two Kane equations associated to the generalized speeds u_1 and u_2

$$F_j^* + Q_j = 0, \ j = 1, 2. \tag{4.60}$$

From Eqs. (4.113) and (4.120) one can find the the reaction force N and the equation of motion for the mechanism.

One can write the angle θ_2 as

$$\theta_2 = \frac{\pi}{2} - \frac{q_1}{2}, \tag{4.61}$$

the vector $\mathbf{e}_{2n}$ as

$$\mathbf{e}_{2n} = -\cos\frac{q_1}{2}\mathbf{I} + \sin\frac{q_1}{2}\mathbf{J}, \tag{4.62}$$

and the reaction force N between the links 2 and 3 as

$$N = m_3 g \sin\frac{q_1}{2}. \tag{4.63}$$

4.3.3 Kineto-static analysis

In this section, the mechanism with no clearance (one degree of freedom) is considered (Fig. 4.1). Friction forces act at the rotational and translational joints. The equation of motion is known and the reaction forces are computed. A Newtonian approach is used, that is, the method of consecutive approximations.

For the translational joint between the links i and j, the friction force $\mathbf{F}_{fji}$ acts on the link i at the contact surface and is proportional to the coefficient of friction μ. The force $\mathbf{F}_{fji}$ has opposite direction to the relative translational velocity $\mathbf{v}_{ij}$ between the links i and j

$$\mathbf{F}_{fji} = -\frac{\mathbf{v}_{ij}}{|\mathbf{v}_{ij}|}\mu F_{ji}, \tag{4.64}$$

where $\mathbf{v}_{ij} = \mathbf{v}_i - \mathbf{v}_j$.

The friction forces induce a moment $\mathbf{M}_{fji}$ that acts at the rotational joint between the links i and j. The moment $\mathbf{M}_{fji}$ is proportional to the coefficient of friction μ, the radius r of the joint, and has opposite sense to the relative angular velocity ω_{ij} between the

links i and j

$$\mathbf{M}_{fji} = -\text{sign}\,(\omega_{ij})\,\mu r F_{ji}, \tag{4.65}$$

where $\omega_{ij} = \omega_i - \omega_j$.

The Newton-Euler equations for the link 1 are (see Fig. 4.3.a)

$$m_1 \mathbf{a}_{C_1} = \mathbf{F}_{01} + \mathbf{F}_{21} + \mathbf{G}_1, \tag{4.66}$$

$$I_{C_1}\boldsymbol{\alpha} = \mathbf{C}_1\mathbf{A} \times \mathbf{F}_{01} + \mathbf{C}_1\mathbf{B} \times \mathbf{F}_{21} + \mathbf{M}_{f21}. \tag{4.67}$$

The Newton-Euler equations for the link 2 are (see Fig. 4.3.b)

$$m_2 \mathbf{a}_{C_2} = \mathbf{F}_{12} + \mathbf{F}_{32} + \mathbf{G}_2 + \mathbf{F}_{f32}, \tag{4.68}$$

$$I_{C_2}\boldsymbol{\alpha}_2 = \mathbf{C}_2\mathbf{B} \times \mathbf{F}_{12} + \mathbf{C}_2\mathbf{Q} \times \mathbf{F}_{32} + \mathbf{M}_{f12}, \tag{4.69}$$

where $\mathbf{F}_{12} = -\mathbf{F}_{21}$ and $\mathbf{M}_{f12} = -\mathbf{M}_{f21}$.

The Newton-Euler equations for the link 3 are (see Fig. 4.3.c)

$$0 = \mathbf{F}_{23} + \mathbf{F}_{03} + \mathbf{G}_3 + \mathbf{F}_{f23}, \tag{4.70}$$

$$I_{C_3}\boldsymbol{\alpha}_3 = \mathbf{CQ} \times \mathbf{F}_{23} + \mathbf{M}_{f03}, \tag{4.71}$$

where $\mathbf{F}_{23} = -\mathbf{F}_{32}$, and $\mathbf{F}_{f23} = -\mathbf{F}_{f32}$.

The application point $Q(x_Q, y_Q)$ of the reaction force $\mathbf{F}_{32}$ is not known but it is located

on the sliding direction

$$\tan q_2 = \frac{y_Q}{x_Q - AC}, \tag{4.72}$$

where $\tan q_2 = \dfrac{L_1 \sin q_1}{L_1 \cos q_1 - AC}$, and $x_Q,\ y_Q$ are the coordinates of the point Q.
The method of consecutive approximations consists of the following steps:

1. Initially, the friction forces and moments are considered zero. From Eqs. (4.66), (4.67), (4.68), (4.69), (4.70), (4.71), and (4.72) one can calculate the unknown joint reaction forces F_{01x}, F_{01y}, F_{21x}, F_{21y}, F_{32x}, F_{32y}, F_{03x}, F_{03y}, and the coordinates x_Q and y_Q.

2. Using the values of the reaction forces computed at the step 1, one can calculate the friction force $\mathbf{F}_{f32}$ and the friction moments $\mathbf{M}_{f21},\ \mathbf{M}_{f03}$ from Eqs. (4.64) and (4.65).

3. Using the value of the friction forces and moments computed at the step 2, one can recalculate the reaction forces from Eqs. (4.66), (4.67), (4.68), (4.69), (4.70), (4.71), and (4.72).

4. Using the new values of the reaction forces computed at the step 3, one can recalculate the friction forces and moments from Eqs. (4.64) and (4.65).

5. Step 3 and step 4 are repeated until

$$\left| F_{ij}^k - F_{ij}^{k+1} \right| < \varepsilon$$

for all reaction forces $\mathbf{F}_{ij}$. The error $\varepsilon \in \mathbf{R}^+$ is known a priori, and $F_{ij}^k,\ F_{ij}^{k+1}$ are the magnitudes of the reaction forces F_{ij} at two consecutive approximations.

The method converges after a finite number of steps and the reaction forces with frictions are calculated.

4.4 R-RTR mechanism with friction and clearance

In order to study the effects of clearances on the motion of a connecting rod in a slider crank mechanism, a simplified model is used, shown in Fig. 4.1. The following basic assumptions are considered. (i) All components are rigid. (ii) All motions occur in a fixed plane. (iii) A motor with a variable torque is used to crank the mechanism. (iv) The clearances for the slider are symmetrically placed about the nominal slider path, that is, without clearance, and have a fixed magnitude. (v) The impacts between the connecting rod and slider are instantaneous and are modelled using a constant coefficient of restitution, a coefficient of friction, and a moment coefficient.

4.4.1 Equations of motion

Various methods are used to derive the equations of motion for the mechanism. It is assumed that during the impacts the system position does not change, because the impact time is very small. It is also assumed that the effect of finite forces is neglected during the impact. When two bodies impact against each other, an unknown impulsive force acts between them. The friction between the impact bodies introduces an tangent impact force. Formulation of rigid body collision problems are based on two physical laws, Coulomb's law of dry friction and balance of momentum. To solve the impact equations, additional relations are obtained using a coefficient of restitution and a coefficient of friction.

Figure 4.4 shows a planar slider joint where the backlash has been made very large in order to make it clearly visible. Figure 4.5 illustrates a possible geometry for the slider joint with clearance and the possible cases consist of: a) No contact (Fig. 4.5.a).

b) Contact or impact on a single point (Fig. 4.5.b).

c) Contact or impact on two opposed points (Fig. 4.5.c).

d) Contact or impact on two points on the same side (Fig. 4.5.d).

The conditions for switching from one case to a different one depend on the positions of the links and the reaction forces at the contact points.

One can consider three lines (L, L_a and L_b) defined on the link 2, and four points (M, N, P, and Q) defined on the link 3 (see Fig. 4.1).

The equations corresponding to the line L, can be expressed as a function of the coordinates of the links 1 and 2 as

Line L: $\quad y - m_2 x - n_2 = 0,$

where $m_2 = \tan\theta_2$ is the slope and $n_2 = L_1 \sin\theta_1 - m_2 \cos\theta_1$ is the displacement of the line L.

The equations corresponding to the lines L_a and L_b can be written as

Line L_a: $\quad y - m_a x - n_a = 0,$

Line L_b: $\quad y - m_b x - n_b = 0,$

where $m_a = m_b = m_2$ are the slopes and $n_a = n_2 - \dfrac{l_2}{2\cos\theta_2}$, $n_b = n_2 + \dfrac{l_2}{2\cos\theta_2}$ are the displacements of the lines L_a and L_b.

The coordinates of the points M, N, P, Q can be expressed as functions of the coordinates of the link 3 as

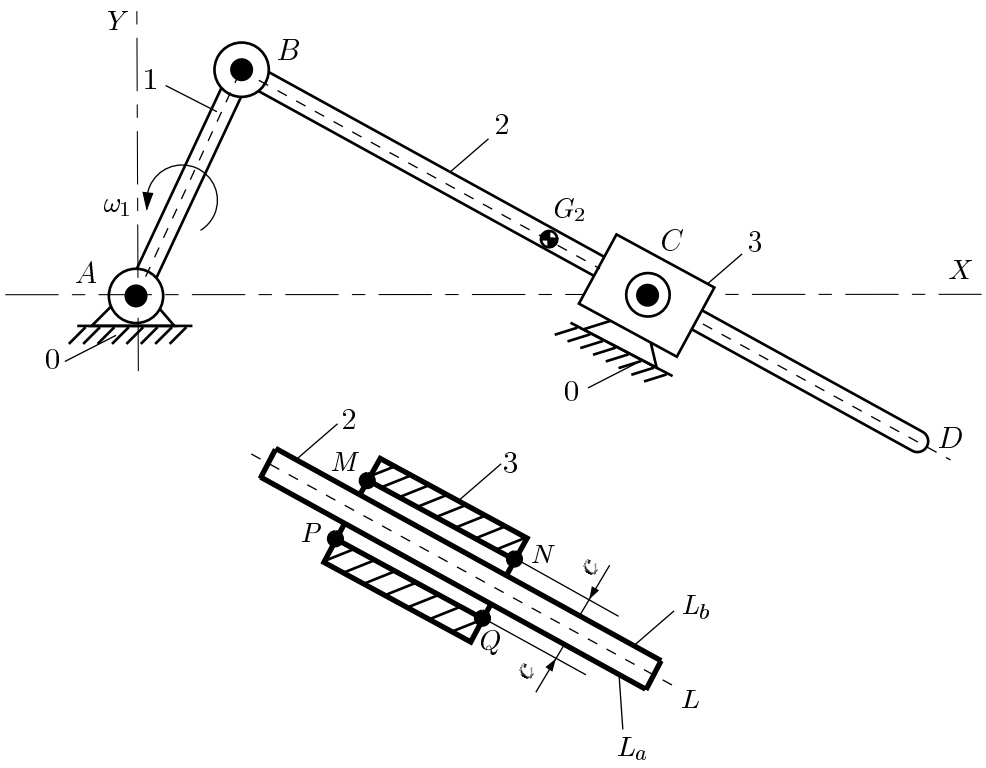

Figure 4.4: Model of the R-RTR mechanism with rotating prismatic joint and clearance.

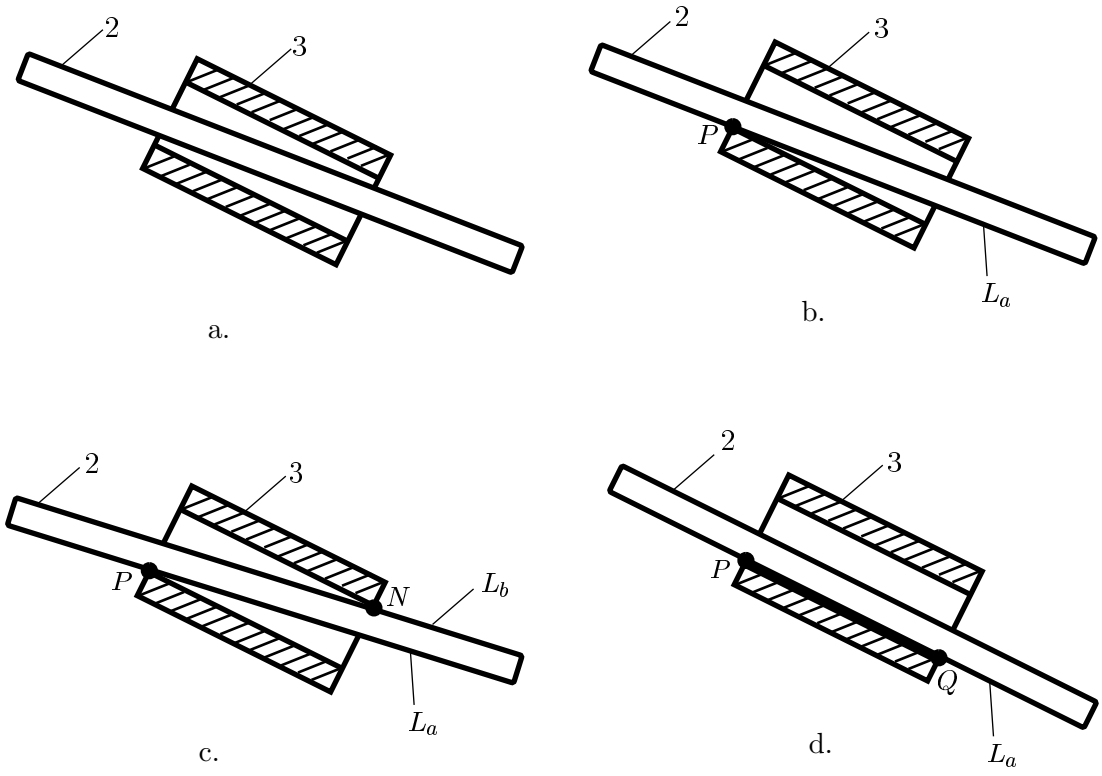

Figure 4.5: Geometry of the slider joint with clearance for: a. no contact; b. contact or impact on a single point; c. contact or impact on two points on the same side; d. contact or impact on two opposed points.

Point P: $x_P = x_C + r\cos\theta_3,\ y_P = y_C + r\sin\theta_3,$

Point Q: $x_Q = x_C + r\cos(\theta_3 - \theta_{30}),\ y_Q = y_C + r\sin(\theta_3 - \theta_{30}),$

Point M: $x_M = x_C + r\cos(\theta_3 - \theta_{30} + \pi),\ y_M = y_C + r\sin(\theta_3 - \theta_{30} + \pi),$

Point N: $x_N = x_C + r\cos(\theta_3 + \pi),\ y_N = y_C + r\sin(\theta_3 + \pi),$

where $x_C = AC$, $y_C = 0$ are the coordinates of the point C, $r = \sqrt{L_3^2 + (l_2 + c)^2}/2$ is the rotation radius of the link 3, and $\theta_{30} = 2\arctan\dfrac{L_3}{l_2 + c}$ is the angle $\angle MCN$.
Using the expressions above, one can set the position conditions corresponding to the four cases shown in Fig. 4.2 as following:

Case a) No conditions are necessary.

Case b) Point P is on the line L_a

$$y_P - m_a x_P - n_a \approx 0. \tag{4.73}$$

Case c) Point P is on the line L_a and point N is on the line L_b

$$\begin{aligned} y_P - m_a x_P - n_a &\approx 0, \\ y_N - m_b x_N - n_b &\approx 0. \end{aligned} \tag{4.74}$$

Case d) Points P and Q are on the line L_a

$$\begin{aligned} y_P - m_a x_P - n_a &\approx 0, \\ y_Q - m_a x_Q - n_a &\approx 0. \end{aligned} \tag{4.75}$$

Impacts can occur when the joint is in either case b), c) or d). The impact conditions depend on the relative linear velocities of the contact points. For example, in case b), one can write the following impact condition

$$\mathbf{v}_{P_2}^n - \mathbf{v}_{P_3}^n \approx 0. \tag{4.76}$$

where $\mathbf{v}_{P_2}^n$ and $\mathbf{v}_{P_3}^n$ are the normal velocities to the collision surface of the contact point P between the links 2 and 3.

The contact conditions also depend on the reaction forces between the links at the contact points. For example, in case b), the force condition can be written as

$$\mathbf{N}_{P_2}^n - \mathbf{N}_{P_3}^n \approx 0. \tag{4.77}$$

where $\mathbf{N}_{P_2}^n$ and $\mathbf{N}_{P_3}^n$ are the reaction forces between the links 2 and 3 at the contact point P.

The motion of the contact point during the impact can be described by one of the following two cases:

1. The contact point is slipping along surface while interacting with it in the normal direction. Since contact is maintained and slipping occurs, the normal and tangential components of the contact forces can be represented for dry friction as $F_t = -\mu_k F_n$.

2. The contact point is not slipping along but interacting with it in the normal direction. The tangential velocity v_t of the contact point is $v_t = 0$ subject to $|F_t/F_n| \leq \mu_s$.

4.4.2 Simulation algorithm

The simulation algorithm for the mechanism automatically determines when a change in the topology occurs and reformulate the equations of motion to reflect the changes in the system topology. The equations of motion depend on the contact and impact conditions. Sets of nonlinear equations are solved for contact and sets of linear equations are solved for impact.

The algorithm consisting of the following steps was written:

Step 1) Set up the input data, those are, the masses, the mass moments of inertia, the dimensions of the links, and the coordinates of the mechanism.

Step 2) Set up the initial conditions: the initial coordinates, velocities and accelerations of the links. Also, set up the initial time, the final time, and the step integration time.

Step 3) Verify the position contact conditions (4.73), (4.75), and (4.74). If case a) then go to step 4). If case b) then go to step 5). If case c) then go to step 6). If case d) then go to step 7).

Step 4) Solve the equations of motion for no contact and go to step 8).

Step 5) Verify the impact condition. If impact is detected then solve the equation of motion for impact on a single point and go to step 8). If no impact is detected then verify the force contact condition. If case a) then go to step 4). If case b) then integrate the equation of motion for contact on a single point and go to step 8).

Step 6) Verify the impact conditions. If impact is detected then solve the equation of motion for impact on two points on the same side and go to step 8). If no impact is detected then verify the force contact condition. If case a) then go to step 4). If case b)

then go to step 5). If case c) then integrate the equation of motion for contact on two points on the same side and go to step 8).

Step 7) Verify the impact conditions. If impact is detected then solve the equation of motion for impact on two opposed points and go to step 8). If no impact is detected then verify the force contact condition. If case a) then go to step 4). If case b) then go to step 5). If case d) then integrate the equation of motion for contact on two opposed points and go to step 8).

Step 8) Increment the integration time with the step integration time. If the integration time is less than the final time then go to step 3).

Step 9) Export the output data for analyzing.

Next, the equations of motion for the previous cases are derived.

4.4.3 No contact

In this section, the mechanism with two degrees of freedom is considered (Fig. 4.6). One can choose the generalized coordinates $q_1 = \theta_1$ and $q_2 = \theta_2$. The equation of motion is derived using the Lagrange's method

$$\frac{d}{dt}\left(\frac{\partial T}{\partial \dot{q}_i}\right) - \frac{\partial T}{\partial q_i} = Q_i, \quad i = 1, 2 \tag{4.78}$$

where T is the kinetic energy, q_i is the generalized coordinate, Q_i is the generalized force associated with the coordinate q_i. The kinetic energy T_1 for the link 1 is

$$T_1 = \frac{1}{2} m_1 \mathbf{v}_{G_1} \cdot \mathbf{v}_{G_1} + \frac{1}{2} I_{G_1} \boldsymbol{\omega}_1 \cdot \boldsymbol{\omega}_1, \tag{4.79}$$

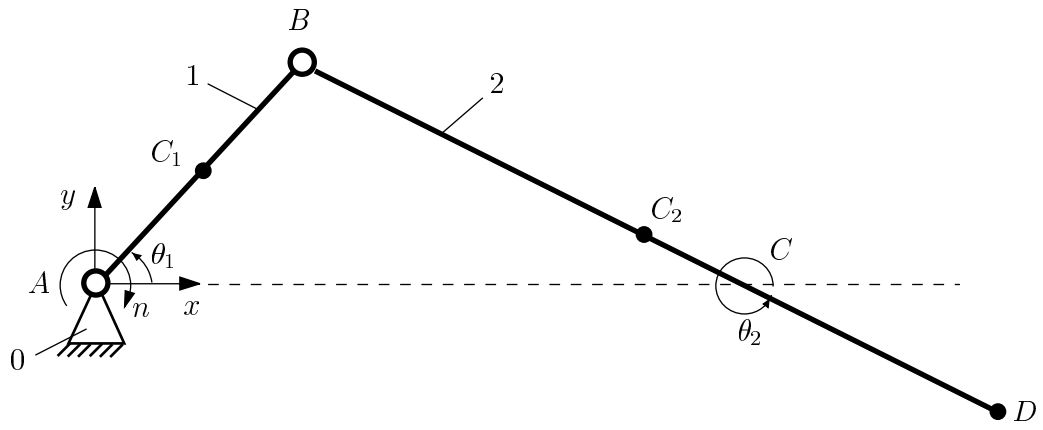

Figure 4.6: Rigid body diagram for the R-RTR mechanism with prismatic joint and clearance in the case of no contact.

where $\boldsymbol{\omega}_1 = \dot{q}_1 \mathbf{k}$.

The kinetic energy T_2 for the link 2 is

$$T_2 = \frac{1}{2} m_2 \mathbf{v}_{G_2} \cdot \mathbf{v}_{G_2} + \frac{1}{2} I_{G_2} \boldsymbol{\omega}_2 \cdot \boldsymbol{\omega}_2, \tag{4.80}$$

where $\boldsymbol{\omega}_2 = \dot{q}_2 \mathbf{k}$.

The kinetic energy T is

$$T = T_1 + T_2. \tag{4.81}$$

One can write the generalized force Q_1 as

$$Q_1 = -\left(\frac{1}{2} m_1 + m_2\right) L_1 g \cos q_1. \tag{4.82}$$

One can write the generalized force Q_2 as

$$Q_2 = -\frac{1}{2} m_2 L_2 g \cos q_2. \tag{4.83}$$

From Eqs. (4.78), (4.81), and (4.82), one can write

$$\left(\frac{m_1 L_1^2}{4} + m_2 L_1^2 + I_{G_2}\right) \ddot{q}_1 + \frac{1}{2} m_2 L_1 L_2 [\ddot{q}_2 \cos(q_2 - q_1) - \dot{q}_2^2 \sin(q_2 - q_1)] = -L_1 \left(\frac{1}{2} m_1 + m_2\right) g \cos q_1. \tag{4.84}$$

From Eqs. (4.78), (4.81), and (4.83), one can write

$$\left(\frac{m_2 L_2^2}{4} + I_{G_2}\right) \ddot{q}_2 + \frac{1}{2} m_2 L_1 L_2 \left[\ddot{q}_1 \cos(q_2 - q_1) + \dot{q}_1^2 \sin(q_2 - q_1)\right] =$$

$$= -\frac{1}{2} L_2 m_2 g \cos q_2. \tag{4.85}$$

Equations (4.84) and (4.85) are used and the equation of motion is derived.

4.4.4 Contact on a single point

In this case, the mechanism has two degrees of freedom (Fig. 4.7.a). One can chose the generalized coordinates $q1 = \theta_1$ and $q_2 = \theta_2$. Kane's equations are used and the equation of motion is derived. The kinetic energy T is

$$T = T_1 + T_2 + T_3. \tag{4.86}$$

One can find the position vector $\mathbf{r}_P$ of the contact point $P(x_P, y_P)$ solving the system of equations

$$\tan q_2 = \frac{y_B - y_P}{x_B - x_P},\ (x_C - x_P)^2 + (y_C - y_P)^2 = r^2. \tag{4.87}$$

The angular velocity and acceleration vectors $\boldsymbol{\omega}_3$ and $\boldsymbol{\alpha}_3$ of the link 3 are

$$\boldsymbol{\omega}_3 = \dot{\theta}_3 \mathbf{k},\ \boldsymbol{\alpha}_3 = \ddot{\theta}_3 \mathbf{k}, \tag{4.88}$$

where $\theta_3 = \arctan \dfrac{y_P}{x_P - AC}$.
One can chose the generalized speeds u_1 and u_2

$$u_1 = \dot{q}_1,\ u_2 = \dot{q}_2. \tag{4.89}$$

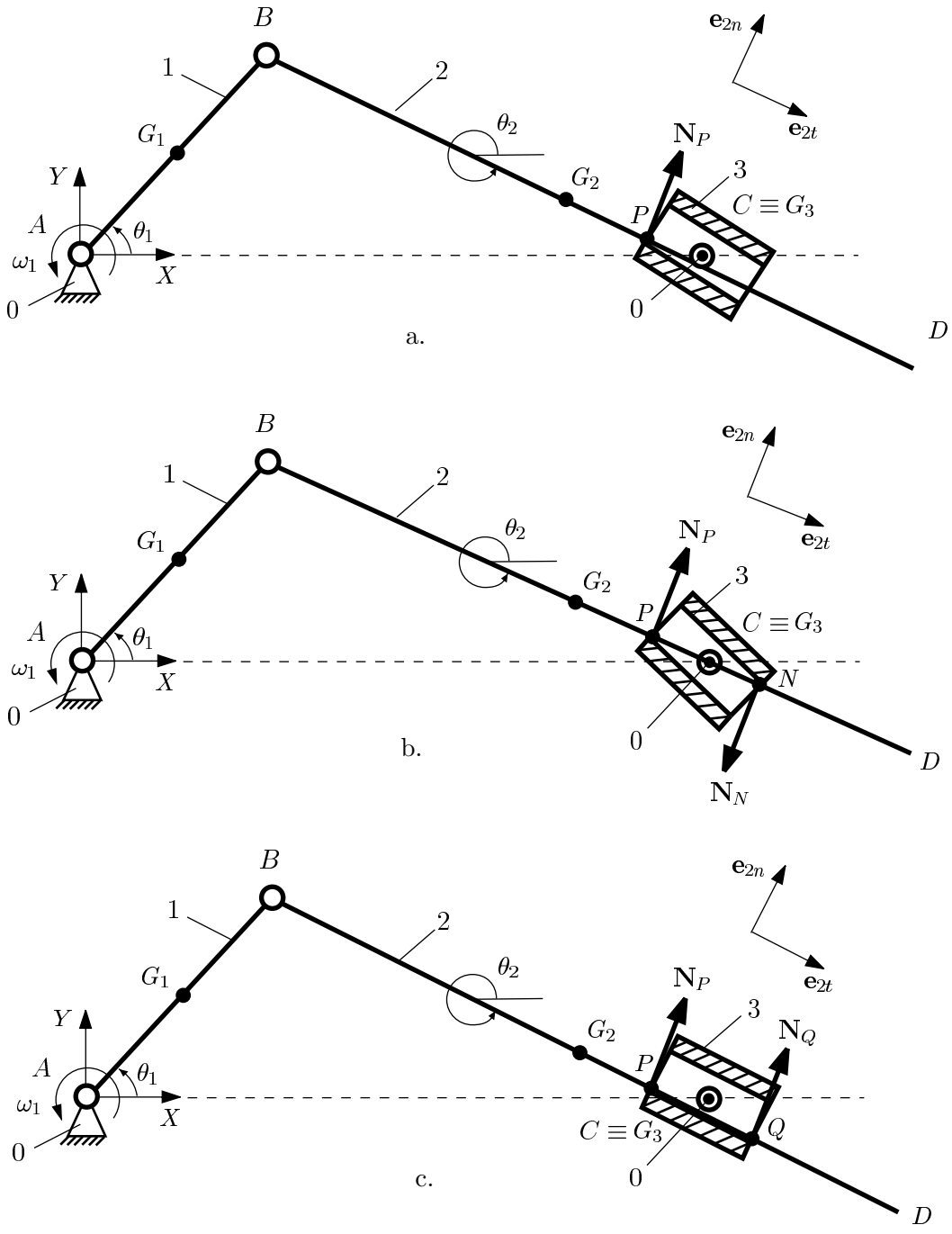

Figure 4.7: Geometry of the mechanism for: a. contact or impact on a single point; b. contact or impact on two opposed points; c. contact or impact on two points on the same side.

In order to take in consideration the reaction force N_P between the links 2 and 3 acting at the point P one can introduce a new generalized speed u_3 in the expression of the relative velocity $\mathbf{v}_{P_{23}}$

$$\mathbf{v}_{P_{23}} = \mathbf{v}_{P_2} - \mathbf{v}_{P_3} + u_3 \mathbf{e}_{2n}, \tag{4.90}$$

where $\mathbf{v}_{P_2} = \mathbf{v}_{G_2} + \boldsymbol{\omega}_2 \times (\mathbf{r}_P - \mathbf{r}_{G_2})$ and $\mathbf{v}_{P_3} = \boldsymbol{\omega}_3 \times (\mathbf{r}_P - \mathbf{r}_C)$.

The reaction force $\mathbf{N}_P$ of the link 3 on the link 2 is

$$\mathbf{N}_P = N_P \mathbf{e}_{2n}. \tag{4.91}$$

The friction force $\mathbf{F}_{f_P}$ that acts on the link 2 at the point P is

$$\mathbf{F}_{f_P} = -\frac{\mathbf{v}_P}{|\mathbf{v}_P|} \mu_k N. \tag{4.92}$$

The generalized forces Q_j, for $j = 1, 2, 3$, can be computed as

$$Q_j = \sum_{i=1}^{3} \frac{\partial \mathbf{v}_{G_i}}{\partial u_j} \cdot \mathbf{G}_i + \frac{\partial \mathbf{v}_{P_2}}{\partial u_j} \cdot (\mathbf{N}_P + \mathbf{F}_{f_P}) + \frac{\partial \mathbf{v}_{P_3}}{\partial u_j} \cdot (-\mathbf{N}_P - \mathbf{F}_{f_P}) + \frac{\partial \boldsymbol{\omega}_1}{\partial u_j} \cdot \mathbf{M}_m. \tag{4.93}$$

The generalized inertia forces F_j^*, for $j = 1, 2, 3$, can be written as

$$F_j^* = \sum_{i=1}^{3} \frac{\partial \mathbf{v}_{G_i}}{\partial u_j} \cdot (-m_i \mathbf{a}_{G_i}) + \sum_{i=1}^{3} \frac{\partial \boldsymbol{\omega}_i}{\partial u_j} \cdot (-I_{G_i} \boldsymbol{\alpha}_i). \tag{4.94}$$

One can write three Kane equations associated to the generalized speeds u_j, for $j = 1, 2, 3$

$$F_j^* + Q_j = 0. \tag{4.95}$$

From Eqs. (4.113) and (4.120) one can find the equation of motion for the mechanism and the reaction force N.

4.4.5 Impact on a single point

Next, the mechanism with three generalized coordinates is considered (Fig. 4.7.a). One can choose $q_3 = \theta_3$ as the third generalized coordinate. To derive the equation of motion for the impact, an integrated form of the Lagrange's equations is used

$$\left(\frac{\partial T}{\partial \dot{q}_i}\right)_{t_s} - \left(\frac{\partial T}{\partial \dot{q}_i}\right)_{t_a} = P_i, \quad i = 1, 2, 3 \tag{4.96}$$

where T is the kinetic energy, $\dot{q}_i$ is the velocity associated with the generalized coordinate q_i, P_i is the generalized impulse associated with the coordinate q_i, and t_a, t_s are the times of approach and separation for the impact.

The kinetic energy T_3 for the link 3 is

$$T_3 = \frac{1}{2} I_{G_3} \boldsymbol{\omega}_3 \cdot \boldsymbol{\omega}_3 = \frac{1}{2} I_{G_3} \dot{q}_3^2, \tag{4.97}$$

where $\boldsymbol{\omega}_3 = \dot{q}_3 \mathbf{k}$.

The kinetic energy T is

$$T = T_1 + T_2 + T_3. \tag{4.98}$$

One can write the left hand sides of Eq. (4.96) as

$$\left(\frac{\partial T}{\partial \dot{q}_i}\right)_{t_s} - \left(\frac{\partial T}{\partial \dot{q}_i}\right)_{t_a} = \left.\frac{\partial T}{\partial \dot{q}_i}\right/_{\dot{q}_i = \Omega_i - \omega_i}, \ i = 1, 2, 3 \tag{4.99}$$

where $\omega_i = \omega_i(t_a) = \dot{q}_i(t_a)$ and $\Omega_i = \omega_i(t_s) = \dot{q}_i(t_s)$ are the angular velocities associated with the coordinates q_i before and after the impact.

One can express the position vector $\mathbf{r}_P$ of the impact point $P(x_P, y_P)$ solving the system of equations

$$\tan q_2 = \frac{y_B - y_P}{x_B - x_P}, \ \ \tan q_3 = \frac{y_C - y_P}{x_C - x_P}. \tag{4.100}$$

The velocity vector of the impact point P is $\mathbf{v}_P = \dot{\mathbf{r}}_P$.

The generalized impulses (right-hand sides of Eq. (4.96)) can be written as

$$P_i = \frac{\partial \mathbf{v}_P}{\partial \dot{q}_i} \cdot (F_n \mathbf{e}_{2n} + F_t \mathbf{e}_{2t}), \ i = 1, 2, 3 \tag{4.101}$$

where $\mathbf{e}_{2n} = -\sin q_2 \mathbf{\imath} + \cos q_2 \mathbf{\jmath}$ and $\mathbf{e}_{2t} = \cos q_2 \mathbf{\imath} + \sin q_2 \mathbf{\jmath}$ are the unit vectors normal and tangential to the contact surface, and F_n, F_t are the normal and the tangential components of the impulse momentum F.

For the link 1, one can write

$$\begin{aligned} &\left(\frac{m_1 L_1^2}{4} + m_2 L_1^2 + I_{G_1}\right)(\Omega_1 - \omega_1) + \frac{1}{2} m_2 L_1 L_2 (\Omega_2 - \omega_2) \\ &\cos(q_2 - q_1) = P_1. \end{aligned} \tag{4.102}$$

For the link 2 one can write

$$\left(\frac{m_2 L_2^2}{4} + I_{G_2}\right)(\Omega_2 - \omega_2) + \frac{1}{2} m_2 L_1 L_2 (\Omega_1 - \omega_1) \cos(q_2 - q_1) = P_2. \tag{4.103}$$

For the link 3 one can write

$$I_{G_3}(\Omega_3 - \omega_3) = P_3. \tag{4.104}$$

The velocities $\mathbf{v}_{P_2}$ and $\mathbf{v}_{P_3}$ of the contact points P_2 and P_3 located on the links 2 and 3 can be expressed as

$$\begin{aligned} \mathbf{v}_{P_2} &= \mathbf{v}_B + \dot{q}_2 \mathbf{k} \times \mathbf{BP}, \\ \mathbf{v}_{P_3} &= \dot{q}_3 \mathbf{k} \times \mathbf{CP}, \end{aligned} \tag{4.105}$$

where $\mathbf{v}_B = \dot{\mathbf{r}}_B$ is the linear velocity of the joint B, and $\mathbf{CP} = \mathbf{r}_P - AC\mathbf{1}$.

One can write the velocity of approach $\mathbf{v}_a$ and separation $\mathbf{v}_s$ for the impact as

$$\mathbf{v}_a = \mathbf{v}_{P_2}(t_a) - \mathbf{v}_{P_3}(t_a), \ \mathbf{v}_s = \mathbf{v}_{P_2}(t_s) - \mathbf{v}_{P_3}(t_s). \tag{4.106}$$

From the definition of the coefficient of restitution e, one can write

$$e = -\frac{v_{sn}}{v_{an}}, \tag{4.107}$$

where $v_{an} = \mathbf{v}_a \cdot \mathbf{e}_{2n}$ and $v_{sn} = \mathbf{v}_s \cdot \mathbf{e}_{2n}$ are the projections of the linear velocities of approach and separation $\mathbf{v}_a$ and $\mathbf{v}_s$ on the normal direction $\mathbf{e}_{2n}$.

The tangential component $\mathbf{v}_{st}$ of the velocity of separation vector $\mathbf{v}_s$ can be expressed as

$$\mathbf{v}_{st} = (\mathbf{v}_s \cdot \mathbf{e}_{2t})\mathbf{e}_{2t}. \tag{4.108}$$

There are two cases of impact with friction at the point P:

1. No slipping. The following condition must be satisfied

$$\left| \frac{F_t}{F_n} \right| < \mu_s. \tag{4.109}$$

In this case, the velocity vector $\mathbf{v}_{st}$ is zero

$$\mathbf{v}_{st} = \mathbf{0}. \tag{4.110}$$

From Eqs. (4.102), (4.103), (4.104), (4.107), and (4.110) one can find the unknown variables F_n, F_t, and Ω_i, $i = 1, 2, 3$.

2. Slipping. The following condition must be satisfied

$$\left|\frac{F_t}{F_n}\right| > \mu_s. \tag{4.111}$$

In this case, the following relation can be written

$$F_t \mathbf{e}_{2n} = -\frac{\mathbf{v}_{st}}{|\mathbf{v}_{st}|}\mu_k \left|F_n\right|. \tag{4.112}$$

From Eqs. (4.102), (4.103), (4.104), (4.107), and (4.112) one can find the unknown variables F_n, F_t, and Ω_i, $i = 1, 2, 3$.

4.4.6 Contact on two opposed points

In this case, the mechanism has one degree of freedom. One can chose $q_1 = \theta_1$ as the generalized coordinate (Fig. 4.7.b). Kane's equations are used and the equation of motion is derived.

One can chose the generalized speed

$$u_1 = \dot{q}_1. \tag{4.113}$$

One can write the position vector $\mathbf{r}_N$ of the contact point $N(x_N, y_N)$ as

$$\mathbf{r}_N = \mathbf{r}_P + 2r\mathbf{e}_{2t}. \tag{4.114}$$

There are two contact points between the link 2 and the link 3, those are P and N. In order to take in consideration the reaction forces N_P and N_N acting at the points P and N one can introduce the generalized speeds u_2 and u_3 in the expressions of the relative velocities $\mathbf{v}_{P_{23}}$ and $\mathbf{v}_{N_{23}}$

$$\mathbf{v}_{P_{23}} = \mathbf{v}_{P_2} - \mathbf{v}_{P_3} + u_2\mathbf{e}_{2n},\ \mathbf{v}_{N_{23}} = \mathbf{v}_{N_2} - \mathbf{v}_{N_3} + u_3\mathbf{e}_{2n}, \tag{4.115}$$

where $\mathbf{v}_{P_2} = \mathbf{v}_{G_2} + \boldsymbol{\omega}_2 \times (\mathbf{r}_P - \mathbf{r}_{G_2})$, $\mathbf{v}_{P_3} = \boldsymbol{\omega}_3 \times (\mathbf{r}_P - \mathbf{r}_C)$, $\mathbf{v}_{N_2} = \mathbf{v}_{G_2} + \boldsymbol{\omega}_2 \times (\mathbf{r}_N - \mathbf{r}_{G_2})$, and $\mathbf{v}_{N_3} = \boldsymbol{\omega}_3 \times (\mathbf{r}_N - \mathbf{r}_C)$.

The reaction forces $\mathbf{N}_P$ and $\mathbf{N}_N$ of the link 3 on the link 2 at the points P and N are

$$\mathbf{N}_P = N_P\mathbf{e}_{2n},\ \mathbf{N}_N = N_N\mathbf{e}_{2n}. \tag{4.116}$$

The friction forces $\mathbf{F}_{f_P}$ and $\mathbf{F}_{f_N}$ that act on the link 2 at the points P and N are

$$\mathbf{F}_{f_P} = -\frac{\mathbf{v}_P}{|\mathbf{v}_P|}\mu_k N_P,\ \mathbf{F}_{f_N} = -\frac{\mathbf{v}_N}{|\mathbf{v}_N|}\mu_k N_N. \tag{4.117}$$

The generalized forces Q_j, for $j = 1, 2, 3$, can be computed as

$$\begin{aligned} Q_j = \sum_{i=1}^{3} \frac{\partial \mathbf{v}_{G_i}}{\partial u_j} \cdot \mathbf{G}_i + \frac{\partial \mathbf{v}_{P_2}}{\partial u_j} \cdot (\mathbf{N}_P + \mathbf{F}_{f_P}) + \frac{\partial \mathbf{v}_{P_3}}{\partial u_j} \cdot (-\mathbf{N}_P - \mathbf{F}_{f_P}) \\ + \frac{\partial \mathbf{v}_{N_2}}{\partial u_j} \cdot (\mathbf{N}_N + \mathbf{F}_{f_N}) + \frac{\partial \mathbf{v}_{N_3}}{\partial u_j} \cdot (-\mathbf{N}_N - \mathbf{F}_{f_N}) + \frac{\partial \boldsymbol{\omega}_1}{\partial u_j} \cdot \mathbf{M}_m. \end{aligned} \tag{4.118}$$

The generalized inertia forces F_j^*, for $j = 1, 2, 3$, can be written as

$$F_j^* = \sum_{i=1}^{3} \frac{\partial \mathbf{v}_{G_i}}{\partial u_j} \cdot (-m_i \mathbf{a}_{G_i}) + \sum_{i=1}^{3} \frac{\partial \boldsymbol{\omega}_i}{\partial u_j} \cdot (-I_{G_i} \boldsymbol{\alpha}_i). \tag{4.119}$$

One can write three Kane equations associated to the generalized speeds u_j, for $j = 1, 2, 3$

$$F_j^* + Q_j = 0. \tag{4.120}$$

From Eqs. (4.113) and (4.120) one can find the equation of motion for the mechanism and the reaction forces N_P and N_N.

4.4.7 Impact on two opposed points

In this case, the mechanism has three generalized coordinates (Fig. 4.7.b). The link 2 impacts the link 3 simultaneously in two points, those are $P(x_P, y_P)$ and $N(x_N, y_N)$. One can express the position vectors $\mathbf{r}_P$ and $\mathbf{r}_N$ of the impact points $P(x_P, y_P)$ and $N(x_N, y_N)$ solving the system of equations

$$\tan q_2 = \frac{y_B - y}{x_B - x},\ (x_C - x)^2 + (y_C - y)^2 = r^2. \tag{4.121}$$

The velocity vectors of the impact points P and N are $\mathbf{v}_P = \dot{\mathbf{r}}_P$ and $\mathbf{v}_N = \dot{\mathbf{r}}_N$.
The generalized impulses can be written as

$$P_i = \frac{\partial \mathbf{v}_P}{\partial \dot{q}_i} \cdot (F_{In} \mathbf{e}_{2n} + F_{It} \mathbf{e}_{2t}) + \frac{\partial \mathbf{v}_N}{\partial \dot{q}_i} \cdot (F_{IIn} \mathbf{e}_{2n} + F_{IIt} \mathbf{e}_{2t}),\ i = 1, 2, 3, \tag{4.122}$$

where F_{In}, F_{It} and F_{IIn}, F_{IIt} are the normal and the tangential components of the impulse momenta F_I and F_{II}.

The velocities $\mathbf{v}_{N_2}$ and $\mathbf{v}_{N_3}$ of the contact points N_2 and N_3 located on the links 2 and 3 can be expressed as

$$\mathbf{v}_{N_2} = \mathbf{v}_B + \dot{q}_2 \mathbf{k} \times \mathbf{BN},\ \mathbf{v}_{N_3} = \dot{\theta}_3 \mathbf{k} \times \mathbf{CN}, \tag{4.123}$$

where $\mathbf{CN} = \mathbf{r}_N - AC\mathbf{\imath}$.

One can write the velocities of approach $\mathbf{v}_{Ia}$, $\mathbf{v}_{IIa}$ and separation $\mathbf{v}_{Is}$, $\mathbf{v}_{IIs}$ for the impact points P and N as

$$\begin{aligned} &\mathbf{v}_{Ia} = \mathbf{v}_{P_2}(t_a) - \mathbf{v}_{P_3}(t_a),\ \mathbf{v}_{IIa} = \mathbf{v}_{N_2}(t_a) - \mathbf{v}_{N_3}(t_a), \\ &\mathbf{v}_{Is} = \mathbf{v}_{P_2}(t_s) - \mathbf{v}_{P_3}(t_s),\ \mathbf{v}_{IIs} = \mathbf{v}_{N_2}(t_s) - \mathbf{v}_{N_3}(t_s). \end{aligned} \tag{4.124}$$

From the definition of the coefficient of restitution e, one can write

$$e = -\frac{v_{Isn}}{v_{Ian}},\ e = -\frac{v_{IIsn}}{v_{IIan}}, \tag{4.125}$$

where $v_{Ian} = \mathbf{v}_{Ia} \cdot \mathbf{e}_{2n}$, $v_{Isn} = \mathbf{v}_{Is} \cdot \mathbf{e}_{2n}$, $v_{IIan} = \mathbf{v}_{IIa} \cdot \mathbf{e}_{2n}$, and $v_{IIsn} = \mathbf{v}_{IIs} \cdot \mathbf{e}_{2n}$.

The tangential components $\mathbf{v}_{Ist}$ and $\mathbf{v}_{IIst}$ of the velocity of separation vectors $\mathbf{v}_{Is}$ and $\mathbf{v}_{IIs}$ can be expressed as

$$\mathbf{v}_{Ist} = (\mathbf{v}_{Is} \cdot \mathbf{e}_{2t})\mathbf{e}_{2t},\ \mathbf{v}_{IIst} = (\mathbf{v}_{IIs} \cdot \mathbf{e}_{2t})\mathbf{e}_{2t}. \tag{4.126}$$

There are two cases of impact with friction:

1. No slipping. The following two conditions must be satisfied

$$\left|\frac{F_{It}}{F_{In}}\right| < \mu_s \text{ and } \left|\frac{F_{IIt}}{F_{IIn}}\right| < \mu_s. \tag{4.127}$$

In this case, the velocity vectors $\mathbf{v}_{Ist}$ and $\mathbf{v}_{IIst}$ are zero

$$\mathbf{v}_{Ist} = \mathbf{v}_{IIst} = \mathbf{0}. \tag{4.128}$$

From Eqs. (4.102), (4.103), (4.125), and (4.128) one can find the unknown variables F_{In}, F_{It}, F_{IIn}, F_{IIt}, and Ω_i, $i = 1, 2, 3$.

2. Slipping. One of the following conditions must be satisfied

$$\left|\frac{F_{It}}{F_{In}}\right| > \mu_s \text{ or } \left|\frac{F_{IIt}}{F_{IIn}}\right| > \mu_s. \tag{4.129}$$

In this case, the following two relations can be written

$$F_{It}\mathbf{e}_{2n} = -\frac{\mathbf{v}_{Ist}}{|\mathbf{v}_{Ist}|}\mu_k \left|F_{In}\right|, \; F_{IIt}\mathbf{e}_{2n} = -\frac{\mathbf{v}_{IIst}}{|\mathbf{v}_{IIst}|}\mu_k \left|F_{IIn}\right|. \tag{4.130}$$

From Eqs. (4.102), (4.103), 4.125), and (4.130) one can find the unknown variables F_{In}, F_{It}, F_{IIn}, F_{IIt}, and Ω_i, $i = 1, 2, 3$.

4.4.8 Contact or impact on two points on the same side

Considering the endpoints, the line contact is kinematically equivalent to two point contact along a line segment [46]. Thus, this case is similar to the case c) for contact or impact on two opposite points (Fig. 4.7.c).

4.5 Working Model and Mathematica simulations

For this section, the mechanism shown in Fig. 4.6 is considered. The numerical results obtained solving the equation of motion for the mechanism using *Mathematica* and data captured from the *Working Model* simulation are compared.

In order to compare the results, the initial conditions used in *Mathematica* are used as input data in *Working Model*. For example, one can set up the variable torque M of the motor in the "Properties" window from "Window" menu by choosing the motor type "Torque" and introducing the value $M = M_0(1-\omega/\omega_0)$, where M_0, ω_0 are constant and ω is the rotational velocity of the driver link (see Fig. 4.8). The graph of the torque M can be visualized by selecting the command "Torque transmitted" from "Measure" menu.

Data from Working Model graphs can be exported choosing the command "Export..." from "File" menu. The data is exported in a plain text file for the desired interval of time and accuracy. This way, the data can be imported and analyzed using various tools. In this case, the simulated data for the motor torque M is exported from *Working Model* and imported in a *Mathematica* program. To import a file in a *Mathematica* program, one can use the command `Import["file", "format"]` which imports data in the specified file format from a file and converts it to a Mathematica expression. For example, if the *Working Model* exported file name is `torque.dta`, the command to import the file in *Mathematica* can be `Import["torque.dta", "Table"]`. Also, the motor torque M can be computed solving the equation of motion using *Mathematica*. In our case, the Lagrange method was used. For a given interval of time, the torque M is computed using *Mathematica* (M_c), and captured from the *Working Model* simulation

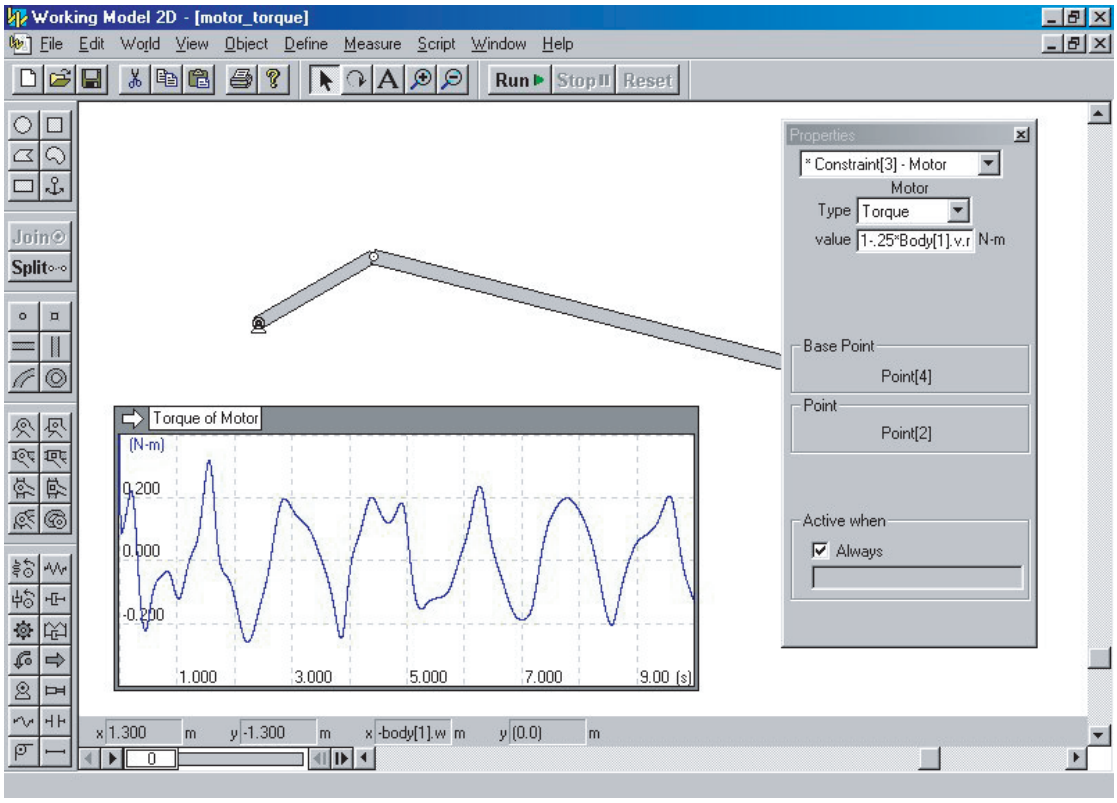

Figure 4.8: Working Model simulation of the driver motor torque for the double pendulum.

(M_s). The graphs of the torques M_c and M_s are compared in Fig. 4.9. The error $err(t)$ between the numerical data $M_c(t)$ and $M_s(t)$ at the time t can be computed as

$$err(t) = |M_c(t) - M_s(t)|.$$

The relative maximal error err^{rel}_{max} can be calculated as

$$err^{rel}_{max} = \frac{\max_{t\in[t_i,t_f]} err(t)}{M_0} \cdot 100,$$

where $[t_i, t_f]$ is the time interval used for the analysis.
In our case, the value of the relative maximal error is computed with the *Mathematica* program shown in Appendix A as $err^{rel}_{max} = 4.5\%$.

4.6 Results

In this section, results from computer simulations are presented using analysis tools. In Fig. 4.4 the mechanism with slider clearance is shown. The masses of the links are $m_1 = 0.008$ kg, $m_2 = 0.038$ kg, and $m_3 = 0.015$ kg. The mass moments of inertia for the links are $I_{G_1} = 6.733 \times 10^{-6}$ Kg m^3, $I_{G_2} = 6.925 \times 10^{-4}$ Kg m^3, and $I_{G_3} = 2.220 \times 10^{-6}$ Kg m^3. The lengths of links are L_1=0.1 m, L_2=0.47 m, and $L_3 = 0.047$ m. The nominal width of the slider (link 3) is $l_3 = 0.025$ m. The distance between the pin joints A and C is $AC = 0.28$ m. The kinetic coefficient of friction μ_k=0.3, the static coefficient of friction μ_s=0.35, and the coefficient of restitution $e = 0.4$ are used. These values are constant through the investigation. The analysis is performed for different values of the

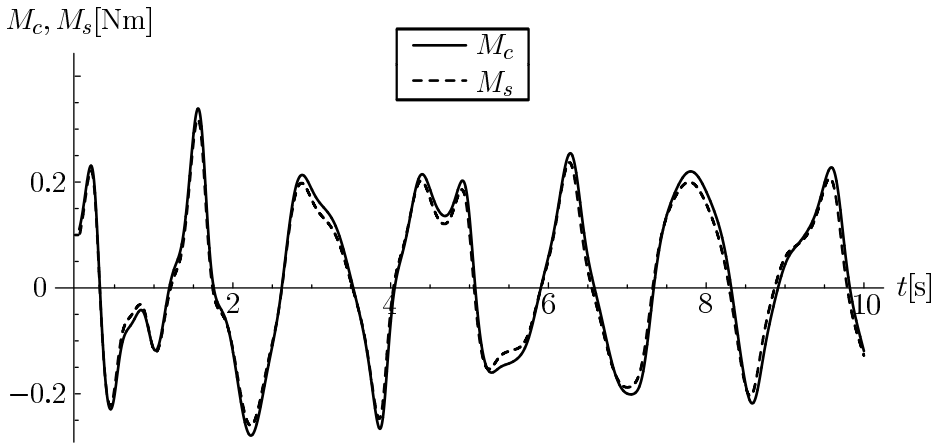

Figure 4.9: Comparison of simulation results obtained using Mathematica and Working Model.

clearance c, varying the nominal angular velocity of the link 1, ω_{10}. The torque of the motor acting at joint A is chosen as $M_m = M_0(1 - \omega_1/\omega_{10})$, where $M_0 = 1$ Nm.

Figure 4.10.a shows the vertical trajectory for the center of mass G_2 of the link 2, y_{G_2}, in the state space for zero clearance (c=0 mm). On the three-dimensional graphic, the coordinate of the position $y_{G_2}(t)$ is plotted along the coordinate $y_{G_2}(t+T)$ and the coordinate $y_{G_2}(t+2T)$, where $T = 3$ is the time lag. The trajectory is a closed loop and the motion is periodic. In this case, the largest Lyapunov exponent is $\lambda = 0$ and all the other exponents are less than zero, that is, a periodic orbit.

Figure 4.10.b shows the vertical trajectory y_{G_2} in the state space for nonzero clearance c=1 mm, and ω_{10} = 200 rpm. The curve is not closed, that is, an unstable orbit. The largest Lyapunov exponent calculated is positive, denoting the chaotic behavior of the system.

Next the largest Lyapunov exponent is computed for a set of simulation results for different values of the nominal angular velocity of the crank: ω_{10}=50 rpm, ω_{10}=100 rpm, ω_{10}=150 rpm, and ω_{10}=200 rpm. Figure 4.11 shows the results for the clearances: c=0.5 mm (Fig. 4.11.a), c=1 mm (Fig. 4.11.b), and c=1.5 mm (Fig. 4.11.c). For constant clearance (c=constant), and for larger values of the nominal angular velocity ω_{10} one can obtain larger values of the Lyapunov exponent λ. For c=0.5 mm, ω_{10}=50 rpm, it results λ=20.54, and for c=0.5 mm, ω_{10}=200 rpm, it results λ=26.55. Also, for constant nominal angular velocity (ω_{10}=constant), and for larger values of the clearance c one can obtain larger values of the Lyapunov exponent λ. For ω_{10}=100 rpm, c=0.5 mm, it results λ=24.66, and for ω_{10}=100 rpm, c=1.5 mm, it results λ=28.90.

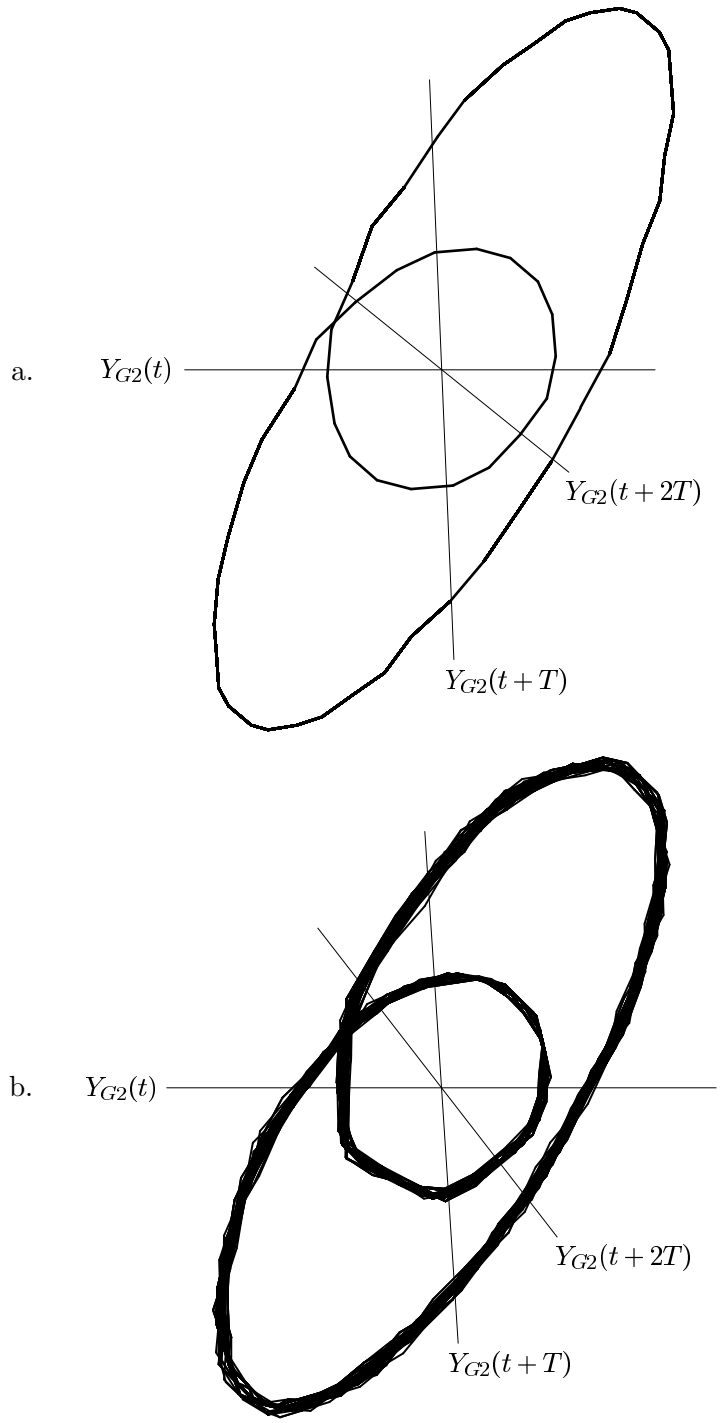

Figure 4.10: Trajectory of the vertical coordinate y_{G_2} in the state space for: a. zero clearance ($c = 0$ mm); b. nonzero clearance ($c = 1$ mm).

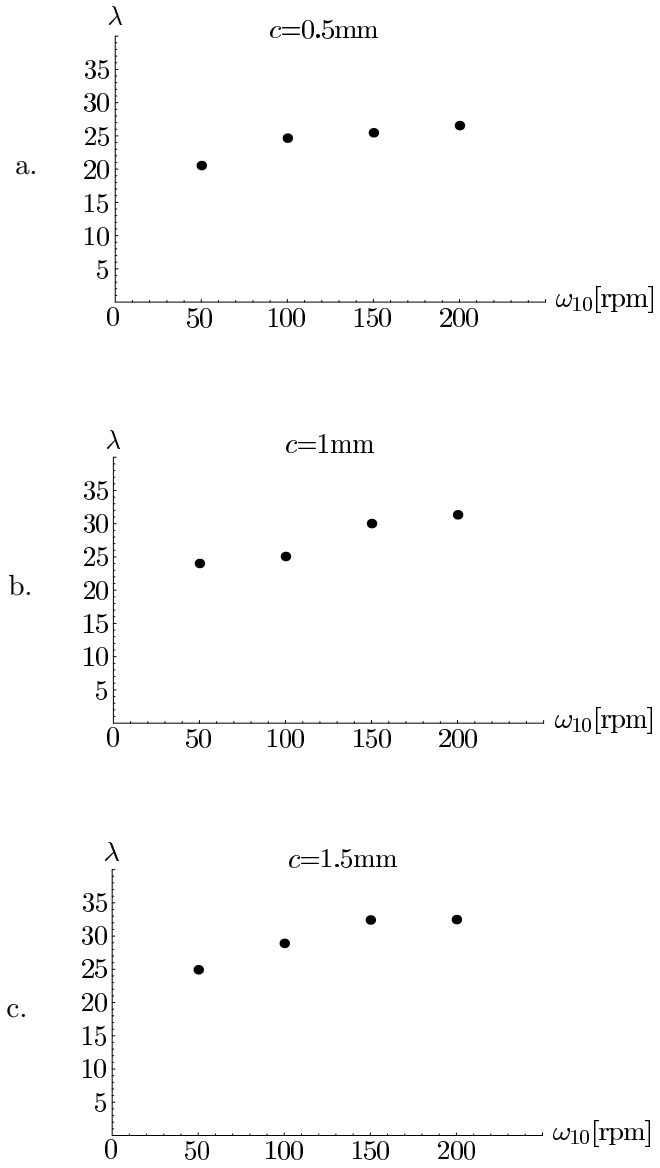

Figure 4.11: Largest Lyapunov exponent computed for a set of values of the nominal angular velocity ω_{10} and for the clearances: a. $c = 0.5$ mm; b. $c = 1$ mm; c. $c = 1.5$ mm.

4.7 Conclusions

The dynamic analysis of a planar mechanism with clearance at the sliding joint is presented. The mathematical model shows that either of four possible contact modes can occur during motion, and the conditions for switching from one case to another. Either contacts or impacts are detected at the contact points between the connecting rod and the slider.

The results present the influence of the slider clearance and the crank speed on the stability of the system. The Lyapunov exponents are computed for the simulated data and used as a diagnostic tool. For the mechanism with no clearance, the motion is periodic. Chaotic motion is observed for the mechanism with slider clearance. The largest Lyapunov exponents are compared for different crank speeds at different values of the clearance. For a constant value of the clearance, larger Lyapunov exponents correspond to higher crank speeds.

Chapter 5

Structural synthesis of spatial mechanisms

A new structural synthesis of spatial mechanisms is studied based on the system group classification. New spatial system groups of different families with one, two, and three independent contours are presented. Several structure configurations of system groups with the same number of independent contours can be obtained for a given family. The advantage of the analysis of spatial mechanisms based on the system group classification lies in its simplicity. The solution of mechanisms can be obtained by composing the partial solutions of system groups.

5.1 Introduction

Structural synthesis of mechanisms with the specified number of contours and joint types is necessary in order to systematize the creative design process. The structural synthesis of mechanisms was accomplished using the graph theory [58, 59]. Tsai [60] applied the graph theory, combinatorial analysis, and computer algorithms to systematically enumerate all possible mechanism topologies having same degrees of freedom and joint types. Belfiore and Pennestri [61] elaborated a method for automatically drawing kinematic chains with specified number of contours using the graph theory. Sen and Mruthynjaya [62] studied the singularities in the workspace of planar closed-loop manipulators. The singularities are determined using the centers of rotation for closed kinematic chains with two degrees of freedom. A classification of Assur groups with multiple joints is presented by Jinkui and Weiqing [63]. Designers also generated collections of

mechanisms classified according to their functional characteristics[64]. Using the theory of symmetric groups, Tuttle and Peterson [65] generated planar linkages by contraction and expansion on a base structure. Huang and Huang [66] described a computer-aided method to generate planar kinematic chains using the approach of contracted link adjacency matrix. The methodology developed by Chiou and Kota [67] systematically generates alternate mechanism concepts using symbolic matrices and constraint vectors representing a library of mechanisms building blocks. Rao and Deshmukh [68] presented a method to generate distinct kinematic chains that does not require the test of isomorphism. Shen, Ting and Yang [69] offers a general and versatile method to identify the possible configurations up to twenty-nine types of basic kinematic chains containing up to four independent contours. A method of computer-aided structure synthesis of multi-loop three-dimensional kinematic chains was presented by Shujun [70]. Structural synthesis of planar and spatial mechanisms with bars was studied by Popescu and Ungureanu [71].

Given the required inputs to any single or multiple degree of freedom mechanism, the mechanism can always be decomposed into system groups. The advantage of the system group classification lies in the fact that the global solution can be obtained by composing the partial solutions. Using subroutines for the system groups the spatial mechanisms can be analyzed in a systematic way. The purpose of this article is to offer a general method to determine all the configurations of complex spatial system groups and to automate the process. Spatial mechanisms can always be decomposed into system groups. The solution of mechanisms can be obtained by composing the partial solutions of system groups.

5.2 Degree of freedom and family

The number of independent coordinates that uniquely determine the relative position of two links connected by a joint is called the degree of freedom of the joint. Alternatively, the term *joint class* is introduced. A joint is called of the j-th class if it diminishes the relative motion of a rigid linked bodies by j degrees of freedom (i.e., j scalar constraint conditions correspond to the given kinematic pair). It follows that such a joint has $(6j)$ independent coordinates.

The *family* f of a mechanism is the number of degrees of freedom that are eliminated from all the links of the system. A free body in space has six degrees of freedom. A system of family f consisting of n movable links has $(6-f)n$ degrees of freedom. Each joint of class j diminishes the freedom of motion of the system by $(j-f)$ degrees of freedom. Denoting the number of joints of class k as c_k, it follows that the number of degrees of freedom M of a particular system is

$$M = (6-f)n - \sum_{j=f+1}^{5} (j-f)c_j. \tag{5.1}$$

In the literature this is referred to as the Dobrovolski formula.

For the general case of planar mechanisms, mechanisms of family $f = 3$, the number of degrees of freedom M is calculated as

$$M = 3n - \sum_{j=4}^{5}(j-3)c_j = 3n - 2c_5 - c_4, \tag{5.2}$$

where n is the number of moving links, c_5 is the number of full joints, and c_4 is the number of half joints. The most common types of planar and spatial joints are shown

in Fig. 5.1. Two planar joints of the class 5 (one degree of freedom joints) are shown, a slider joint in Fig. 5.1.a and a pin joint in Fig. 5.1.b. Figure 5.1.c represents a cylindrical joint of the class 4 (two degrees of freedom joints). A spherical joint of the class 3 (three degree of freedom joints) is shown in Fig. 5.1.d.

Of special interest are the kinematic chains which do not change their degree of freedom after being connected to an arbitrary system. Kinematic chains defined this way are called *system groups*. A structurally new system can be created connecting them to or disconnecting them from a given system. For the case of planar systems, from Eq. (5.2) one can obtain

$$3n - 2c_5 = 0, \tag{5.3}$$

according to which the number of system group links n is always even. The simplest fundamental kinematic chain is the binary group with two links ($n = 2$) and three full joints ($c_5 = 3$). This binary group is called *dyad*.

The cartesian reference frame $xOyz$ is chosen for the mechanical systems (Fig.5. 2). The rotations about the axis are represented by R and the translations along the axis are represented by T.

5.3 Independent contours

A *contour* or *loop* is a configuration described by a polygon consisting of links connected by joints. The presence of loops can be used to determine the type of kinematic chains. Closed kinematic chains have one ore more loops so that each link and each joint is contained in at least one loop. A closed kinematic chain has no open attachment points.

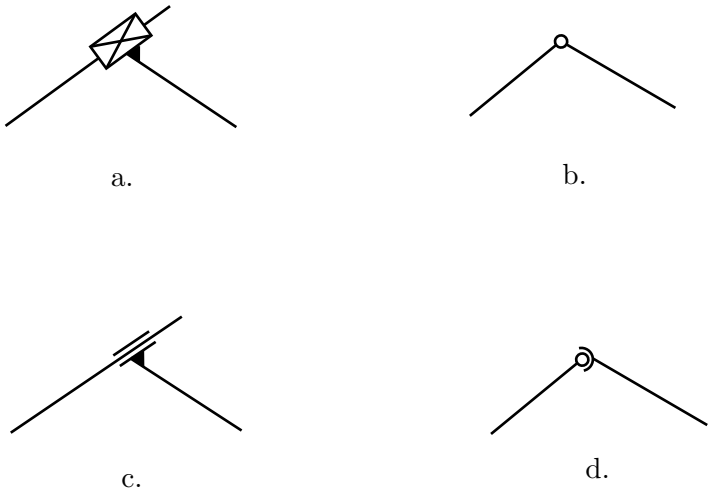

Figure 5.1: Types of joints: a. Slider joint (class 5); b. Pin joint (class 5); c. Cylindrical joint (class 4); d. Spherical joint (class 3).

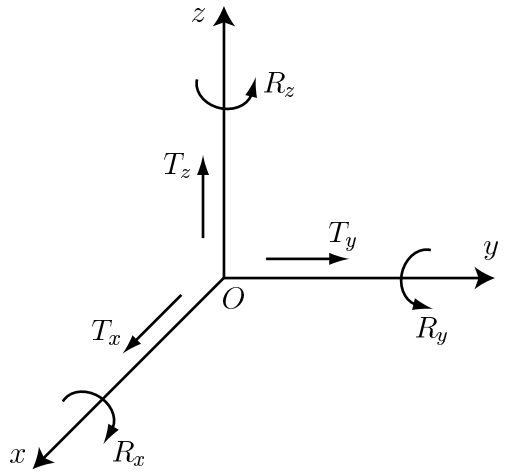

Figure 5.2: The cartesian spatial reference frame $xOyz$.

An open kinematic chain contains no loops. Mixed kinematic chains are a combination of closed and open kinematic chains.

A contour with at least one link that is not included in any other contour of the chain is called *independent contour*. The number of independent contours N of a kinematic chain can be computed as

$$N = c - n, \tag{5.4}$$

where c is the number of joints, and n is the number of moving links.

Planar kinematic chains are presented in Fig.5. 3. The kinematic chain shown in Fig. 5.3.a has two moving links 1 and 2 ($n = 2$), three joints ($c = 3$), and one independent contour ($N = c - n = 3 - 2 = 1$). This kinematic chain is a dyad. In Fig. 5.3.b, a new kinematic chain is obtained by connecting the free joint of the link 1 to the ground (link 0). In this case, the number of independent contours is also $N = c - n = 3 - 2 = 1$. The kinematic chain shown in Fig. 5.3.c has three moving links 1, 2, and 3 ($n = 3$), four joints ($c = 4$), and one independent contour ($N = c - n = 4 - 3 = 1$). A closed chain with three moving links 1, 2, and 3 ($n = 3$), and one fixed link 0, connected by four joints ($c = 4$) is shown in Fig. 5.3.d. This is a four-bar mechanism. In order to find the number of independent contours, only the of moving links are considered. Thus, there is one independent contour ($N = c - n = 4 - 3 = 1$). The kinematic chain presented in Fig. 5.3.e has four moving links 1, 2, 3, and 4 ($n = 4$), and six joints ($c = 6$). There are three contours: 1-2-3, 1-2-4, and 3-2-4. Only two contours are independent contours ($N = 6 - 4 = 2$).

Spatial kinematic chains are depicted in Fig. 5.4. The kinematic chain shown in Fig. 5.4.a has five links 1, 2, 3, 4, and 5 ($n = 5$), six joints ($c = 6$), and one independent

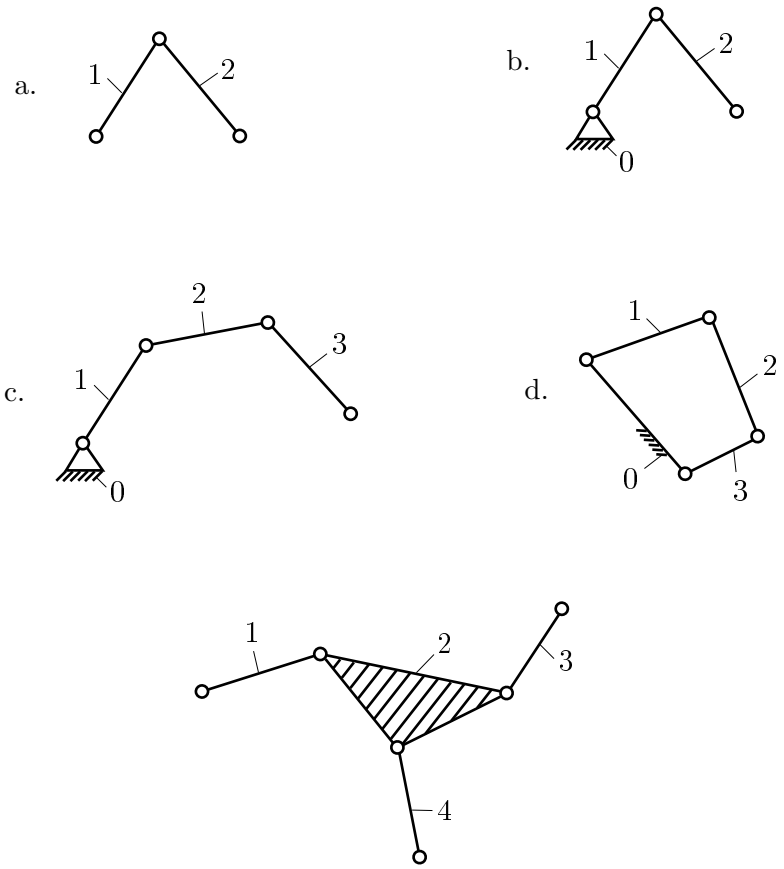

Figure 5.3: Planar kinematic chains.

contour ($N = c - n = 6 - 5 = 1$). For the spatial kinematic chain shown in Fig. 5.4.b, there are six links 1, 2, 3, 4, 5, and 6 ($n = 6$), eight joints ($c = 8$), and three contours 1-2-3-4-5, 1-2-3-6, and 5-4-3-6. In this case, two of the contours are independent contours ($N = c - n = 8 - 6 = 2$).

5.4 Spatial system groups

One can determine the system groups for spatial mechanisms by analogy to the system groups for the planar mechanisms. The system groups have the degree of freedom $M = 0$. All possible system groups can be determined for each family of chains.
For the family $f = 0$, for system groups, from Eqs. (5.1) and (5.4) the mobility is

$$M = 6n - 5c_5 - 4c_4 - 3c_3 - 2c_2 - c_1 = 0, \tag{5.5}$$

and the number of moving links is

$$n = c - N. \tag{5.6}$$

From Eqs. (5.5) and (5.6) one can express the number of joints of class 5 as

$$c_5 = 6N - 5c_1 - 4c_2 - 3c_3 - 2c_4, \tag{5.7}$$

and the number of moving links as

$$n = -N + c_1 + c_2 + c_3 + c_4 + c_5. \tag{5.8}$$

a.

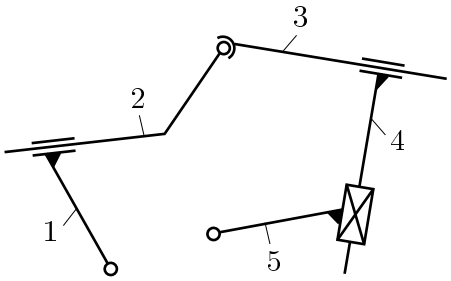

b.

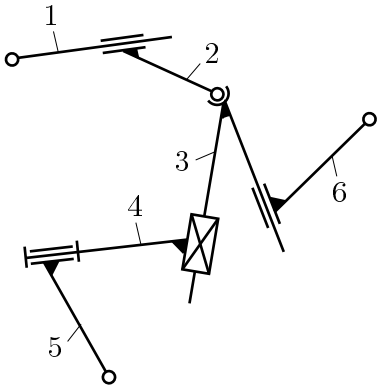

Figure 5.4: Spatial kinematic chains.

For the family $f = 1$, $c_1 = 0$ and it results

$$c_5 = 5N - 4c_2 - 3c_3 - 2c_4,\ n = -N + c_2 + c_3 + c_4 + c_5. \tag{5.9}$$

For the family $f = 2$, $c_1 = 0,\ c_2 = 0$ and it results

$$c_5 = 4N - 3c_3 - 2c_4,\ n = -N + c_3 + c_4 + c_5. \tag{5.10}$$

For the family $f = 3$, $c_1 = 0,\ c_2 = 0,\ c_3 = 0$ and it results

$$c_5 = 3N - 2c_4,\ n = -N + c_4 + c_5. \tag{5.11}$$

For the family $f = 4$, $c_1 = 0,\ c_2 = 0,\ c_3 = 0,\ c_4 = 0$ and it results

$$c_5 = 2N,\ n = -N + c_5. \tag{5.12}$$

Using the above conditions, all the possible solutions for spatial system groups can be determined. The number of joints $c_1,\ c_2,\ ,c_3$, and c_4 are cycled from 0 to w, where w is a positive integer, for system groups with one or more independent contours ($N \geq 1$). The number of joints c_5 and the number of moving links n are computed for each system group. An acceptable solution has to verify the conditions $n > 0$ and $c_5 > 0$. In Table 1, the number of possible solutions is presented for some values of w between 0 and 40 and for kinematic chains with one contour ($N = 1$), two contours ($N = 2$), and three contours ($N = 3$). For $N = 1$ and $w \geq 3$, there are 23 possible solutions. For $N = 2$, there are 85 solutions for $w \geq 6$, and for $N = 3$ there are 220 solutions for $w \geq 9$.

5.4.1 System groups with one independent contour

The combinations of spatial system groups with one independent contour ($N = 1$) are presented in Table 2. The number of joints $c_1,\ c_2,\ c_3$, and c_4 are cycled from 0 to 3, and the number of joints c_5 and the number of moving links n are computed. System groups from Table 2 are exemplified next for each of the families $f = 0,\ 1,\ 2,\ 3$, and 4.

For the family $f = 0$, four system groups are illustrated in Fig. 5.5. The values c_5 and n are computed from Eqs. (5.7) and (5.8), respectively. A spatial system group with no joints of class $1,\ 2,\ 3$, and 4 ($c_1 = c_2 = c_3 = c_4 = 0$) is shown in Fig. 5.5.a. The system group has six joints of class 5 ($c_5 = 6(1) = 6$), and five moving links ($n = -1 + 6 = 5$). A system group with one joint of class 4 ($c_4 = 1$) and no joints of class $1,\ 2$, and 3 ($c_1 = c_2 = c_3 = 0$) is shown in Fig. 5.5.b. The system group has four joints of class 5 ($c_5 = 6(1) - 2(1) = 4$), and four moving links ($n = -1 + 1 + 4 = 4$). A system group with two joints of class 4 ($c_4 = 2$) and no joints of class $1,\ 2$, and 3 ($c_1 = c_2 = c_3 = 0$) is shown in Fig. 5.5.c. The system group has two joints of class 5 ($c_5 = 6(1) - 2(2) = 2$), and four moving links ($n = -1 + 2 + 2 = 3$). A system group with one joint of class 3 ($c_3 = 1$) and no joints of class $1,\ 2$, and 4 ($c_1 = c_2 = c_4 = 0$) is shown in Fig. 5.5.d. The system group has three joints of class 5 ($c_5 = 6(1) - 3(1) = 3$), and three moving links ($n = -1 + 1 + 3 = 3$).

The spatial mechanism presented in Fig. 5.6 is built from the system group shown in Fig. 5.5.b. The mechanism has one degree of freedom ($M = 6n - 5c_5 - 4c_4 - 3c_3 - 2c_2 - c_1 = 6(5) - 5(5) - 4(1) = 1$). The driver link is the link 5. The relative linear velocities are symbolized by v_{ij} and the relative angular velocities are symbolized by ω_{ij}, where i and j

w	0	1	2	3	4	5	6	7	8	9	10	20	30
$N=1$	5	18	22	23	23	23	23	23	23	23	23	23	23
$N=2$	5	30	62	76	82	84	85	85	85	85	85	85	85
$N=3$	5	31	100	158	190	205	214	218	218	220	220	220	220

Table 5.1: The number of configurations of system groups with one, two and three independent contours ($N = 1$, 2, and 3)

Index	f	c_1	c_2	c_3	c_4	c_5	n
1	0	0	0	0	0	6	5
2	0	0	0	0	1	4	4
3	0	0	0	0	2	2	3
4	0	0	0	0	3	0	2
5	0	0	0	1	0	3	3
6	0	0	0	1	1	1	2
7	0	0	0	2	0	0	1
8	0	0	1	0	0	2	2
9	0	0	1	0	1	0	1
10	0	1	0	0	0	1	1
11	1	0	0	0	0	5	4
12	1	0	0	0	1	3	3
13	1	0	0	0	2	1	2
14	1	0	0	1	0	2	2
15	1	0	0	1	1	0	1
16	1	0	1	0	0	1	1
17	2	0	0	0	0	4	3
18	2	0	0	0	1	2	2
19	2	0	0	0	2	0	1
20	2	0	0	1	0	1	1
21	3	0	0	0	0	3	2
22	3	0	0	0	1	1	1
23	4	0	0	0	0	2	1

Table 5.2: The configurations of system groups with one independent contour ($N = 1$)

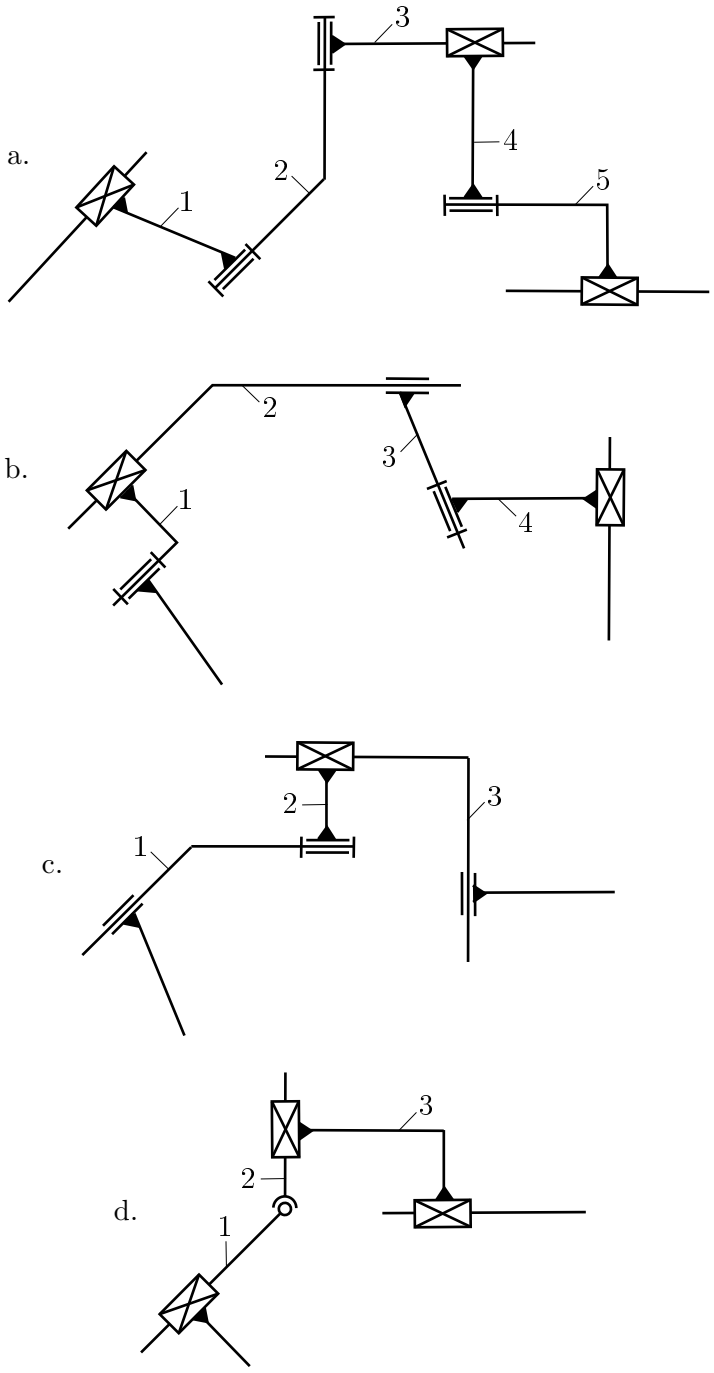

Figure 5.5: System groups with one independent contour ($N = 1$) of the family $f = 0$.

are the numbered links. Only one relative velocity is represented on the reference frame in order to show that the respective motion exists.

For the family $f = 1$, three systems groups are depicted in Fig. 5.7. The values c_5 and n are computed from Eq. (5.9). The missing translations and rotations with respect to the axis of the reference frame $xOyz$ are specified further on for each system group. A spatial system group with no joints of class 1, 2, 3, and 4 ($c_1 = c_2 = c_3 = c_4 = 0$) is shown in Fig. 5.7.a. The system group has five joints of class 5 ($c_5 = 5(1) = 5$), and four moving links ($n = -1 + 5 = 4$). There are no rotations R_x for the links. A system group with no joints of class 1, 2, and 3 ($c_1 = c_2 = c_3 = 0$) and one joint of class 4 ($c_4 = 1$) is shown in Fig. 5.7.b. The system group has three joints of class 5 ($c_5 = 5(1) - 2(1) = 3$), and three moving links ($n = -1 + 1 + 3 = 4$). There are no translations T_z for the links. A system group with one joint of class 3 ($c_3 = 1$) and no joints of class 1, 2, and 4 ($c_1 = c_2 = c_4 = 0$) is shown in Fig. 5.7.c. The system group has two joints of class 5 ($c_5 = 5(1) - 3(1) = 2$), and two moving links ($n = -1 + 3 = 2$). There are no translations T_y for the links.

For the family $f = 2$, four system groups are presented in Fig. 5.8. The values c_5 and n are computed from Eq. (5.10). Two spatial system groups with no joints of class 1, 2, 3, and 4 ($c_1 = c_2 = c_3 = c_4 = 0$) are shown in Figs. 8.a and 8.b. The system groups have four joints of class 5 ($c_5 = 4(1) = 4$), and three moving links ($n = -1 + 4 = 3$). For the system group in Fig. 5.8.a, there are no translations T_x and no rotations R_y for the links. For the system group in Fig. 5.8.b, there are no translations T_y and no rotations R_x for the links. A system group with no joints of class 1, 2, and 3 ($c_1 = c_2 = c_3 = 0$) and one joint of class 4 ($c_4 = 1$) is shown in Fig. 5.8.c. The system group has two joints

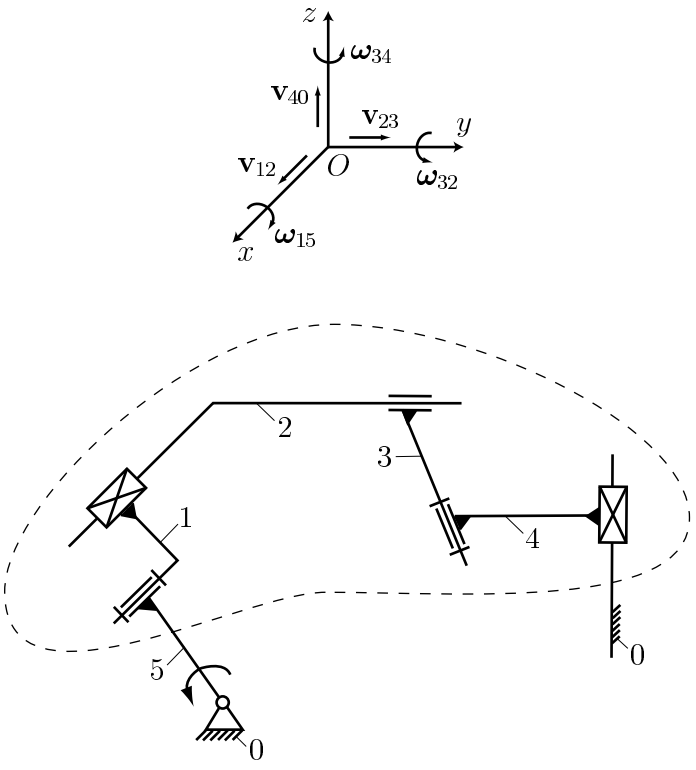

Figure 5.6: Spatial mechanism with one independent contour and a system group of the family $f = 0$.

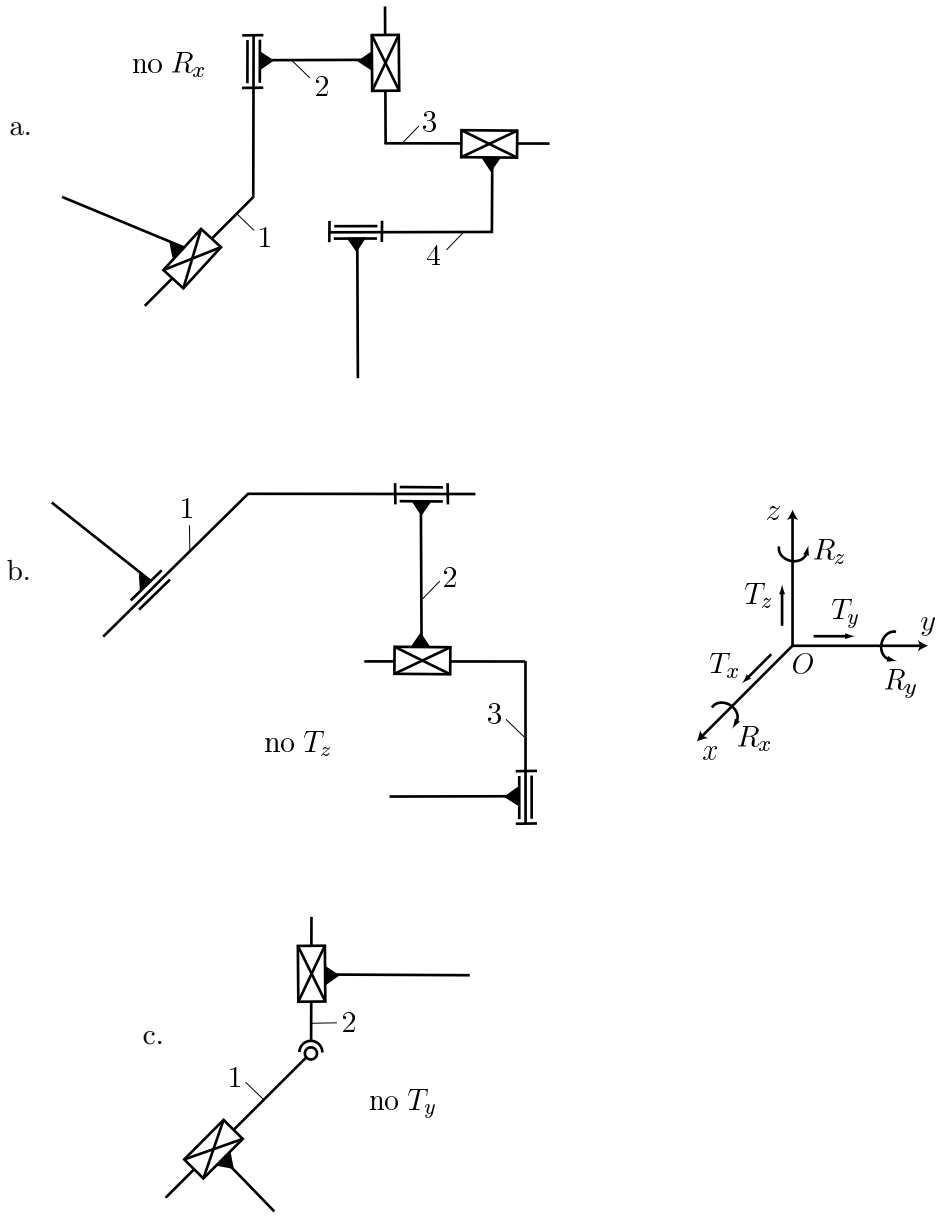

Figure 5.7: System groups with one independent contour ($N = 1$) of the family $f = 1$.

of class 5 ($c_5 = 4(1) - 2(1) = 2$), and two moving links ($n = -1 + 1 + 2 = 2$). There are no translations T_z and no rotations R_y for the links. A system group with one joint of class 3 ($c_3 = 1$) and no joints of class 1, 2, and 4 ($c_1 = c_2 = c_4 = 0$) is shown in Fig. 5.8.d. The system group has one joints of class 5 ($c_5 = 4(1) - 3(1) = 1$), and one moving link ($n = -1 + 1 + 1 = 1$). There are no translations T_x and T_z for the links.

The spatial mechanism presented in Fig. 5.9 is built from the system group shown in Fig. 5.8.b. The mechanism has one degree of freedom ($M = 4n - 3c_5 - 2c_4 - c_3 = 4(4) - 3(5) = 1$). The link 4 is the driver link.

For the family $f = 3$, three system groups are presented in Fig. 5.10. The values c_5 and n are computed from Eq. (5.11). Three system groups with no joints of class 1, 2, 3, and 4 ($c_1 = c_2 = c_3 = c_4 = 0$) are shown in Fig. 5.10. The system groups have three joints of class 5 ($c_5 = 3(1) = 3$), and two moving links ($n = -1 + 3 = 2$). There are no translations T_x and no rotations R_y and R_z for the system group in Fig. 5.10.a. There are no translations T_x and no rotations R_x and R_z for the system group in Fig. 5.10.b. There are no translations T_z and no rotations R_x and R_y for the system group in Fig. 5.10.c.

For the family $f = 4$, two planar system groups with no joints of class 1, 2, 3, and 4 ($c_1 = c_2 = c_3 = c_4 = 0$) are shown in Fig. 5.11. The values c_5 and n are computed from Eq. (5.12). for each system group, there are two joints of class 5 ($c_5 = 2(1) = 2$), and one moving link ($n = -1 + 2 = 1$). Also, there are two planar translations for the links and thus the family of the systems is $f = 6 - 2 = 4$.

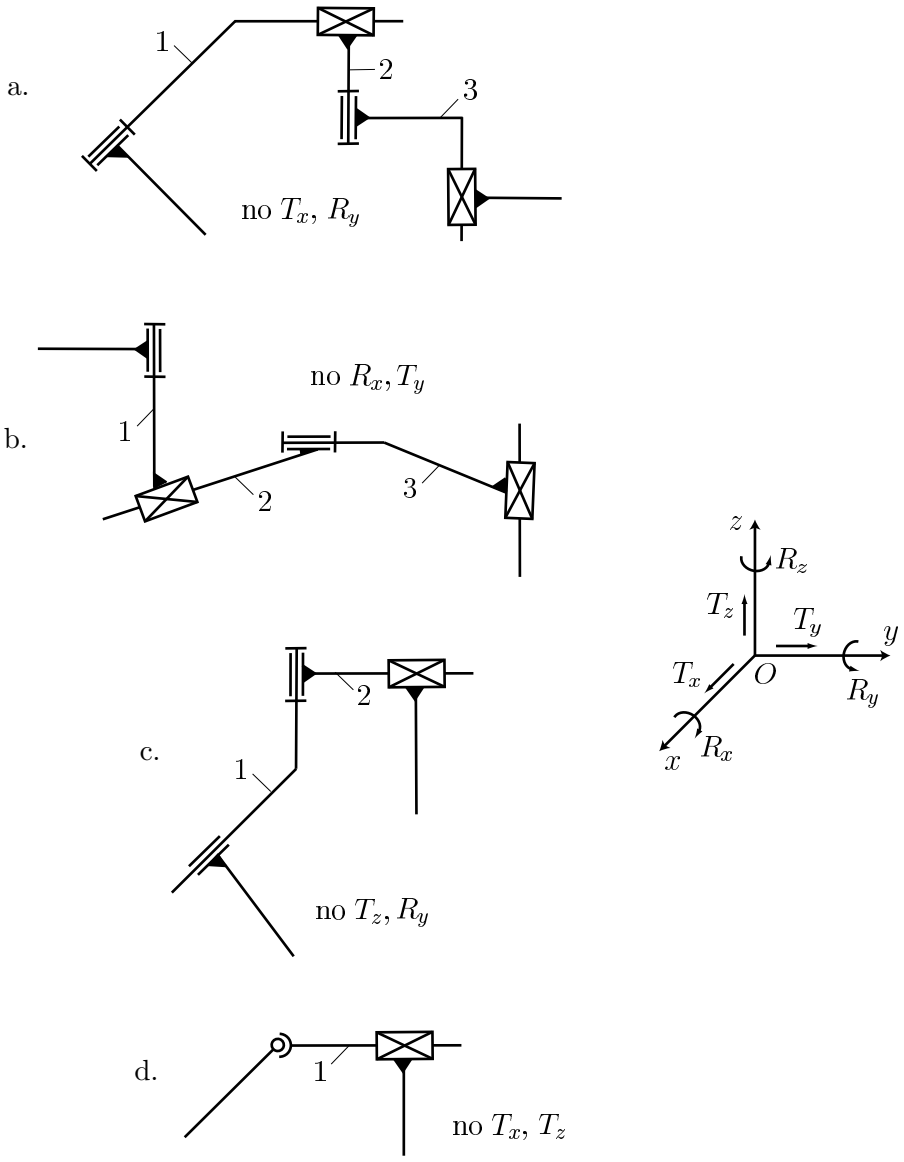

Figure 5.8: System groups with one independent contour ($N = 1$) of the family $f = 2$.

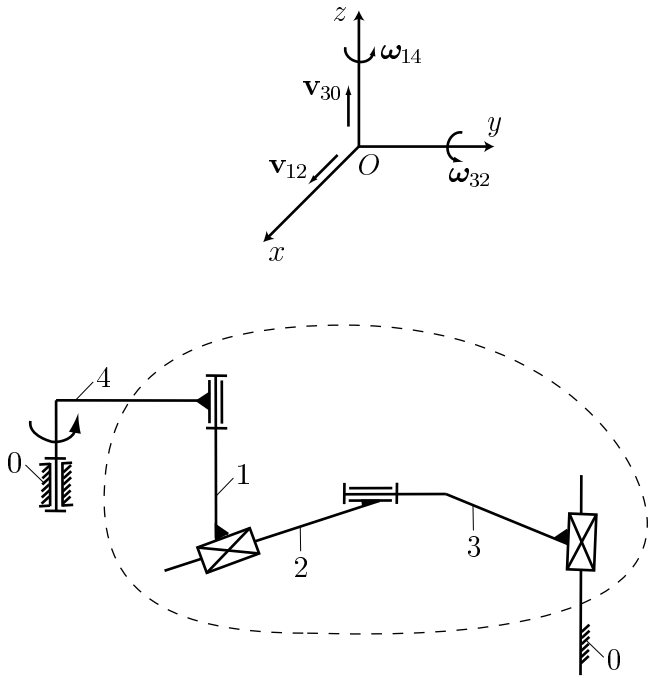

Figure 5.9: Spatial mechanism with one independent contour and a system group of the family $f = 2$.

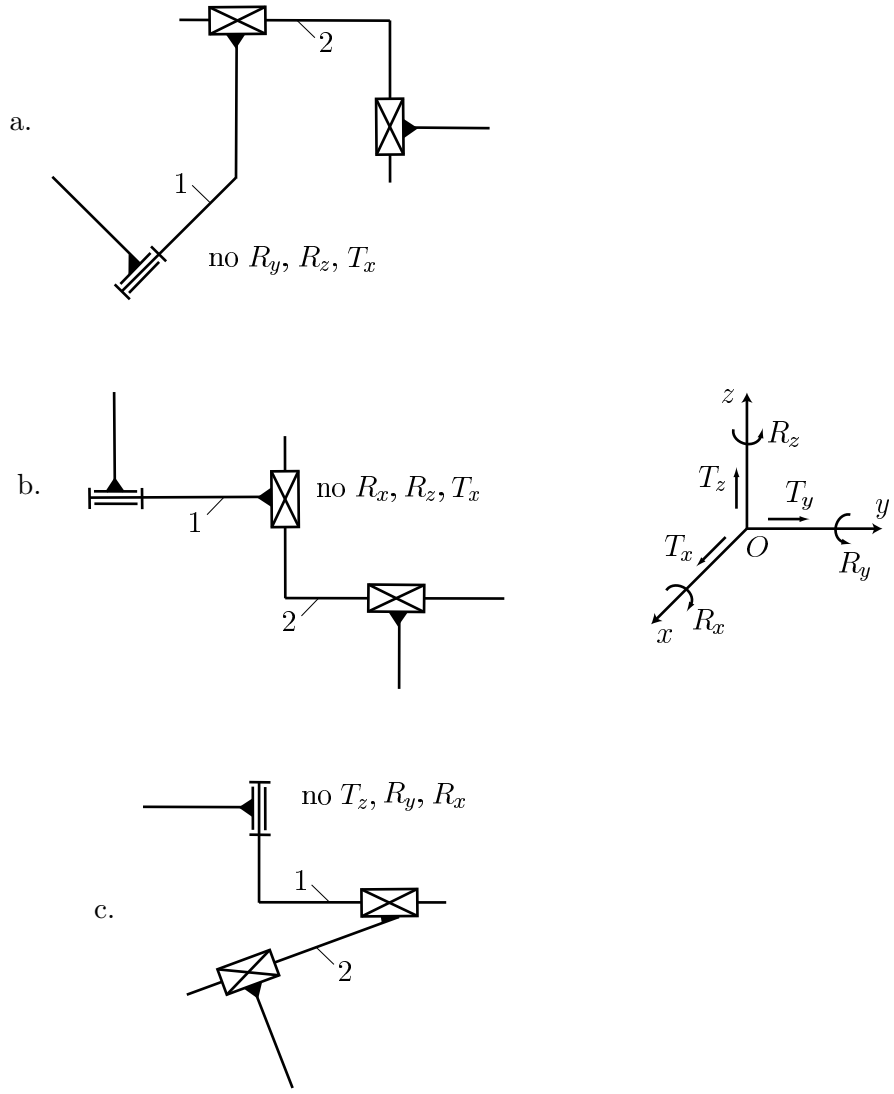

Figure 5.10: System groups with one independent contour ($N = 1$) of the family $f = 3$.

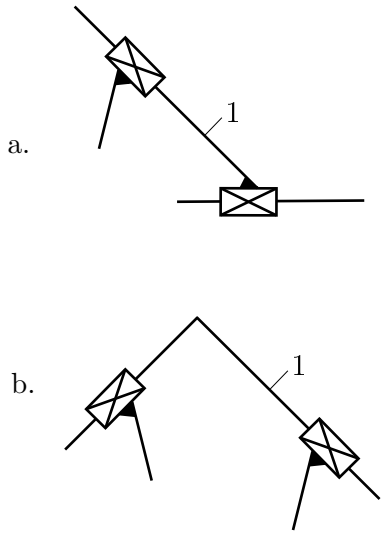

Figure 5.11: System groups with one independent contour ($N = 1$) of the family $f = 4$.

5.4.2 System groups with two independent contours

Spatial system groups with two independent contours ($N = 2$) are presented. The number of joints $c_1,\ c_2,\ c_3$, and c_4 are cycled, and the number of joints c_5 and the number of moving links n are computed. Examples of system groups with $N = 2$ are described next for each of the families $f = 1,\ 2,\ 3$, and 4.

For the family $f = 1$, a system group is depicted in Fig. 5.12. The system group has no joints of class 1, 2, 3, and 4 ($c_1 = c_2 = c_3 = c_4 = 0$). There are ten joints of class 5 ($c_5 = 5(2) = 10$), and eight moving links ($n = -2 + 10 = 8$). There are no translations T_x for the links.

For the family $f = 2$, two system groups are illustrated in Fig. 5.13. A system group with no joints of class 1, 2 and 3 ($c_1 = c_2 = c_3 = 0$) and one joint of class 4 ($c_4 = 1$) is shown in Fig. 5.13.a. The system group has six joints of class 5 ($c_5 = 4(2) - 2(1) = 6$), and five moving links ($n = -2+1+6 = 5$). There are no translations T_x and no rotations R_x for the links. A system group with no joints of class 1 and 2 ($c_1 = c_2 = 0$), one joint of class 3 ($c_3 = 1$), and one joint of class 4 ($c_4 = 1$) is shown in Fig. 5.13.b. The system group has three joints of class 5 ($c_5 = 4(2) - 3(1) - 2(1) = 3$), and three moving links ($n = -2 + 1 + 1 + 3 = 3$). There are no translations T_x and T_y for the links.

For the family $f = 3$, three system groups are presented in Fig. 5.14. A system group with no joints of class 1, 2, 3, and 4 ($c_1 = c_2 = c_3 = c_4 = 0$) is shown in Fig. 5.14.a. The system group has six joints of class 5 ($c_5 = 3(2) = 6$), and four moving links ($n = -2 + 6 = 4$). There are no translations T_x, T_y, and T_z for the links. A spatial system group and a planar system group with no joints of class 1, 2 and 3 ($c_1 = c_2 = c_3 = 0$) and one joint of class 4 ($c_4 = 1$) are shown in Fig. 5.14.b and Fig.14.c,

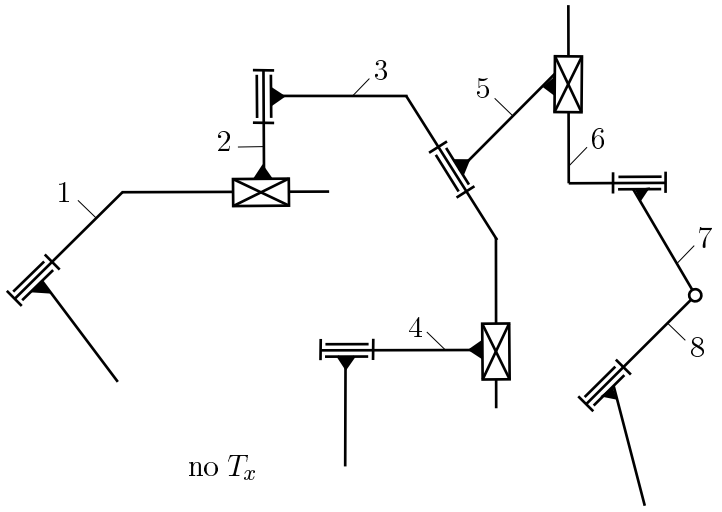

Figure 5.12: System group with two independent contours ($N = 2$) of the family $f = 1$.

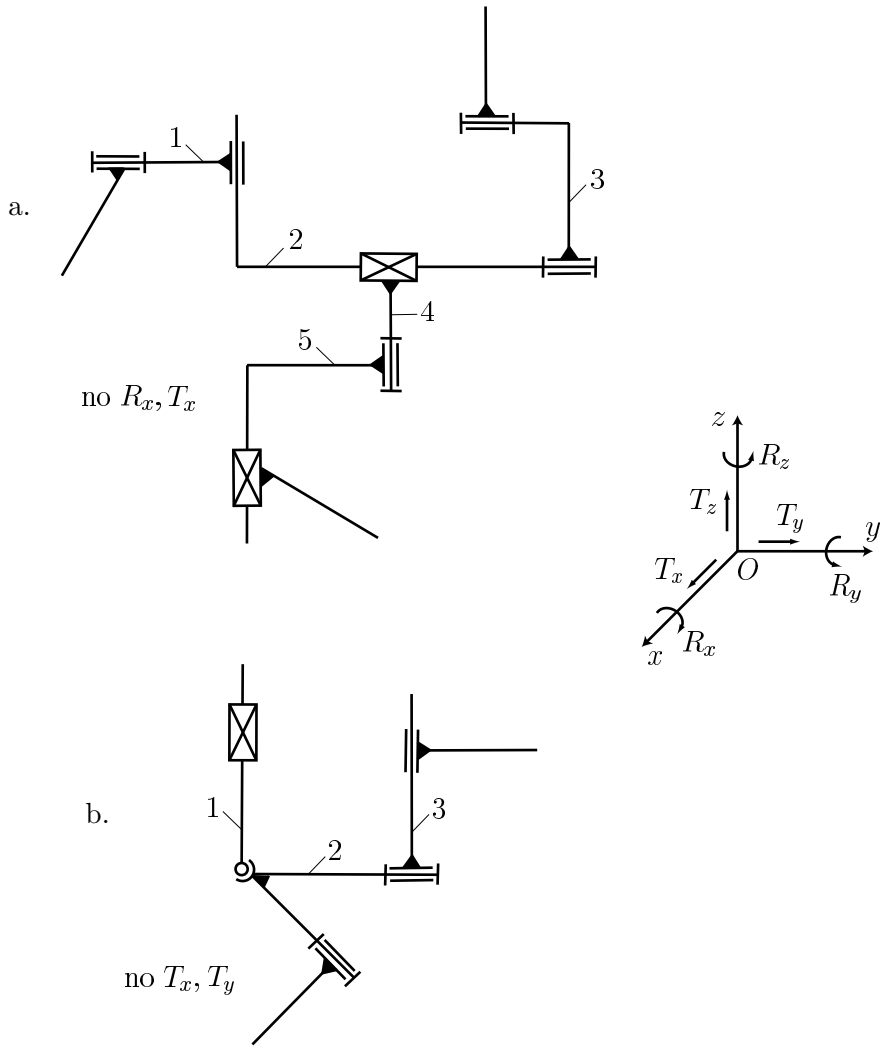

Figure 5.13: System groups with two independent contours ($N = 2$) of the family $f = 2$.

respectively. The system groups have four joints of class 5 ($c_5 = 3(2) - 2(1) = 4$), and three moving links ($n = -2 + 1 + 4 = 3$). There are no translations T_y, T_z and no rotations R_z for the spatial system in Fig. 5.14.b.

For the family $f = 4$, a planar system group with no joints of class 1, 2, 3, and 4 ($c_1 = c_2 = c_3 = c_4 = 0$) is shown in Fig. 5.15. The system group has four joints of class 5 ($c_5 = 2(2) = 4$), and two moving links ($n = -2 + 4 = 2$).

The spatial mechanism shown in Fig. 5.16 contains a system group of the family $f = 0$ that has $c_1 = c_2 = 0$, $c_3 = 1$, $c_4 = 2$, $c_5 = 6(2) - 3(1) - 2(2) = 5$, and $n = -2 + 1 + 2 + 5 = 6$. The mechanism has two degrees of freedom $M = 6n - 5c_5 - 4c_4 - 3c_3 - 2c_2 - c1 = 6(8) - 5(7) - 4(2) - 3(1) = 2$. The links 7 and 8 are driver links.

5.4.3 System groups with three independent contours

Spatial system groups with three independent contours ($N = 3$) are presented. The number of joints c_1, c_2, c_3, and c_4 are cycled and the number of joints c_5 and the number of moving links n are computed. System groups with $N = 3$ are exemplified next for each of the families $f = 2$, 3, and 4.

For the family $f = 2$, a spatial system group with no joints of class 1 and 2 ($c_1 = c_2 = 0$), one joint of class 3 ($c_3 = 1$), and one joint of class 4 ($c_4 = 1$) is shown in Fig. 5.17. The system group has seven joints of class 5 ($c_5 = 4(3) - 3(1) - 2(1) = 7$), and six moving links ($n = -3 + 1 + 1 + 7 = 6$). There are no translations T_x and T_z for the links.

For the family $f = 3$, a planar system group with no joints of class 1, 2, and 3 ($c_1 = c_2 = c_3 = 0$) and one joint of class 4 ($c_4 = 1$) is depicted in Fig. 5.18. The

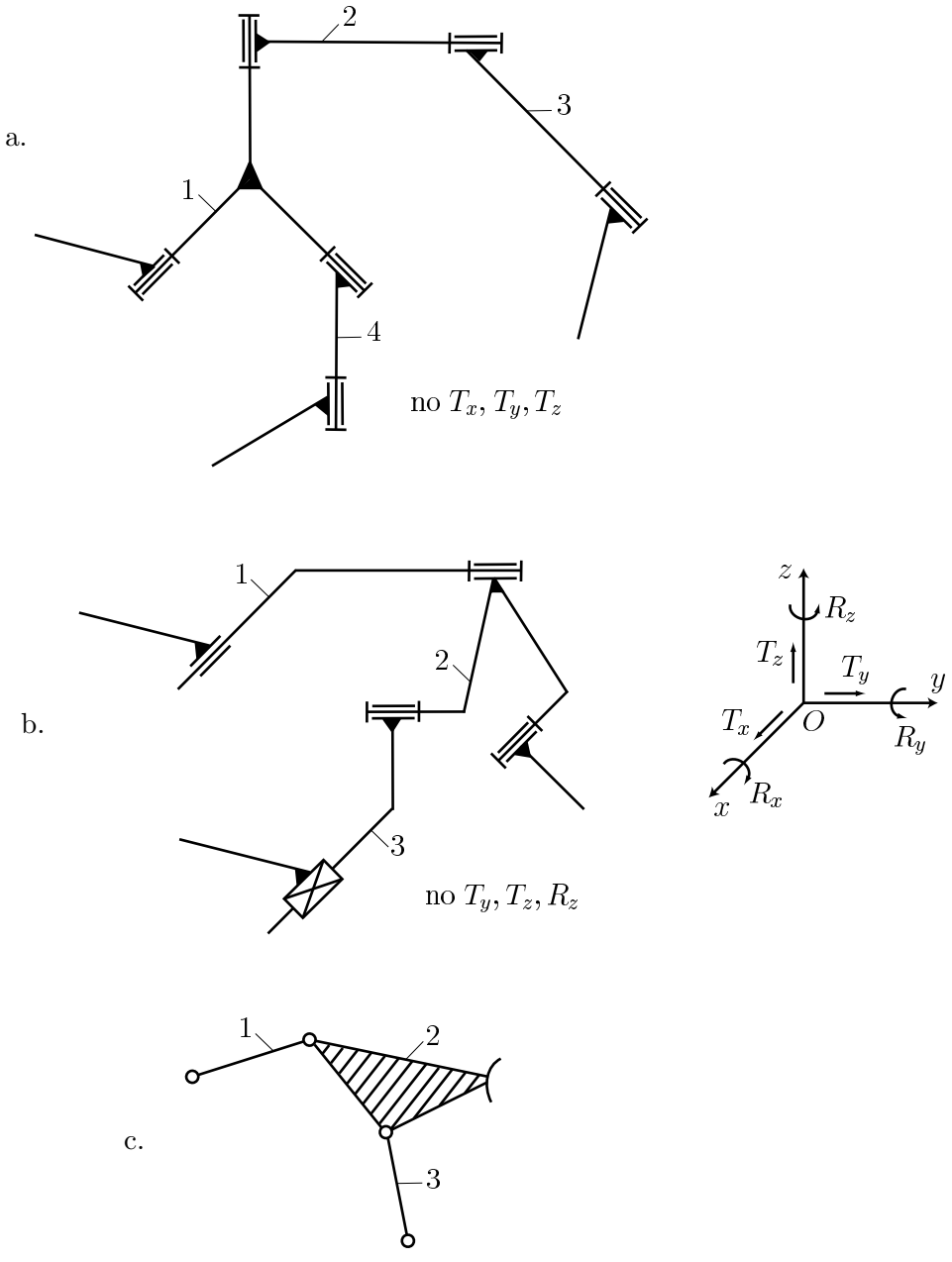

Figure 5.14: System groups with two independent contours ($N = 2$) of the family $f = 3$.

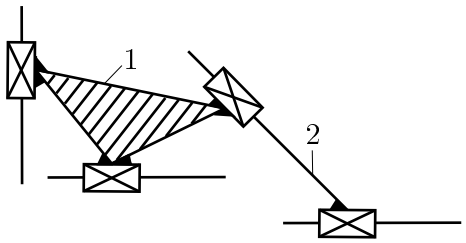

Figure 5.15: System group with two independent contours ($N = 2$) of the family $f = 4$.

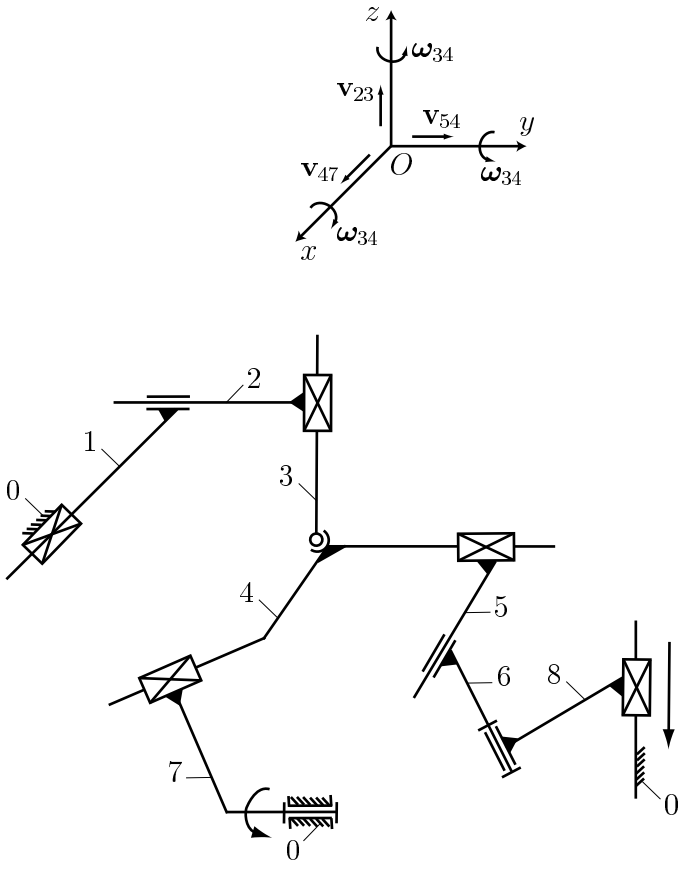

Figure 5.16: Spatial mechanism with two independent contours and a system group of the family $f = 0$.

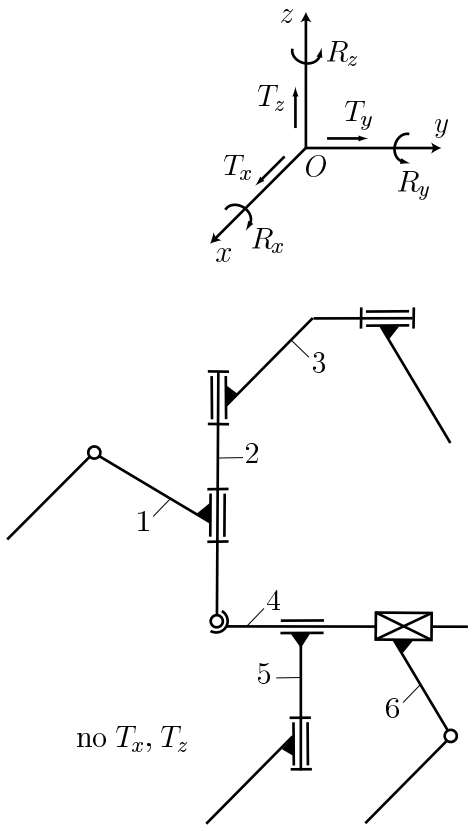

Figure 5.17: System group with three independent contours ($N = 3$) of the family $f = 2$.

system group has seven joints of class 5 ($c_5 = 3(3) - 2(1) = 7$), and five moving links ($n = -3 + 1 + 7 = 5$).

For the family $f = 4$, a planar system group with no joints of class 1, 2, 3, and 4 ($c_1 = c_2 = c_3 = c_4 = 0$) is shown in Fig. 5.19. The system group has six joints of class 5 ($c_5 = 2(3) = 6$), and three moving links ($n = -3 + 6 = 3$).

The spatial mechanism presented in Fig. 5.20 contains a system group of the family $f = 0$ that has $c_1 = c_2 = 0$, $c_3 = 3$, $c_4 = 4$, $c_5 = 6(3) - 3(3) - 2(4) = 1$, and $n = -3 + 3 + 4 + 1 = 5$. The mechanism has three degrees of freedom $M = 6n - 5c_5 - 4c_4 - 3c_3 - 2c_2 - c1 = 6(8) - 5(4) - 4(4) - 3(3) = 3$. The links 6, 7 and 8 are driver links.

5.5 Conclusions

The method of computer-aided structural synthesis of spatial mechanisms presented in this paper is based essentially on system group formation using the number of independent contours and joints as inputs. The number of joints of different classes are cycled for different families and several structures of spatial system groups with one, two, or more independent contours are obtained. For a given family, different configurations of system groups with the same number of independent contours can be obtained. Spatial mechanisms can be structured based on spatial system groups.

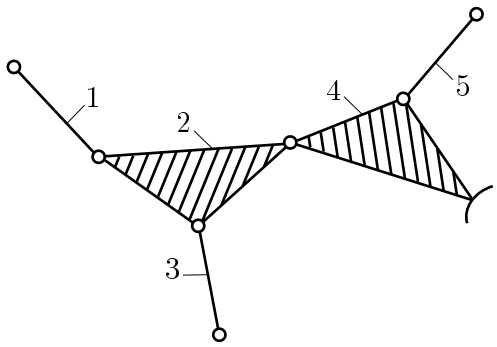

Figure 5.18: System group with three independent contours ($N = 3$) of the family $f = 3$.

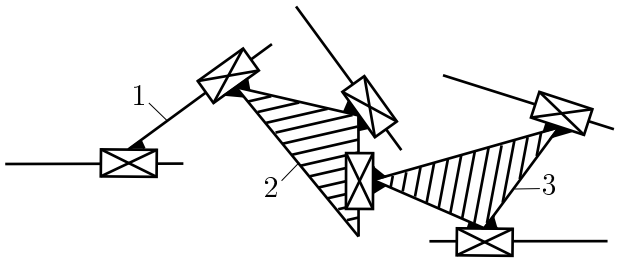

Figure 5.19: System group with three independent contours ($N = 3$) of the family $f = 4$.

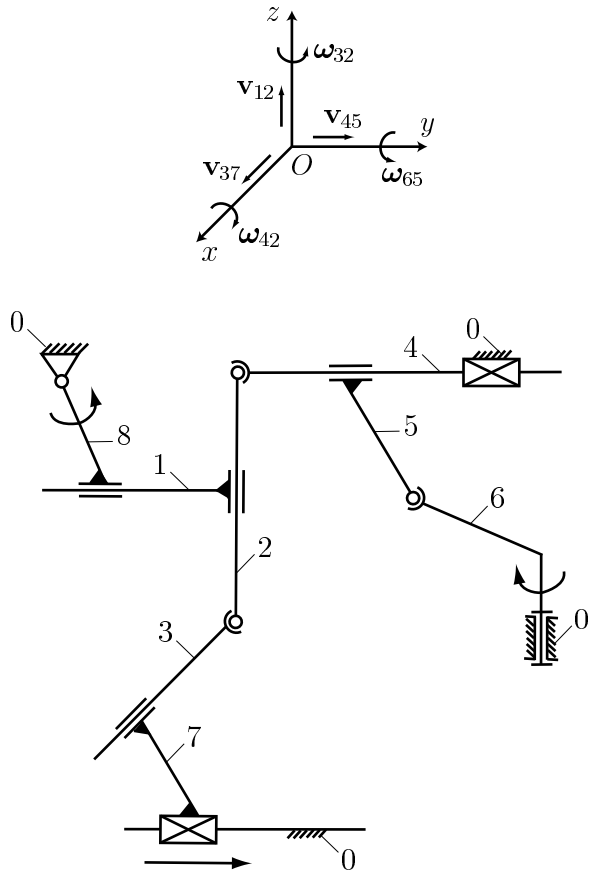

Figure 5.20: Spatial mechanism with three independent contours and a system group of the family $f = 0$.

Chapter 6

Discussions and conclusions

In this dissertation the nonlinear dynamics of a mechanical system with joint clearance is investigated. Modeling this system leads to modeling contacts and impacts that occur between the links and the joints. Also, at high speeds, the joint moment of inertia may significantly influence the behavior of the system.

In Chapter 2, the influence of the moment of rolling friction on the energy dissipated by friction during the impact for different values of the geometrical parameters of the links is analyzed. More energy is dissipated during impact for larger values of the coefficient of rolling friction. An energy increase is observed in some cases when the kinematic coefficient of restitution is used to model the impact. One can partially solve this problem and obtain energetically consistent results introducing the moment of rolling friction to the impact equations.

In Chapter 3, the effect of joint inertia on the dynamics of kinematic chains is presented. The application point of the joint contact forces changes its position for different values of the slider inertia. Dynamic response characteristics of a planar robot arm are compared for different values of the prismatic joint inertia.

In Chapter 4, the influence of the prismatic joint clearance and the crank speed on the stability of mechanisms is studied. The Lyapunov exponents are computed for simulated data and used as a diagnostic tool. The largest Lyapunov exponents are compared for different crank speeds at different values of the clearance.

In Chapter 5, a computer-aided structural synthesis of spatial mechanisms is presented. The method is based essentially on system group formation using the number of independent contours and joints as inputs. For each family, the number of joints are cycled and several structures of spatial system groups are obtained. The solution of a spatial mechanism can be obtained by composing the partial solutions of the system groups.

Future work includes experimental approaches of dynamics and control of robotic arms with joint clearance. The influence of the clearance at joints and the effect of joint inertia on the control parameters of the systems should be investigated.

Bibliography

[1] Newton, I., 1686, *Philosophiae naturalis principia mathematica*, Reg. Soc. Praeses, London.

[2] Poisson, S.D., 1817, *Mechanics*, Longmans, London.

[3] Routh, E.J., 1860, *Dynamics of a System of Rigid Bodies*, Macmillan & Co., London.

[4] Whittaker, E. T., 1904, *A Treatise on the Analytical Dynamics of Particles and Rigid Bodies*, Cambridge, U.K.

[5] Kane, T. R., and Levinson, D. A., 1985, *Dynamics: Theory and applications*, New York, McGraw-Hill.

[6] Keller, J. B., 1986, "Impact with Friction", *Journal of Applied Mechanics*, Vol. 53, pp. 1-4.

[7] Stronge, W.J., 1990, "Rigid Body Collisions with Friction", *Proceedings of Royal Society*, Vol. 431, Part A, pp. 169-181.

[8] Stronge, W.J., 1994, "Swerve During Three-Dimensional Impact of Rough Bodies", *Journal of Applied Mechanics*, Vol. 61, pp. 605-611.

[9] Brach, R. M., 1960, "Rigid Body Collisions", *Journal of Applied Mechanics*, Vol. 56, pp. 133-138.

[10] Brach, R. M., 1991, *Mechanical Impact Dynamics*, New York, John Wiley and Sons.

[11] Brach, R. M., and Dunn, P. F., 1995, "Macrodynamics of Microparticles", *Journal of Aerosol Science and Technology*, Vol. 23, pp. 51-71.

[12] Marghitu, D. B., 1995, "Frictional Impact of an Elastic Body", *Design Engineering Technical Conference*, DE 87-1, Vol. 3, Part A, pp. 191-201.

[13] Stioanovici, D., and Hurmuzlu, I., 1996, "A Critical Study of the Applicability of Rigid-Body Collision Theory", *Journal of Applied Mechanics*, Vol. 63, pp. 307-316.

[14] Calsamiglia, J., Kennedy, S. W., Chatterjee, A., Ruina, A., and Jenkins, J. T., 1999, "Anomalous Frictional Behavior in Collision of Thin Disks", *Journal of Applied Mechanics*, Vol. 66, pp. 146-152.

[15] Osakue, E. E., and Rogers, R. J., 2001, "An Experimental Study of Friction During Planar Elastic Impact", *ASME Journal of Pressure Vessel Technology*, Vol. 123, pp. 493-500.

[16] Johansson, L., and Klarbring, A., 2000, "Study of Frictional Impact Using a Nonsmooth Equations Solver", *ASME Journal of Applied Mechanics*, Vol. 67, pp. 267-273.

[17] Pfeiffer, F., and Glocker, C., 1996, *Multibody Dynamics with Unilateral Contacts*, New York, John Wiley and Sons.

[18] Marghitu, D.B., and Hurmuzlu, Y., 1995, "Three Dimensional Rigid Body Collisions with Multiple Contact Points", *Journal of Applied Mechanics*, Vol. 62, pp. 725-732.

[19] Hurmuzlu, Y., 1998, "An Energy-Based Coefficient of Restitution for Planar Impacts of Slender Bars With Massive External Surfaces", *Journal of Applied Mechanics*, Vol. 65, pp. 952-962.

[20] Ceanga, V., and Hurmuzlu, Y., 2001, "A New Look at an Old Problem: Newton's Cradle", *Journal of Applied Mechanics*, Vol. 68, pp. 575-583.

[21] Chatterjee, A., and Ruina, A., 1998, "A New Algebraic Rigid-Body Collision Law Based on Impulse Space Considerations", *Journal of Applied Mechanics*, Vol. 65, pp. 939-951.

[22] Lankarani, H. M., 2000, "A Poisson-Based Formulation for Frictional Impact Analysis of Multibody Mechanical Systems with Open or Closed Kinematic Chains", *ASME Journal of Mechanical Design*, Vol. 122, pp. 489-495.

[23] R.D. Howe, M.R. Cutkoski, 1996, "Practical Force-Motion Models for Sliding Manipulation", *International Journal of Robotic Research*, Vol. 15, pp. 557-572.

[24] P. Song, M. Yashima, V. Kumar, 2000, "Dynamic Simulation for Grasping and Whole Arm Manipulation", *Proceedings of the 2000 IEEE International Conference on Robotics and Automation*, Vol. 2, pp. 1082-1087.

[25] J. Trinkle, J.-S. Pang, S. Sudarsky, G. Lo, 1997, "On Dynamic Multi-Rigid-Body Contact Problems with Coulomb Friction", *Z. Angew. Math. Mech.*, Vol. 77, No. 4, pp. 267-280.

[26] M.T. Mason, Y. Wang, 1988, "On the Inconsistency of Rigid-Body Frictional Planar Mechanics", *Proceedings of the 2000 IEEE International Conference on Robotics and Automation*, pp. 524-528.

[27] Y.-K. Kim, 1988, "Adaptive Control of Robotic Manipulators with a Sliding Flexible Link", PhD thesis, University of California, Los Angeles.

[28] K.W. Buffinton, 1992, "Dynamics of Elastic Manipulators with Prismatic Joints", *Journal of Dynamic Systems, Measurements, and Control*, Vol. 114, pp. 41-49.

[29] F. Gordaninejad, A. Azhdari, N.G. Chalhoub, 1991, "Nonlinear Dynamic Modelling of a Revolute-Prismatic Flexible Composite-Material Robot Arm", *Journal of Vibration and Acoustics*, Vol. 113, pp. 461-468.

[30] R.C. Benson, F.E. Talke, 1987, "The Transition Between Sliding and Flying of a Magnetic Recording Slider", *IEEE Transactions on Magnetics*, Vol. 23, No. 5, pp. 3441-3443.

[31] W.Q.D. Do, D.C.H. Yang, 1988, "Inverse Dynamic Analysis and Simulation of a Platform Type of Robot", *Journal of Robotic Systems*, Vol. 5, No. 3, pp. 209-227.

[32] D. Stewart, 1965, "A platform with six degrees of freedom", *Proceedings of the Institute of Mechanical Engineerings, Part I*, Vol. 180, No. 15, pp. 371-386.

[33] Z. Ji, 1993, "Study of the effect of leg inertia in Stewart platforms", *Proceedings of the IEEE International COnference of Robotics and automation*, Vol. 1, pp. 121-126.

[34] B. Dasgupta, T.S. Mruthyunjaya, 1998, "A Newton-Euler formulation for the inverse dynamics of the Stewart platform manipulator", *Mechanism and Machine Theory*, Vol. 33, No. 8, pp. 1135-1152.

[35] F. Xi, R. Sinatra, W. Han, 2001, "Effect of Leg Inertia on Dynamics of Sliding-Leg Hexapods", *Journal of Dynamic Systems, Measurment, and Control*, Vol. 123, pp. 265-271.

[36] F. Gao, W. Li, X. Zhao, Z. Jin, H. Zhao, 2002, "New kinematic structures for 2-, 3-, 4-, and 5-DOF parallel manipulator designs", *Mechanism and Machine Theory*, Vol. 37, pp. 1395-1411.

[37] J.E. Bobrow, S. Dubowski, J.S. Gibson, 1985, "Time-Optimal Control of Robotic Manipulators Along Specified Paths", it International Journal of Robotics Research, Vol. 4, No. 3, pp. 3-17.

[38] Farahanchi, F., and Shaw, S.W., 1994, "Chaotic and periodic dynamics of a slider-crank mechanism with slider clearance", *Journal of Sound and Vibration*, Vol. 177, No. 3, pp. 307-324.

[39] Abarbanel, H.D.I., 1995, "Tools for analysing observed chaotic data", Springer-Verlag, New York.

[40] Abarbanel, H.D.I., 1996, "Analysis of Observed Chaotic Data", Springer-Verlag, New York.

[41] Abarbanel, H.D.I., Frison, T.W., and Tsimring, L.S., 1998, "Time-Domain Analysis of Nonlinear and Chaotic Signals", *IEEE Signal Processing Machine*.

[42] Nayfeh, A. H., and Balachandran, B., 1995, "Applied Nonlinear Dynamics", John Wiley and Sons, New York.

[43] Kapitaniak, T., 1991, "Chaotic oscillations in mechanical systems", Manchaster University Press, Manchaster.

[44] Ott, E., Sauer, T., and Yorke, J.A., 1994, "Coping with Chaos", John Wiley and Sons, New York.

[45] Deck, J.F., and Dubowski, S., 1992, "On the limitations of predictions of the dynamic response of machines with clearance connections", *Flexible mechanisms, Dynamics, and Analysis*, Vol. 47, pp. 461-469.

[46] Gilmore, B.J., and Cipra, R.J., 1991, "Simulation of Planar Dynamic Mechanical Systems with Changing Topologies: part I - Characterization and Prediction of the Kinematic Constraint Changes, part II - Implementation Strategy and Symulation Results for Example Dynamic Systems", *Journal of Mechanical Design*, Vol. 113, pp. 70-83.

[47] Conti, C., Corron, P., and Michotte, P., 1992, "A Computer Aided Kinematic Analysis System for Mechanism Design and Computer Simulation", *Mechanism and Machine Theory*, Vol. 27, pp. 563-574.

[48] Pfeiffer, F., 1993, "Complimentarity problems of stick-slip vibrations", *Dynamics and Vibration of Time-Varying Systems and Structures*, Vol. 56, pp. 43-50.

[49] Brach, R. M., 1989, "Rigid Body Collisions", *Journal of Applied Mechanics*, Vol. 56, pp. 133-138.

[50] Wang, Y., and Mason, M.T., 1992, "Two Dimensional Rigid-Body Collision with Friction", *Journal of Applied Mechanics*, Vol. 59, pp. 635-642.

[51] Jean, M. and Moreau, J.J., 1992, "Unilaterality and Dry Friction in the Dynamics of Rigid Body Collections", *Proceedings of Contact Mechanics International Symposium*, Lausanne, pp. 31-48.

[52] Marghitu, D.B., and Hurmuzlu, Y., 1996, "Nonlinear Dynamics of an Elastic Rod with Frictional Impact", *Journal of Nonlinear Dynamics*, Vol. 10, pp. 187-201.

[53] Marghitu, D.B., 1997, "Impact of Flexible Link with Solid Lubrication", *Journal of Sound and Vibration*, Vol. 205, No. 4, pp. 712-720.

[54] Marghitu, D.B., Guran, A., 1998, "The Dynamics of a Flexible Beam with a Lubricated Prismatic Kinematic Pair", *Journal of Vibration and Acoustics*, Vol. 120, No. 4, pp. 880-885.

[55] Marghitu, D.B., Stoenescu, E.D., 2000, "Dynamic stability of children gait", *Advanced Topics in Electrical Engineering Conference*, Bucharest, December 8.

[56] Stoenescu, E.D., Marghitu, D.B., 2003, "Dynamic analysis of a planar rigid-link mechanism with rotating slider joint and clearance", *Journal of Sound and Vibration*, Vol. 266, pp. 394-404.

[57] Marghitu, D.B., Stoenescu, E.D., 2001, "Dynamics of mechanisms with slider joints and clearance", *Design Engineering Technical Conferences and Computers and Information*, Pittsburg, September 9-12.

[58] F.R.E. Crossley, 1965, "The Permutation of Kinematic Chains of Eight Members or Less from the Graph-Theoretic Viewpoint", *Developments in Theoretical and Applied Mechanics*, Vol. 2, pp. 467-486.

[59] T.H. Davies, 1968, "An Extension of Manolescu's Classification of Planar Kinematic Chains and Mechanisms of Mobility m>1 Using Graph Theory", *Journal of Mechanisms*, Vol. 3, pp. 87-100.

[60] L.W. Tsai, 2000, "Mechanism Design: Enumeration of Kinematic Structures According to Function", CRC Press, Boca Raton.

[61] N.P. Belfiore, E. Pennestri, 1994, "Automatic skeching of planar kinematic chains", *Mechanism and Machine Theory*, Vol. 29, pp. 177-193.

[62] D. Sen, T.S. Mruthynjaya, 1998, "A Centro-Based Characterization of Singularities in the Workspace of Planar Closed-Loop Manipulators", *Mechanism and Machine Theory*, Vol. 8, pp. 1091-1104.

[63] C. Jinkui, C. Weiqing, 1998, "Sistemics of Assur Groups with Multiple Joints", *Mechanism and Machine Theory*, Vol. 8, pp. 1127-1133.

[64] P.W. Jensen, 1991, "Classical and Modern Mechanisms for Engineers and Inventors", Marcel Dekker, Inc., New York.

[65] E.R. Tuttle, S.W. Peterson, J.E. Titus, 1989, "Enumeration of basic kinematic chains using the theory of finit groups", *J. Mech., Trans. Automat. Design*, Vol. 111, pp. 498-503.

[66] W.M. Hwang, Y.W. Hwang, 1992, "Computer-aided structural synthesis of planar kinematic chains with simple joints", *Mechanism and Machine Theory*, Vol. 27, No. 2, pp. 189-199.

[67] S.J. Chiou, S. Kota, 1999, "Automated conceptual design of mechanisms", *Mechanism and Machine Theory*, Vol. 34, No. 3, pp. 467-495.

[68] A.C. Rao, P.B. Deshmukh, 2001, "Computer aided structural synthesis of planar kinematic chains obviating the test for isomorphism", *Mechanism and Machine Theory*, Vol. 36, pp. 489-506.

[69] H. Shen, K.-L. Ting, T. Yang, 2000, "Configuration analysis of complex multiloop linkages and manipulators", *Mechanism and Machine Theory*, Vol. 35, pp. 353-362.

[70] L. Shujun, 1990, "Computer-Aided Structure Synthesis of Spatial Kinematic Chain", *Mechanism and Machine Theory*, Vol. 6, pp. 645-653.

[71] I. Popescu, C. Ungureanu, 2000, "Structural Synthesis and Kinematics of Mechanisms with Bars", Universitaria Press, Craiova.